Julius-Maximilians-
UNIVERSITÄT
WÜRZBURG

PAF1 complex and MYC couple transcription elongation with double-strand break repair

Koordination von Transkriptionselongation und Doppelstrangbruchreparatur durch den PAF1 Komplex und MYC

Doctoral Thesis
for a doctoral degree at the Graduate School of Life Sciences,
Julius-Maximilian Universität Würzburg,
Section Biomedicine

submitted by
Theresa Endres
from Bad Neustadt a. d. Saale

Würzburg 2021

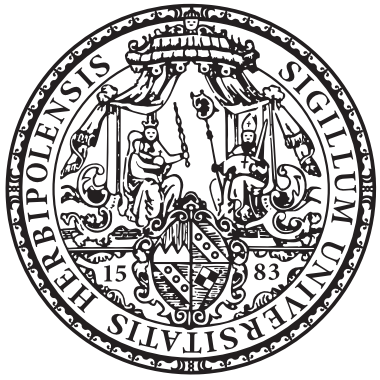

Members of the Thesis Committee:

Chairperson: Prof. Dr. Alexander Buchberger

First Supervisor: Prof. Dr. Martin Eilers
Second Supervisor: Prof. Dr. Elmar Wolf
Third Supervisor: Prof. Dr. Caroline Kisker
Fourth Supervisor: Prof. Dr. Patrick Cramer

Submitted on:

Date of Public Defense:

Date of Receipt of Certificates:

Version August 17, 2021

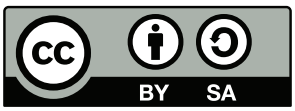

Satz: PDF-LaTeX 2$_\varepsilon$

Contents

Abbreviation ix

Summary xvi

Zusammenfassung xvii

1 Introduction 1

1.1 The oncogenic transcription factor MYC . . . 1
1.2 Functions of MYC . . . 4
1.2.1 The transcription factor MYC . . . 4
1.2.2 Target genes of MYC . . . 6
1.2.3 Models of MYC function . . . 7
1.3 MYC and the ubiquitin system . . . 11
1.4 RNA Polymerase II transcription . . . 14
1.4.1 Initiation . . . 15
1.4.2 Promoter-proximal pausing . . . 15
1.4.3 Elongation and termination . . . 16
1.5 DRB-sensitive inducing factor (DSIF) . . . 17
1.6 RNA Polymerase II associated factor 1 complex (PAF1c) . . . 18
1.6.1 Subunits of PAF1c . . . 19
1.6.2 PAF1c and the transcriptional cycle . . . 20
1.7 DNA damage repair . . . 22
1.8 Objective of the thesis . . . 24

2 Material 25

2.1 Strains and cell lines . . . 25
2.1.1 Bacterial strains . . . 25

2.1.2 Human cell lines . . . 25
2.2 Cultivation media and supplements . . . 26
2.2.1 Media and antibiotics for bacterial cell culture . . . 26
2.2.2 Media for mammalian cell culture . . . 27
2.2.3 Antibiotics for mammalian cell culture . . . 27
2.2.4 Additional supplements . . . 27
2.3 Consumables . . . 28
2.4 Consumables for immunoblot . . . 28
2.5 Equipment . . . 28
2.6 Programs . . . 30
2.7 Enzymes, inhibitors and antibodies . . . 31
2.8 Beads . . . 34
2.9 Dyes . . . 34
2.10 Ready-made kits . . . 35
2.11 EdU labelling reagents . . . 36
2.12 Protein and DNA Ladders . . . 36
2.13 Chemicals . . . 36
2.14 Buffers and solutions . . . 36
2.15 Nucleic acids . . . 43
2.15.1 Plasmids . . . 43
2.15.2 Primer . . . 47

3 Methods **52**

3.1 Cell biology methods . . . 52
3.1.1 Cultivation of eukaryotic cells . . . 52
Passaging of cells . . . 52
Freezing and thawing of cells . . . 52
3.1.2 Transfection of plasmid DNA . . . 53
Transfection with polyethilenimine (PEI) . . . 53
Production of lentiviruses . . . 53
3.1.3 Lentiviral infection of cells . . . 54
3.1.4 Colony formation assay (Crystal violet staining) . . . 54

3.1.5 BrdU Propidium iodide staining for flow cytometry (BrdU-PI FACS) . . . 55
3.2 Molecular biology methods . . . 55
3.2.1 Transformation of competent cells with plasmid DNA followed by plasmid amplification . . . 55
3.2.2 Overexpression and isolation of recombinant proteins in *E.coli* . . . 56
3.2.3 Analytical preparation of plasmid DNA from bacteria (Miniprep) 57
3.2.4 Preparative isolation of plasmid DNA (Maxiprep) . . . 57
3.2.5 Restriction analysis of DNA . . . 57
3.2.6 Gel electrophoretic separation of DNA fragments . . . 58
3.2.7 Extraction and purification of DNA fragments and PCR products 58
3.2.8 Ligation of DNA fragments . . . 59
3.2.9 Nucleic acid quantification . . . 59
Nanodrop . . . 60
PicoGreen . . . 60
Experion . . . 60
Fragment Analyzer . . . 60
3.2.10 RNA Isolation . . . 61
RNA isolation with TriFAST . . . 61
RNA Isolation with RNeasy ® Mini Columns and DNase digestion (Qiagen) . . . 61
3.2.11 cDNA Synthesis . . . 62
3.2.12 Polymerase chain reaction (PCR) . . . 62
PCR to amplify DNA for cloning . . . 62
3.2.13 Quantitative real-time PCR (qPCR) . . . 63
3.3 Biochemical methods . . . 65
3.3.1 Preparation of whole cell protein extracts . . . 65
3.3.2 Total protein quantification by bicinchoninic acid assay (BCA) . 66
3.3.3 SDS Polyacrylamide gel electrophoresis (SDS-PAGE) . . . 66
3.3.4 Immunoblot . . . 66
3.3.5 Coomassie staining of proteins in polyacrylamide gels . . . 67
3.3.6 Silver staining of proteins in in polyacrylamide gels . . . 67
3.3.7 *In vitro* pulldown assay . . . 68

3.3.8 Chromatin immunoprecipitation (ChIP) . . . 68
Formaldehyde fixation . . . 68
Chromatin isolation and Fragmentation . . . 69
Chromatin size control . . . 69
Coupling of antibodies to Dynabeads . . . 70
Immunoprecipitation . . . 70
Washing and elution of chromatin . . . 70
Decrosslinking and DNA purification . . . 70
3.4 Next generation sequencing . . . 71
3.4.1 ChIP for deep sequencing . . . 71
3.4.2 mRNA Isolation, fragmentatiuon and cDNA synthesis for RNA sequencing . . . 71
3.4.3 BLISS and BLISS8 . . . 72
Seeding and fixation of cells in a 24-well plate . . . 72
Cell lysis . . . 72
In-situ AsiSI digestion for BLISS8 . . . 73
In-situ double strand break blunting . . . 73
In-situ ligation . . . 74
Removal of unligated adapters and extraction of genomic DNA . 75
Fragmentation and concentration of DNA . . . 75
In vitro transcription . . . 76
RNA clean up . . . 76
3.4.4 Library Preparation . . . 77
NEBNext® Ultra RNA Library Prep Kit for Illumina® . . . 77
NEBNext® ChIP-Seq Prep Master Mix Set for Illumina® . . . 78
NEBNext® Ultra II DNA Library Prep for Illumina® . . . 78
NEBNext® Multiplex Small RNA Library Prep Kit for Illumina® 79
3.4.5 Sequencing data analysis . . . 81
ChIP Sequencing analysis . . . 81
RNA Sequencing analysis . . . 82
BLISS and BLISS8 Sequencing analysis . . . 82

4 Results **85**

4.1 MYC is directly interacting with PAF1 complex and DSIF 85

4.2 PAF1c enhances association of MYC with active promoters 89

4.3 MYC-mediated transfer of SPT5 is required to maintain RNA Polymerase II processivity 96

4.4 MYC-mediated transfer of PAF1c is required to maintain elongation of RNA Polymerase II 99

4.5 MYC squelches SPT5 from chromatin at oncogenic MYC levels 100

4.6 PAF1c is rapidly transferred from MYC onto RNA Polymerase II . . . 102

4.7 HUWE1 drives the transfer of PAF1c from MYC onto RNAPII 110

4.8 MYC promotes Double Strand Break repair in a PAF1c-dependent manner 112

4.9 PAF1c knockdown reduces MYC dependent transcriptional regulation . 115

4.10 PAF1c suppresses transcription-dependent DNA damage 118

5 Discussion **127**

5.1 MYC directly interacts with SPT5 and PAF1c 127

5.2 SPT5 and MYC: an interaction to keep the chromatin accessible 129

5.3 PAF1c and MYC: another interaction partner at the elongation step? . 131

5.4 PAF1c and MYC - interactors for the DNA damage repair 135

5.5 MYC-dependent PAF1c transfer: a struggle to maintain the integrity of the genome? 137

5.6 PAF1c and MYC - a gene regulation-independent function of MYC . . 140

Bibliography **142**

List of Publications **163**

Abbreviation

2x	Double concentrated
E.coli	*Escherichia coli*
A	Ampere
Amp	Ampicillin
AURKA	Aurora kinase A
BCA	Bicinchoninic acid assay
BLISS	Breaks labelling *In Situ* and Sequencing
BrdU	Bromdesoxyuridin
brHLHLZ	basic region of a Helix-Loop-Helix Leucin Zipper
$CaCl_2$	Calcium chloride
CDK	Cyclin-dependent kinases
cDNA	complementary DNA
CDS	Coding sequence
ChIP	Chromatin immunoprecipitation
CHK	Checkpoint kinase
CMV	Cytomegalovirus
CRC	Colorectal cancer
CTD	C-terminal domain
DDR	DNA damage response
DEPC	Diethylpyrocarbonat
DMSO	Dimethyl sulfoxide
DNA	Desoxyribonuclein acid
dNTP	Deoxy-nucleotide triphosphate
Dox	Doxycycline

dsDNA	double stranded DNA
DSIF	DRB-sensitive inducing factor
DTT	1,4-Dithiothreitol
E-box	Enhancer box
ECL	Electrochemiluminescence
EdU	5-Ethynyl-2'-deoxyuridine
EtBr	Ethidium bromide
EtOH	Ethanol
FACS	Fluorescence-activated cell sorting
FBS	Fetal bovine serum
gDNA	Genomic DNA
GFP	Green fluorescent protein
H2Bub	H2B monoubiquitylation
H3K4	histone 3 lysine 4
HA	Human influenza hemagglutinin
HRP	Horseradish peroxidase
IAA	Indole-3-acetic-acid
IB	Immuno blot
IDR	Intrinsicially disordered domains
IF	Immune fluorescence
Ig	Immuno globulin
IPTG	Isopropyl β-d-1-thiogalactopyranoside
IVT	*In vitro* transcription
m	Milli
MB	MYC box
$MgCl_2$	Magnesium chloride
mut	Mutant
MW	molecular weight
NaCl	Natrium Chloride
NELF	Negative elongation factor

nm	Nano meter
OD	Optical density
P-TEFb	Positive transcription elongation factor
pA	Poly Adenylation
PAF1c	RNA polymerase II associated factor 1 complex
PAGE	Polyacrylamid gel electrophoresis
PBS	Phosphate buffered saline
PCC	Pearson correlation coefficient
PCR	Polymerase Chain Reaction
PEI	Polyethylenimin
PI	Propidium iodide
PIC	Pre-initiation complex
PLA	Proximity Ligation Assay
PLA	Proximity ligation assay
PP2A	Protein phosphatase 2A
qPCR	quantitative PCR
RNAPII	RNA polymerase II
ROS	Reactive oxygen species
RQI	RNA quality indicator
RT	Reverse transcriptase
RT	Reverse transcription
SCC	Squamous cell cancer
SD	Standard deviation
SDS	Sodium dodecyl sulfate
SEC	Super elongation complex
SFFV	spleen focus forming virus
sh	Short hairpin
SKP2	S-phase kinase-associated protein 2
ssDNA	single stranded DNA
TAE	Tris-Acetat-EDTA

TBP	TATA box binding protein
TCEP	Tris(2-carboxyethyl)phosphin-hydrochlorid
TFIIF	Transcription factor IIF subunit 1
TRIS	Tris-(hydroxymethyl)-aminomethan
TRRAP	Transformation/transcription domain-associated protein
U	Unit
UMI	Unique modifier index
USP	Ubiquitin-specific-processing protease
USP11	Ubiqutin C-terminal hydrolase 11
V	Volt
VCP	Valosin-containing protein
wt	Wildtype

List of Tables

4.1 MYC target gene sets activated after MYC induction in U2OS MYC-Tet-On . . . 117
4.2 Gene sets repressed after PAF1c knockdown at oncogenic MYC levels . 118

List of Figures

1.1 Hallmarks of the oncogene MYC . . . 3
1.2 MYCBoxes and their canonical functions . . . 6
1.3 Models of MYC's function . . . 9
1.4 MYC-associated proteins from different interactome analysis . . . 11
1.5 MYC and the ubiquitin system . . . 13
1.6 Transcription by the RNA Polymerase II . . . 15
1.7 Elongating RNAPII-DSIF-PAF1c-SPT6 complex . . . 18
1.8 DNA Damage and DNA Damage Repair . . . 24

4.1 Diagram of MYC protein structure . . . 86
4.2 Input of *in vitro* pulldown experiments . . . 87
4.3 PAF1c and DSIF are interacting directly with MYC . . . 88
4.4 PAF1c interacts directly with MYC independent of MYCBox I or II . . 89
4.5 Knockdown efficiency of CDC73 or CTR9 in U2OS using constitutively active pGIPZ vector . . . 90
4.6 PAF1c knockdown reduces association of MYC on chromatin . . . 92

4.7 PAF1c knockdown reduces association of MYC at promoters but not enhancers . . . 93
4.8 Knockdown efficiency of CDC73 or CTR9 in U2OS using doxycycline inducible pInducer10 vector . . . 94
4.9 PAF1c knockdown reduces association of MYC on chromatin in a MYC oncogenic environment . . . 95
4.10 PAF1c knockdown reduces MYC promoter association in a MYC oncogenic environment. . . . 96
4.11 MYC-mediated transfer of SPT5 is required to maintain RNA Polymerase II processivity . . . 98
4.12 MYC mediated transfer of PAF1c is required to maintain RNA Polymerase II elongation . . . 100
4.13 MYC squelches SPT5 from chromatin . . . 101
4.14 Overexpression of MYC enhances occupancy of PAF1c on chromatin . 103
4.15 Acute activation of MYC enhances MYC occupancy at promoters . . . 104
4.16 Acute activation of MYC enhances MYC occupancy globally . . . 105
4.17 Acute activation of MYC enhances PAF1c and pS2 RNAPII occupancy on chromatin . . . 106
4.18 Acute depletion of MYC abolishes MYC occupancy at promoters . . . 108
4.19 Acute depletion of MYC reduces PAF1c occupancy on chromatin . . . 109
4.20 HUWE1 drives the transfer of PAF1c from MYC onto RNAPII and recruits histone modifiers. . . . 111
4.21 Depletion of MYC enhances accumulation of DSB. . . . 113
4.22 MYC promotes Double Strand Break repair in a PAF1c-dependent manner . . . 114
4.23 Attenuation of MYC-dependent gene expression upon PAF1c knockdown 116
4.24 Reduced proliferation upon knockdown of PAF1c . . . 119
4.25 PAF1c knockdown leads to a delay in DNA replication at oncogenic MYC levels . . . 120
4.26 PAF1c knockdown at oncogenic MYC levels leads to an activation of the ATM kinase . . . 121
4.27 MYC-stimulated increase in DNA Damage upon PAF1c knockdown . . 122

4.28 MYC-stimulated increase in DNA Damage upon PAF1c knockdown during DNA synthesis 125
4.29 Quantification of MYC-stimulated increase in DNA Damage upon PAF1c knockdown during DNA synthesis 126

5.1 Suggested transfer model of PAF1c from MYC onto RNAPII via PTMs 129
5.2 Proposed model for MYCs involvement in the transcriptional cycle . . . 134
5.3 Proposed model for subcomplex assembly of MYC, PAF1c and RNAPII 135
5.4 MYC-PAF1c interaction controls genomic integrity in an oncogenic environment 139

Summary

The oncogene MYC is deregulated and overexpressed in a high variety of human cancers and is considered an important driver in tumorigenesis. The MYC protein binds to virtually all active promoters of genes which are also bound by the RNA Polymerase II (RNAPII). This results in the assumption that MYC is a transcription factor regulating gene expression. The effects of gene expression are weak and often differ depending on the tumor entities or MYC levels. These observations could argue that the oncogene MYC has additional functions independent of altering gene expression. In relation to this, the high diversity of interaction partners might be important. One of them is the RNAPII associated Factor I complex (PAF1c).

In this study, direct interaction between PAF1c and MYC was confirmed in an *in-vitro* pulldown assay. ChIP sequencing analyses revealed that knockdown of PAF1c components resulted in reduced MYC occupancy at active promoters. Depletion or activation as well as overexpression of MYC led to reduced or enhanced global occupancy of PAF1c in the body of active genes, arguing that MYC and PAF1c bind cooperatively to chromatin. Upon PAF1c knockdown cell proliferation was reduced and additionally resulted in an attenuation of activation or repression of MYC-regulated genes. Interestingly, knockdown of PAF1c components caused an accumulation in S-phase of cells bearing oncogenic MYC levels. Remarkably, enhanced DNA damage, measured by elevated γH2AX and pKAP1 protein levels, was observed in those cells and this DNA damage occurs specifically during DNA synthesis. Strikingly, MYC is involved in double strand break repair in a PAF1c-dependent manner at oncogenic MYC levels.

Collectively the data show that the transfer of PAF1c from MYC onto the RNAPII couples the transcriptional elongation with double strand break repair to maintain the genomic integrity in MYC-driven tumor cells.

Zusammenfassung

Das Onkogen MYC ist in einer Vielzahl verschiedener Krebsarten dereguliert und überexprimiert und deshalb ein wichtiger Faktor in der Tumorgenese. Zwei zentrale Beobachten sind: Erstens, das MYC Protein bindet grundsätzlich an allen zugänglichen Promotoren von Genen, die ebenfalls von der RNA Polymerase II gebunden sind. Das resultiert in der Annahme, dass MYC als ein Transktiptionfaktor klassifiziert werden kann, der Genexpression reguliert. Zweitens, die Effekte auf die Genregulation sind schwach und oftmal abhängig von der Tumorart als auch von der unterschiedlichen MYC Proteinmenge. Diese Beobachtungen lassen die Schlussfolgerung zu, dass MYC eine zusätzliche Funktion neben der des Transktiptionfaktors haben könnte. Darauf bezogen könnte die große Anzahl an Interaktionspartnern eine entscheidende Rolle spielen. Einer dieser Interaktionspartner ist der RNA Polymerase II assoziierte Faktor I Complex (PAF1c). In dieser Arbeit konnte die direkte Interaktion zwischen PAF1c und MYC mittels *in-vitro* Pulldown Assays bestätigt werden. ChIP-Sequenzierungen illustrierten, dass der Knockdown verschiedener Untereinheiten des PAF1c zur einer verminderten Bindung von MYC an aktiven Promotoren führt. Andererseits zeigte die Depletion oder Aktivierung sowie Überexpression des MYC Proteins entweder eine reduzierte oder aber eine gesteigerte PAF1c Bindung im Genkörper aktiver Gene. Folglich wird angenommen, dass MYC und PAF1c kooperativ an das Chromatin binden. Unabhängig von den MYC Proteinmengen, führte der Knockdown von PAF1c Untereinheiten zu einer reduzierten Proliferation von Zellen. Zusätzlich resultierte in RNA Sequenzierexperimenten, dass der PAF1c Knockdown zu einer abgeschwächten Aktivierung oder Repression von MYC regulierten Genen führt. Interessanterweise führte der Knockdown von PAF1c Untereinheiten zu einer Ansammlung in der S-Phase des Zellzyklus für viele Zellen, die onkogene MYC Proteinmengen aufweisten. Auffallend dabei war, dass diese Zellen erhöhten DNA Schaden, gemessen an erhöhten

Proteinmengen von γH2AX und pKAP1, aufwiesen. Dieser DNA Schaden ereignete sich spezifisch während der DNA Synthese. Bemerkenswert ist, dass MYC, vor allem bei onkogenen MYC Proteinmengen, in die Doppelstrangbruchreparatur involviert ist und das dies in Zusammenarbeit mit PAF1c erfolgt.
Zusammenfassend zeigen die Daten, dass der Transfer des PAF1c von MYC auf die RNAPII die transkriptionelle Elongation mit der Doppelstrangbruchreparatur vereint um die genomische Integrität in MYC getriebenen Tumoren zu gewährleisten.

1 Introduction

MYC is an oncogene which is deregulated and overexpressed in a majority of human cancers. MYC deregulation occurs downstream of multiple cellular phenomena: therefore, a big effort was undertaken in the last decades to precisely define MYC biology with the aim of harnessing this knowledge cancer therapy.
MYC is classified as a transcription factor, it is quite surprising that MYC only mildly induces up- or downregulation of genes transcribed by the RNA polymerase II (RNAPII). Interestingly, MYC is interacting with a high diversity of proteins which are as well involved in the transcriptional cycle of the RNAPII. One of those factors is the elongation factor RNAPII associated factor 1 complex (PAF1c).
As this study focuses on the interaction of MYC and PAF1c, the detailed mechanism of this interaction and involvement in the double strand break repair, this chapter gives an broad overview of the common knowledge of the individual topics.

1.1 The oncogenic transcription factor MYC

The MYC oncogene belongs to a family consisting of *MYC*, *MYCN* and *MYCL* (Brodeur et al., 1984; Kohl et al., 1984; Nau et al., 1985). While only few studies focused on *MYCL* there is more known about the two isoforms *MYC* or *MYCN*. In this study, the main focus will be on *MYC*.
Originally, MYC was found in early research steps of chicken tumors caused by retroviruses leading to *my*elo*c*ytomatosis, where its name is resulting from (Duesberg and Vogt, 1979; Hu et al., 1979; Sheiness and Bishop, 1979). The idea, that retrovirus are the cause of human tumors was discarded. Nevertheless, MYC's function in tumor progression is still valid.
MYC is frequently translocated or highly amplified in a high variety of human

cancers. Translocation of the *MYC* locus is described in Burkitt lymphoma or multiple myeloma (Dalla-Favera et al., 1982; Shou et al., 2000; Taub et al., 1982). It is highly amplified in different cancer types (Beroukhim et al., 2010). Defects in Wnt-APC signaling in colon carcinoma (He et al., 1998) or deregulated Notch signaling in T-cell leukemia (Palomero et al., 2006; Sharma et al., 2006; Weng et al., 2006) lead to activation of MYC. Hence, there are different ways how MYC can get activated in entities of human tumors.

Figure 1.1 highlights MYC as a classified *bona fide* human oncogene (Chen et al., 2018b; Dang, 2006; Meyer and Penn, 2008). MYC affects diverse cellular functions including cell cycle progression, signal transduction, protein biosynthesis, cell adhesion, translation, metabolism, transcription and DNA repair (Berwanger et al., 2002; Blanco-Bose et al., 2008; He et al., 1998; Kress et al., 2015; Muhar et al., 2018; Murphy et al., 2011; Wanzel et al., 2005; Yin et al., 2001; Yustein et al., 2010).

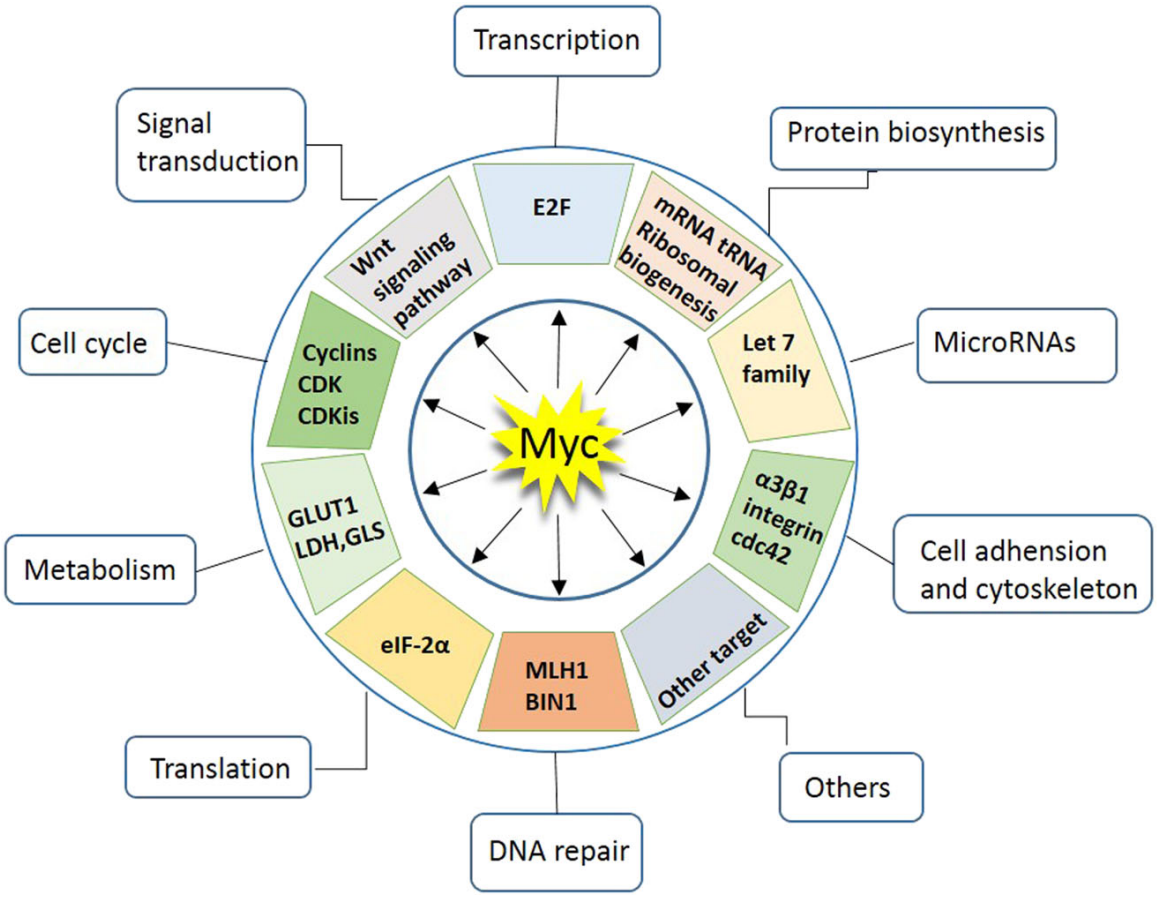

Figure 1.1: Hallmarks of the oncogenic transcription factor MYC.
MYC regulates different cellular functions. MYC alters the expression of protein coding and non-coding genes and therefore regulates different cellular processes such as signal transduction, transcription, protein biosynthesis, microRNAs, cell adhesion and cytoskeleton, DNA repair, translation, metabolism and cell cycle. [Adapted from Chen et al. (2018b)].

A majority of tumors depend on enhanced expression of MYC and downregulation of the MYC protein results in stalling and eradication of tumor growth (Gabay et al., 2014). Although MYC knockout embryos earlier showed defects in developement it was shown that this observation is based on placental insufficiency (Dubois et al., 2008). Furthermore, MYC depletion is tolerated in adult mice for a period of time. Additionally, recent data shows, that MYC is involved in the eviction of the immune system in tumor cells (Casey et al., 2016; Kortlever et al., 2017; Topper et al., 2017). Moreover, Omomyc, which is a protein inhibiting the interaction between MYC and MAX, reverses MYC-driven tumorigenesis *in vivo* (Soucek et al., 2004). Collectively, these studies suggest, that MYC is a valid target for tumor therapy.

Biochemical studies have been made to understand the properties of this protein to

find ways to target MYC. Strikingly, very limited success was achieved concerning MYC-related therapeutic approaches. Remarkably, recent interactome data shows novel insights in MYC network, especially in its interaction with the RNAPII machinery. As better clarified in the next paragraphs, these findings point out a view where MYC not only changes expression of target genes, but also affects basic transcription-related mechanisms.

1.2 Functions of MYC

As stated above, MYC can be involved in multiple cellular processes, a complete description of which would go beyond the scope of this thesis. The next sections will therefore cover the aspects which are relevant for the aims of this study.

1.2.1 The transcription factor MYC

At its C-terminus MYC contains a basic region of a Helix-Loop-Helix Leucin Zipper (brHLHLZ, figure 1.2) necessary for its binding affinity towards chromatin. For DNA binding MYC needs to form a heterodimer with the protein MAX. The heterodimer binds to chromatin at promoter regions containing an enhancer-box (E-box) bearing the consensus sequence CAC(G/A)TG. (Blackwood et al., 1992; Prendergast and Ziff, 1991).

The interaction of MYC with MAX is counteracted by other proteins competing with MYC for MAX binding. This can be MAX homodimers which are transcriptionally inactive as well as other factors such as MAD or MGA/MNT forming a heterodimer with MAX (Wolf et al., 2015). An additional way to repress MYC function is the interaction with MIZ1. At high MYC levels, MIZ1 is recruited to MYC-bound promoters to attenuate MYC-mediated transcriptional activation (Wiese et al., 2015). The ratio of the MYC-MIZ1 protein complex at promoters determines if genes are activated or repressed by MYC (Walz et al., 2014). In cells expressing low MYC levels, MIZ1 binds to a specific MIZ1-motif and activates genes which are involved in autophagy (Wolf et al., 2013). In cell systems with elevated MYC levels, MIZ1 binds to MYC to reduce MYC's transcriptional activity on those genes (Walz et al.,

2014; Wiese et al., 2015). MIZ1 itself is degraded by the E3 ligase HUWE1 (Inoue et al., 2013). Additionally, the tumor supressor protein ARF is not only inhibiting MYC's transcriptional activity via direct interaction but also inhibiting HUWE1 which stabilizes MIZ1 (Chen et al., 2005; Herkert et al., 2010; Peter et al., 2014). Arguing, that ARF and MIZ1 are involved in a stress response to high oncogenic MYC protein levels (Peter et al., 2014).

Aside from the brHLHLZ, MYC contains structured, conserved regions which are termed as MYCBoxes (MB). Common consensus in literature is that there are six MYCBoxes: 0, I, II, IIIa, IIIb, IV (Baluapuri et al., 2020) (see figure 1.2).

MB I is important for proteasome-mediated degradation of MYC (Farrell and Sears, 2014). It contains serines and threonines, which are acceptor sites for phosphorylation. On MB I are four conserved amino acid residues which can be phosphorylated: T58, S62, S64 and S67. S62 phosphorylation by cyclin-dependent kinases (CDKs) primes the phosphorylation of T58 by GSK3 (Welcker et al., 2004). The best understood phosphorylation site is T58, which is targeted by the GSK3 kinase. The T58 phosphorylation is a docking site for E3 ubiquitin ligases as SCF^{FBXW7} and SCF^{FBXL3}. Their binding to pT58 displace the interaction between MYC and the C-terminal hydrolase 11 (USP11) (Herold et al., 2019). Which kinase phosphorylates S64 or S67 and if they are involved in proteasomal degradation is still unknown. The serine/threonine-protein phosphatase 2A (PP2A) and the peptidyl-prolyl cis/trans isomerase PIN1 interact with MYC as well via MYCBox I (Yeh et al., 2004).

The binding of the E3 ubiquitin ligase SCF^{FBXW7} is antagonized by Aurora kinase A (AURKA) binding to MB 0 and I, an event that promotes MYC stabilization (Dauch et al., 2016; Otto et al., 2009; Richards et al., 2016). The transformation/transcription domain-associated protein (TRRAP) interacts with MYC via MB II (McMahon et al., 1998; Zhang et al., 2014). TRRAP is a scaffolding protein known to be involved in chromatin remodelling, recruitment of the histone acetyltransferase complex NuA4 or association of the helicase P400. MB IIIb is promoting interaction with WDR5 which facilitates histone 3 lysine 4 (H3K4) methylation. As H3K4 methylation is an indicator for active promoters, WDR5 interaction with MYC is important to increase the affinity of MYC to active promoters (Thomas et al., 2015). Additionally, the general transcription factor IIF subunit 1 (TFIIF) interacts with MB 0 and the transcriptional co-regulator HCFC1 with MB IV (Kalkat et al., 2018; Thomas et al.,

2016).

Besides of the few structured regions, MYC is a disordered protein, which only folds in complex with other proteins. Intrinsically disordered proteins have the property to interact with each other to promote liquid liquid phase separation (Hnisz et al., 2017), so it is possible that MYC forms condensates via its N-terminal transactivation domain.

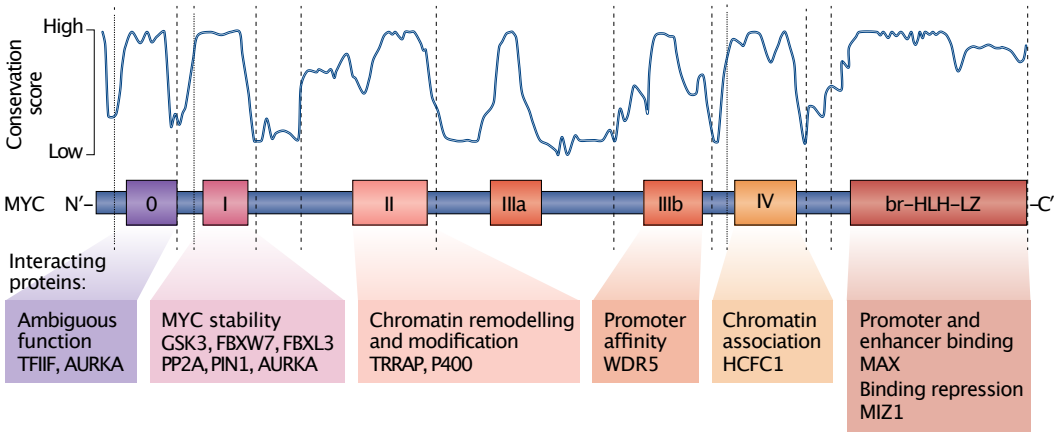

Figure 1.2: MYCBoxes and their canonical functions.
Conservation score is based on amino acid sequence analysis resulting in three different degrees of conservation raging from high to low. Structure of the MYC protein ranging from N-terminus (N') until C-terminus (C'). Structured regions are MYCBoxes highlighted as 0, I, II, IIa, IIIb, IV and the basic region-Helix-Loop-Helix-Leucin Zipper (br-HLH-LZ). Examples of proteins which interact with the different MYCBoxes are listed below.
AURKA, Aurora kinase A; FBXL3, F-box and leucine rich repeat protein 3; FBXW7, F-box and WD repeat domain containing 7; GSK3, glycogen synthase kinase 3; HCFC1, host cell factor C1; MAX, MYC associated factor X; MIZ1, MYC interacting zing finger protein 1; P400, E1A binding protein p400; PIN1, peptidylprolyl cis/trans isomerase NIMA-interaction 1; PP2A, serine/threonine protein phosphatase 2A; TFIIF, general transcription factor IIF subunit 1; TRRAP, transformation/transcription domain-associated protein; WDR5, WD repeat domain 5. [Adapted from Baluapuri et al. (2020)]

1.2.2 Target genes of MYC

Over the last 20 years a lot of effort was placed in investigating the role of MYC and how MYC is activating or repressing its target genes. Yet, there is no clear consensus within the MYC field, which highlights how difficult it is to understand MYC's exact function; specifically the function as a transcription factor.

Genes which are transcribed by the RNAPI, II or III can be regulated by MYC (Gomez-Roman et al., 2003; Grandori et al., 2005). Binding of MYC on promoters

transcribed by the RNAPI or III promotes a positive gene expression (Sabò et al., 2014). Genes transcribed by the RNAPII can be either positively or negatively regulated by MYC occupancy. The regulation of MYC on RNAPII transcribed target genes includes genes which drive the hallmarks of cancer (see figure 1.1). The controversional observations of activation or repression of MYC target genes are often caused by the different cell type or cell system and even then, the observations differ within the same cell system (Berwanger et al., 2002; Blanco-Bose et al., 2008; Eilers et al., 1989; Kress et al., 2015; Muhar et al., 2018; Murphy et al., 2011; Stine et al., 2015; Wanzel et al., 2005; Yin et al., 2001; Yustein et al., 2010). The gene sets which are repressed by MYC's transcriptional activity are even more variable and depend on expression levels and tissue specificity. Also the underlying mechanism how MYC function can be repressed is quite multifaceted (Baluapuri et al., 2019; Gebhardt et al., 2006; Herold et al., 2002; Seoane et al., 2002; Tu et al., 2018).

1.2.3 Models of MYC function

Two main observations can be drawn of MYC behaviour: First, MYC is classified as a transcription factor which is binding to virtually all active promoters and known to interact with its partner MAX to bind to E-boxes (see subsection 1.2.1). But, only one third of the binding sites of MYC are considered to be E-boxes (Lorenzin et al., 2016). Thus, the binding affinity for a specific DNA motif is not sufficient to explain MYC function on transcriptional regulation (Gerlach et al., 2017; Lorenzin et al., 2016; Thomas et al., 2015). Second, genes transcribed by the RNAPII are activated or repressed upon MYC activation (Herold et al., 2019; Kress et al., 2015). Nevertheless, changes in overall gene expression are weak and also not sufficient to understand the importance of MYC in so many different tumor entities. These two main observations are reproducible in different tumors and MYC levels. Based on those observations, different models are existing to explain MYC function.

The specific-gene regulation model is based on structural analysis. MYC binds as a heterodimer with MAX to the consensus sequence of an E-box. After binding to the target sequence, it activates or represses specific sets of genes (see figure 1.3 A). But even though virtually all active promoters are bound by MYC, only a small portion

of those genes reacts to altered MYC levels (Sabò et al., 2014; Staller et al., 2001; Walz et al., 2014). Stimulation of primary murine B-cells either harbouring wildtype MYC or lacking MYC did not result in direct global alterations of gene expression even though MYC was bound to all promoters with an open chromatin structure (Tesi et al., 2019). This and other examples lead to the conclusion that MYC binds to all active promoters but does not affect steady-state mRNA levels (Kress et al., 2015).

The global gene activation model is based on the finding that elevated MYC levels can enhance overal global transcription rate (Lin et al., 2012). Originally, it was shown that upon primary B-cell stimulation elevated total mRNA levels depend on MYC (Nie et al., 2012) (see figure 1.3 B). The "global amplifier" model of MYC function underlies the view that the normalization algorithm used in gene expression studies falsifies the global increase in transcription in a MYC-dependent manner (Lewis et al., 2018). Based on ChIP sequencing data of MYC and RNAPII, this model shows, that MYC binds to all promoters of genes which are as well bound by RNAPII. After MYC binds to the promoter, it acts as a transcription factor and enhances the transcription rate of the RNAPII. This model postulates that enhanced overall transcription is the central oncogenic function of MYC. Several publications cannot support this model: The observed mRNA amplification - if at all - is mostly a late, indirect consequence of MYC activation (Muhar et al., 2018; Tesi et al., 2019; Walz et al., 2014). In particular, the MYC-dependency stimulation of primary B-cells was needed for ATP production (Tesi et al., 2019). ATP production supports chromatin remodeling and decompaction (Kieffer-Kwon et al., 2017) and led in turn to a delayed increase of overal mRNA levels. Meaning that the elevated mRNA levels are an indirect result of MYC activation and therefore MYC did not have an impact on direct changes of overal RNA levels (Tesi et al., 2019).

The gene-specific affinity model is based on observations from ChIP sequencing data of samples with different MYC levels. This models differentiates between two classes of target site. On one side there are the high affinity targets and on the other side are low affinity targets. Whereas at physiological levels of MYC high affinity promoters are already saturated, MYC only binds to low affinity promoters at supraphysiological, oncogenic levels (Staller et al., 2001) (see figure 1.3 C). The binding

specificity of MYC/MAX heterodimers to E-boxes is relatively low and therefore protein-protein interactions between MYC and other factors might be relevant (Guo et al., 2014; Thomas et al., 2015). So, this model argues that other interaction partners are needed for the binding to low affinity targets at oncogenic MYC levels (Guo et al., 2014; Lorenzin et al., 2016).

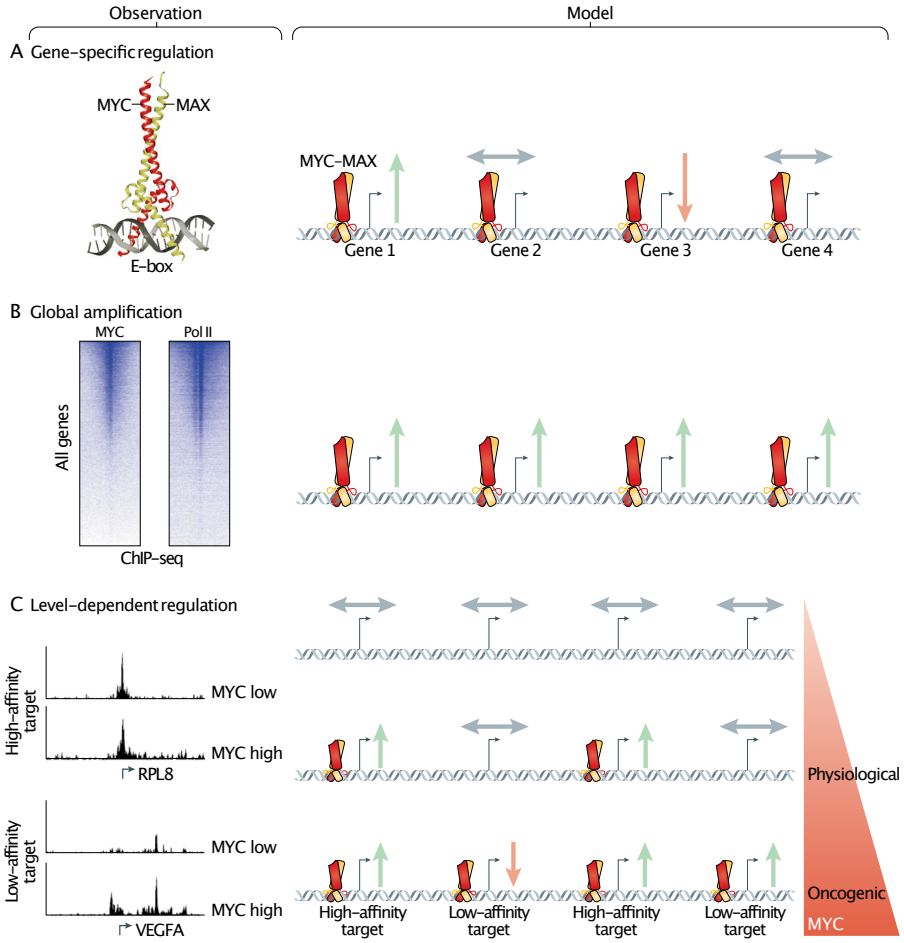

Figure 1.3: Models of MYC's function.
A) The specific-gene regulation model: MYC binds with MAX to its consensus sequence of an E-box. Model is based on the structural analysis of MYC binding to DNA to the consensus sequence.
B) The global activation model: MYC binds to virtually all open promoters and activates transcription. The model is based on ChIP sequencing data of MYC and RNAPII.
C) The gene-specific affinity model: Even though MYC binds to virtually all open promoters, the affinity towards specific promoters differs. At physiological levels of MYC high affinity promoters are saturated and MYC binds to low affinity promoters only at supraphysiological levels. The model is based on ChIP sequencing data of samples with different MYC levels.
Green arrows represent activation, red arrows represent repression and grey arrows represent no gene regulation. RPL8: 60S ribosomal protein L8; VEGFA: vascular endothelial growth factor A. [Adapted from Baluapuri et al. (2020)]

The gene regulation-independent model is based on the observation that MYC does not alter the gene expression of a specific set of genes. Unlike p53, which regulates specific sets of genes involved in inducing cell cylce arrest, senescence or apoptosis (Kastenhuber and Lowe, 2017; Simabuco et al., 2018), there is no consensus which genes or specific classes of genes are regulated by MYC.

Within the last years a number of proteomic analysis of the MYC or MYCN interactome were performed (Baluapuri et al., 2019; Büchel et al., 2017; Heidelberger et al., 2018; Kalkat et al., 2018). Common proteins found in the different interactomes are illustrated in figure 1.4. There are different classes of proteins found which are related to transcription: transcription factors, transcription elongation factors as well as chromatin remodelling or RNA processing splicing factors. Surprisingly, some of the known interaction partners of MYC are very weakly found in those global analysis if not at all. This is for example the case for the general transcription factor TFIIH or the transcription related kinase CDK9. In addition to that, there are also factors found in the MYC and MYCN proteome which are not directly linked to transcription: The E3 ligases HUWE1 or UBR5 and the deubiquitylating enzyme USP7 are very well present in the interactome analysis (Besche et al., 2009). Arguing, that the proteasome is involved in MYC function, which is consistent with a report that proteasome subunits are recruited to promoters (von der Lehr et al., 2003). Furthermore, factors involved in double strand break (DSB) repair such as NuA4 complex or Tip60 were also found in the MYC and MYCN interactome (Gorrini et al., 2007; Jacquet, 2016).

The observation that MYC is interacting with proteins which are not directly connected to transcription in addition to the unaltered steady-state mRNA levels upon elevated MYC levels lead to the possibility that MYC oncogenic function is independent of regulating gene expression.

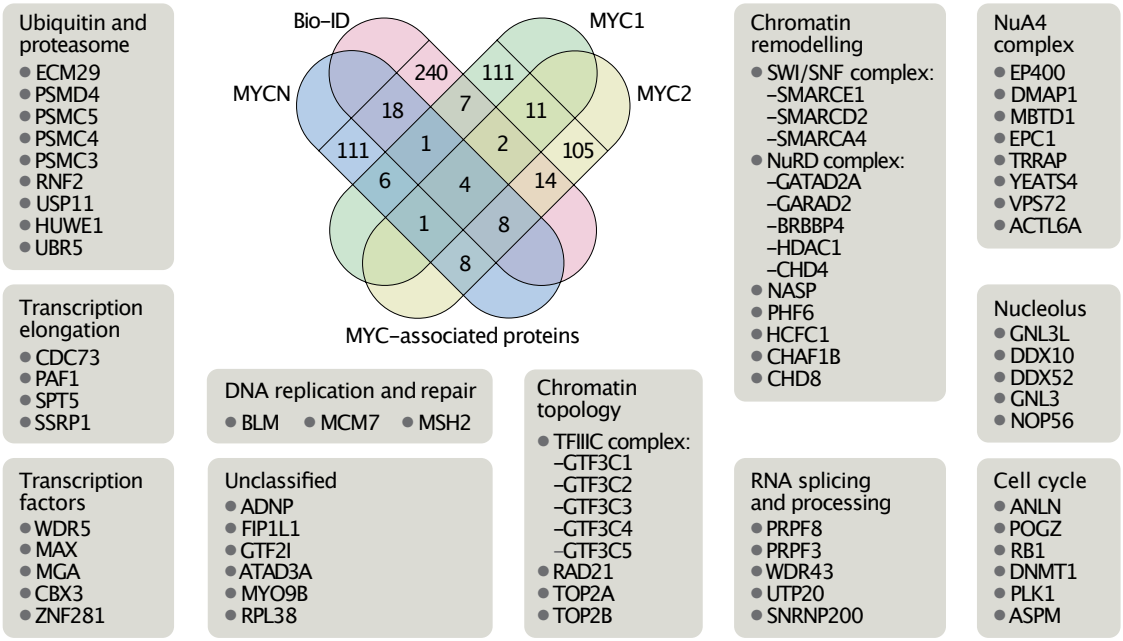

Figure 1.4: MYC-associated proteins from different interactome analysis. Shown is the overlap of recently published MYC and MYCN interacting proteins (Baluapuri et al., 2019; Büchel et al., 2017; Heidelberger et al., 2018; Kalkat et al., 2018). Proteins appearing in at least two datasets are presented in the surrounding boxes and were used for functional annotation. "Bio-ID" dataset was published in (Kalkat et al., 2018), "MYC1" inBaluapuri et al. (2019), "MYC2" in Heidelberger et al. (2018) and "MYCN" in Büchel et al. (2017). [Adapted from Baluapuri et al. (2020)]

1.3 MYC and the ubiquitin system

Ubiquitylation belongs like phosphorylation to known modifications of MYC. The Ubiquitin-Proteasome-System consists of a cascade of three enzymes which transfer ubiquitin to target proteins. Although typically ubiquitin transfer primes proteins for degradation, the outcome of ubiquitylation can differ depending on the linkages, branches and chains. The best studied ubiquitin ligase degrading MYC is SCF^{FBXW7}. It recognizes the T58 phosphorylation on MB I (Welcker et al., 2004; Yada et al., 2004). The ubiquitylation of MYC can get reverted by deubiquitinating enzymes termed DUBs or USPs (Ubiquitin-specific-processing protease). USP28 is reported to antagonize FBXW7 and subsequently stabilizing MYC (Popov et al., 2007). USP28 is highly abundant in colorectal cancer (CRC) and squamous cell cancer (SCC) cells which are MYC-driven tumor cells (Diefenbacher et al., 2015; Popov et al., 2007). As a proof of principle deletion of USP28 attenuates tumorigenesis and prolongs survival

in mouse models of CRC and SCC (Diefenbacher et al., 2015; Prieto-Garcia et al., 2020).

There is increasing evidence that ubiquitylation of MYC is important for MYC's transcriptional activity. S-phase kinase-associated protein 2 (SKP2) results in proteasomal turnover of MYC but also stimulates MYC-dependent gene expression. Additionally, other components of the proteasome are present at promoters, arguing that ubiquitin-dependent turnover of MYC is occuring on chromatin (Adhikary and Eilers, 2005; Kim et al., 2003; von der Lehr et al., 2003). Another link between MYC and the ubiquitin system is HUWE1. Peter et al. (2014) showed that a small inhibitor targeting HUWE1 abrogates the MYC-dependent gene expression in CRC (Peter et al., 2014). HUWE1 not only ubiquitylates MYC but also degrades MIZ1 (see figure 1.5 A). Upon HUWE1 inhibition, MIZ1 is accumulating and therefore changing the MYC-MIZ1 ratio from activating complexes toward repressive complexes (Peter et al., 2014; Walz et al., 2014). Knockdown or inhibition affects MYC function on target genes in embryonic stem cells, epithelium cells or intestine cells which opens a therapeutic window in targeting HUWE1 (Peter et al., 2014; Zhao et al., 2008).

The ubiquitylation of MYC by HUWE1 does not result in its degradation. Heidelberger et al. (2018) showed that Valosin-containing protein (VCP) extracts MYC from MYC/MAX heterodimers and as a consequence MYC is removed from chromatin before it gets degraded by the proteasome. VCP inhibition resulted in increased ubiquitylated MYC and enhanced MYC occupancy at promoters. Furthermore, they could show that HUWE1 predominantly ubiquitylates MYC at K148. This lysine is also acetylated via p300, suggesting that the modification of this lysine residue regulates the interaction with VCP and could influence the transcriptional outcome of MYC target genes (see figure 1.5 B).

Jaenicke et al. (2016) could show that ubiquitylation of MYC has an important function in transcriptional elongation. RNAPII sequencing revealed that cells, expressing a lysine-free MYC mutant - termed as K-less MYC - did not have any effect on initiation of RNAPII but on elongation. Additionally, Jaenicke et al. (2016), shows, that the ubiquitin-dependent turnover of MYC serves as a checkpoint at the transition to positive elongation. In the presence of the proteasome inhibitor MG132 the positive elongation factor PAF1c is interacting with MYC, arguing that it is an intermediate inhibitory complex. Finally, Jaenicke et al. (2016) proposes a model, by

which histone acetylation is regulated by TRRAP and E3 ligases competing for MB II. MYC and P-TEFb (positive transcription elongation factor) require stabilization by acetylated histones at core promoters. The PAF1c/MYC interaction is enhanced upon phosphorylation of T58 or S62, suggesting that this interaction is MB I dependent. In summary, PAF1c and MYC interact with each other at the transition to positive elongation to serve as a checkpoint for productive elongation (see figure 1.5 C).

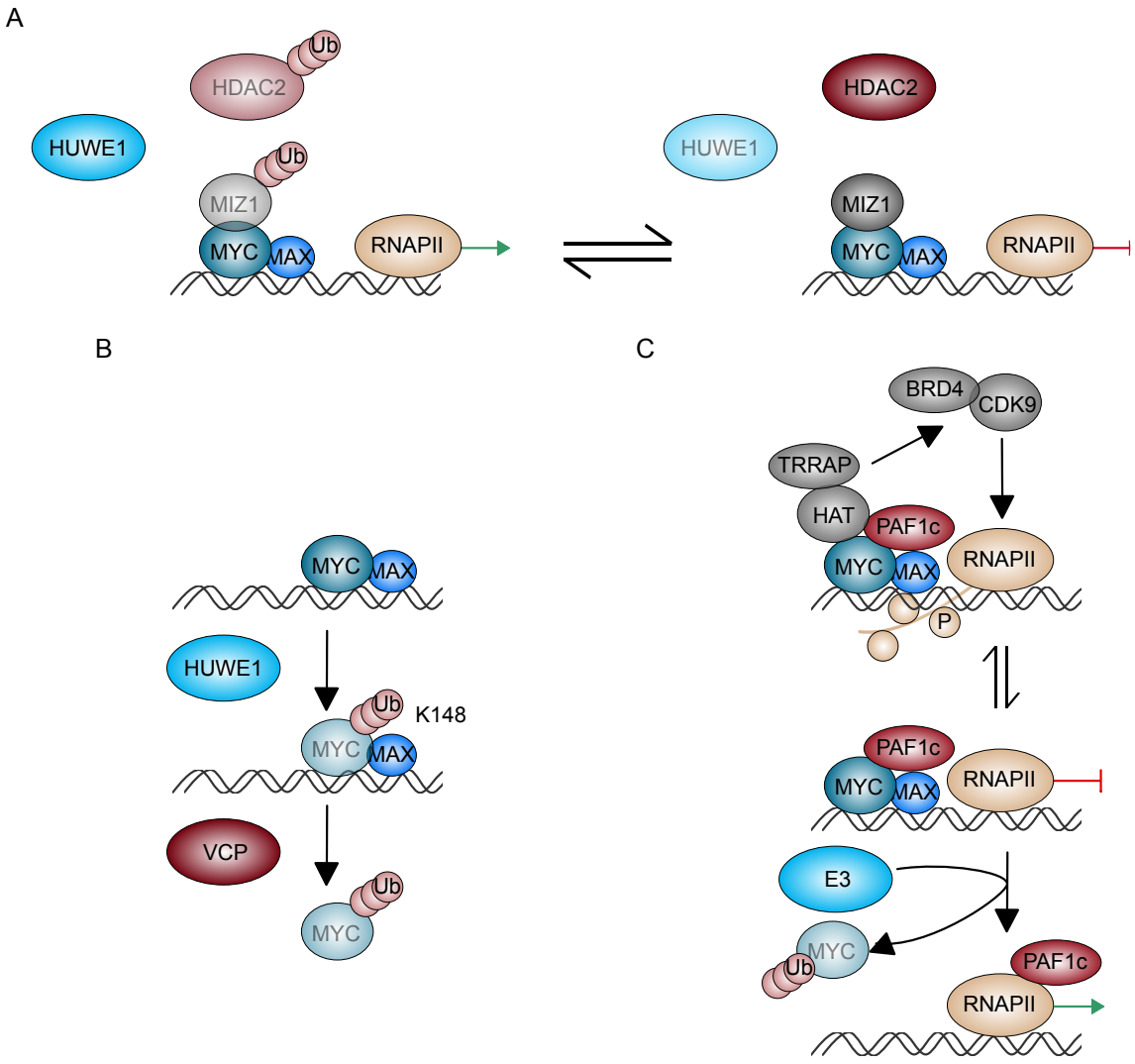

Figure 1.5: MYC and the ubiquitin system.
A: Model adapted from Peter et al. (2014). In the presence of HUWE1 MYC is transcriptionally active. In the absence of HUWE1 MIZ1 is getting stabilized and therefore attenuating MYC transcriptional activity.
B: Model adapted from Heidelberger et al. (2018). MYC is ubiquitylated at K148 by HUWE1 which recruits VCP to extract MYC from chromatin.
C: Model adapted from Jaenicke et al. (2016). The accumulation of an intermediate inhibitory MYC-PAF1c complex is counteracted by an productive MYC-PAF1c-TRRAP complex at core promoters. This active complex promotes histone acetylation and recruits P-TEFb which leads to phosphorylation and finally the transfer of PAF1c from MYC onto the RNAPII.

1.4 RNA Polymerase II transcription

Transcription by RNAPII is a regulated process. Multiple studies have been made to understand the mechanism in detail. The three major steps of transcription are initiation, elongation and termination.
The C-terminal domain (CTD) of the RNAPII and its modifications play an important role during the trancriptional cycle. The human CTD consists of 52 repeats of the heptad YSPTSPS (Eick and Geyer, 2013). The different phosphorylation status of the CTD in an indicator for different steps during the transcription by the RNAPII. The two best studied phosphorylation sites are at Ser5 and at Ser2 of the CTD. Ser5 is phosphorylated by CDK7 and is a marker for initiation (Kornberg, 2005). Ser2 phosphorylation is a marker for RNAPII elongation and conveyed by CDK9 (Zhou et al., 2012).
To early detect problems and mistakes throughout its transcriptional cycle, every step is regulated by different factors. Structural analysis gave detailed insights of the initiation and elongation step. Based on this data, mechanisms are elucidated how transcription by RNAPII is regulated to determine cell identity and function (Cramer, 2019). Additionally, microscopy studies revealed that phase separation might be involved in those processes. The RNAPII may shuttle in between those so called "transcriptional hubs"(Boehning et al., 2018; Cho et al., 2018; Chong et al., 2018; Cisse et al., 2013; Hnisz et al., 2017; Sabari et al., 2018). Still, a lot of research investigation is needed to reveal how those transcriptional hubs are getting assembled and dissolved .

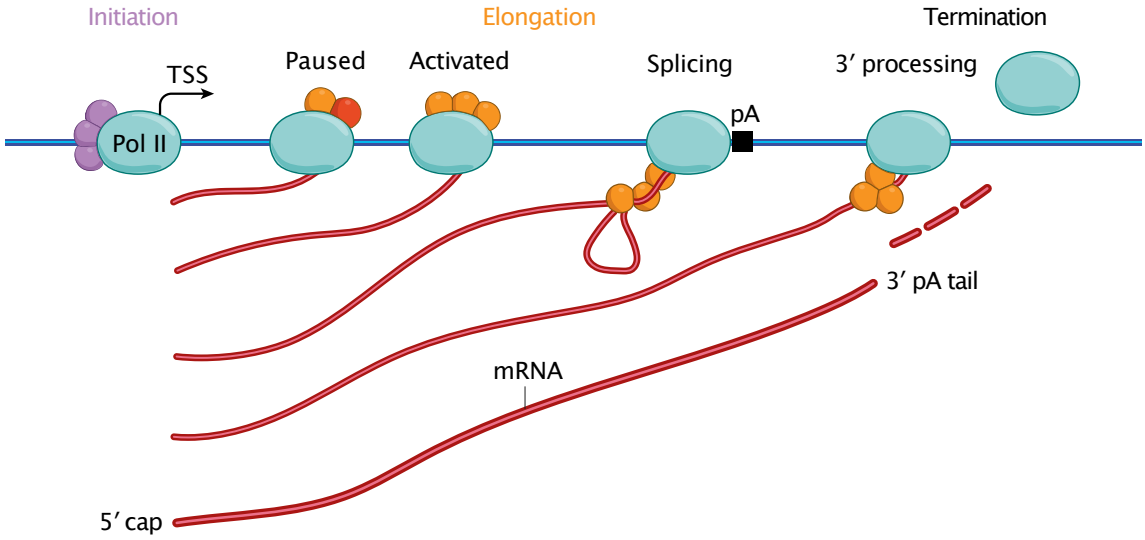

Figure 1.6: Transcription by the RNA Polymerase II.
The transcription by the RNAPII contains different steps: Initiation, elongation including pausing, activation and splicing and termination including 3' processing of the mRNA. [Published in Cramer (2019)].

1.4.1 Initiation

On active promoters a preinitiation complex (PIC) consisting of class II transcription factors including TATA box binding protein (TBP) is formed (Kornberg, 1999; Schones et al., 2008; Talbert et al., 2019). After binding of TFIIB the RNAPII-TFIIF complex is recruited (Bushnell et al., 2004; Chen and Hahn, 2004). TFIIH, which binds the DNA downstream of RNAPII and contains the catalytic subunit XPB, a DNA translocase, opens the promoter region (Egly and Coin, 2011; Kim et al., 2000). Next, the mediator complex is binding and contacts RNAPII, TFIIH and TFIIB (Nozawa et al., 2017; Plaschka et al., 2015; Tsai et al., 2017). CDK7, the catalytic subunit of TFIIH phosphorylates the CTD at Ser5 to finalize the initiation of the RNAPII (Eick and Geyer, 2013; Kornberg, 2005).

1.4.2 Promoter-proximal pausing

After initiation, the transcription of the majority of genes undergoes an additional regulatory step: the promoter-proximal pausing. Shortly downstream of the

TSS the RNAPII is stalling which ist termed as promoter proximal pausing. After promoter-proximal pausing, the transcription cycle can either be resumed or terminated. One important factor for this regulation is TFIIS (Cheung and Cramer, 2011; Conaway et al., 2000; Landick, 2006). TFIIS binds close to the RNA exit where it can cleave off the backtracked RNA so that the RNAPII can restart transcripiton. In general, pausing is a regulated step and can limit the frequency of initiation. Pausing happens approximately 50 bp downstream of the TSS, and is stabilized by the DRB-sensitive inducing factor (DSIF) and the negative elongation factor (NELF)(Yamaguchi et al., 2013). DSIF binds close to the RNA exit - the site where the freshly synthesised RNA is released from the RNAPII- (Bernecky et al., 2017; Ehara et al., 2017) whereas NELF binds the RNAPII on the other side and impairs TFIIS or PAF1c binding (Palangat et al., 2005; Vos et al., 2018b).

1.4.3 Elongation and termination

RNAPII is released from its pausing state by CDK9, the catalytic subunit of P-TEFb (Marshall and Price, 1995). CDK9 phosphorylates DSIF, NELF and the CTD at Ser2 (Zhou et al., 2012). CDK9 triggers the transformation of DSIF into a positive elongation factor and, concomitantly, NELF dissociation from RNAPII (Oss et al., 2017; Vos et al., 2018a,b). NELF blocks the binding site of he positive elongation factor PAF1c. Therefore, the dissociation of NELF makes RNAPII accessible for PAF1c. Phosphorylated DSIF, SPT6 and PAF1c, which are bound to the RNAPII, form an activating elongation complex (Kwak and Lis, 2013; Vos et al., 2018a). Elongation complexes have two functions. First, they recruit other factors needed for the elongation process. Second, they protect the RNAPII physically from "negative influences" which might disturb the elongation by enclosing the surface of the RNAPII. The phosphorylated CTD serves as a plattform for other elongation factors to be recruited during the transcriptional cycle by the RNAPII such as RNA processing, histone modification and chromatin remodelling factors (Bentley, 2014; Chen et al., 2018a; Kwak and Lis, 2013). Also other factors can have an impact on the elongation process: the oncogene MYC is known to promote transcriptional elongation as well (Gressel et al., 2017; Rahl et al., 2010). At the end of the gene, the RNAPII slows down. To terminate transcription, RNA needs to be cleaved and polyadenylated.

The freshly synthesized RNA is polyadenylated when the RNAPII reaches a specific sequence in the genome which serves as signal to add several A nucleotides (polyA) to the freshly synthesized RNA. By reaching polyadenylation (pA) sites RNAPII decelerates, to allow the cleavage of RNA (which is later polyadenylated) (Chen et al., 2018a). Subsequently, the RNA strand still attached to RNAPII is degraded and RNAPII evicted from chromatin. The exact mechanism of these latter events have been widely debated. Two alternative models have been proposed: the torpedo and the allosteric model (Kuehner et al., 2011; Porrua and Libri, 2015). The torpedo model proposes that the 5'-3' exoribonuclease 2 (XRN2) which cleaves the nascent RNA chases down the RNAPII which in the end leads to eviction of the RNAPII from chromatin (Fong et al., 2015). The allosteric model shows, that a pA signal-dependent conformation change results in termination and frees the RNAPII from chromatin (Zhang et al., 2015).

1.5 DRB-sensitive inducing factor (DSIF)

The DRB-sensitive inducing factor (DSIF) consists of the two subunits SPT5 and SPT4. After TFIIE and Mediator dissociate from the RNAPII, DSIF can bind and is associated with the RNAPII after initiation (Diamant et al., 2016; Grohmann et al., 2011; Vos et al., 2018b). This indicates that DSIF promotes promoter escape. DSIF binds close to the RNA exit of the RNAPII (Vos et al., 2018b), suggesting that DSIF is an important factor for promoter proximal pausing as it binds close to the RNA exit and conformational changes at this site control the pausing step. NELF, DSIF and RNAPII form a promoter-proximal paused elongation complex. After phosphorylation by CDK9, DSIF is converted into a positive elongation factor, travels along the gene associated with the RNAPII and increases the processivity of transcription (Decker, 2020). But how DSIF regulates the two processes remains unclear. SPT5 is also involved in termination as depletion of SPT5 resulted in delayed termination (Baejen et al., 2017; Fitz et al., 2018). Additionally, dephosphorylation of SPT5 leads to a deceleration of the RNAPII close to the pA site, a step considered a pre-requisite of transcription termination (Cortazar et al., 2019). Taken together, DSIF is involved in promoter-proximal pausing, transcripitonal elongation and termination.

But how exactly the different processes are regulated by DSIF and which role the phosphorylation of DSIF plays in these remains still unknown.

1.6 RNA Polymerase II associated factor 1 complex (PAF1c)

The RNA Polymerase II associated factor 1 complex (PAF1c) was discovered in *S. cerevisae* (Wade et al., 1996). This complex is regulating different steps of the transcriptional cycle. The PAF1c is transferred onto the RNAPII at the transition to positive elongation. The crystal structure of RNAPII with PAF1c and two other elongation factors DSIF and SPT6 (see figure 1.7) shows that all the accessory proteins decorate the RNAPII surface and provide a mechanical barrier against negative factors which could disturb the efficient elongation of the RNAPII. Generally, the PAF1c is involved in transcription, chromatin remodelling and the control of gene regulation.

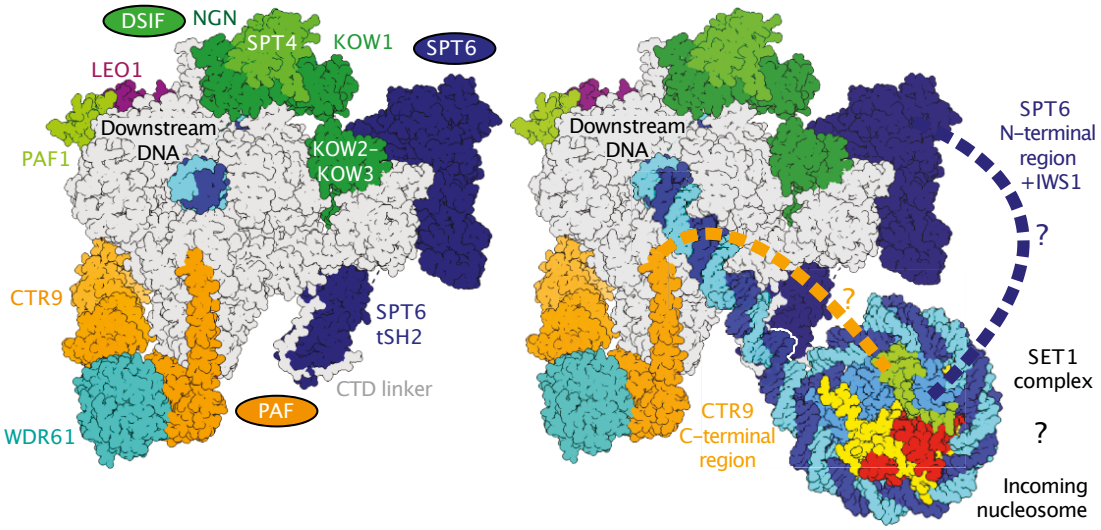

Figure 1.7: Elongating RNAPII-DSIF-PAF1c-SPT6 complex.
The elongating complex of the RNAPII (grey) contains the phosphorylated DSIF (SPT4 and SPT5, green), SPT6 (dark blue) and the PAF1c. Some subunits of the PAF1c are highlighted: CTR9 (orange), PAF1(light green), LEO1 (magenta) and WDR61 (light blue). Structure shows, that the positive elongation factors are binding the transcribing RNAPII - a mechanical barrier for negative factors. [Published in Vos et al. (2018a)]

1.6.1 Subunits of PAF1c

The PAF1c consists of six different subunits in humans: CTR9, LEO1, PAF1, CDC73, RTF1 and SKI8 (WDR61).

CTR9 is the largest subunit of the complex and is important for its integrity in combination with the core subunit PAF1 (Chu et al., 2013; Kim et al., 2010). Additionally, *CTR9* is an essential gene and plays an important role in multiple stages of the nervous development (Bahrampour and Thor, 2016; Mosimann et al., 2006). Furthermore, it was shown, that germ line mutations of *CTR9* predispose for Wilms tumor - a childhood disease (Hanks et al., 2014).

LEO1 binds RNA and is involved in the recruitment of the complex (Dermody and Buratowski, 2010). Furthermore PAF1 and LEO1 promote the transition from heterochromatin to euchromatin by enhancing histone turnover (Sadeghi et al., 2015). Additionally it was observed in *D. melanogaster* that LEO1 helps to recruit MYC to chromatin (Gerlach et al., 2017).

PAF1 was the first identified subunit of the complex and has several different roles in combination with other factors of the complex as it lays in the center of the complex. Like CTR9, PAF1 is involved in cancer specifically ovarian cancer (Karmakar et al., 2017). It was also shown that overexpression of PAF1 leads to tumor growth in NIH-3T3 cells, and in non-small cell lung cancer MYC and PAF1c were positively correlated in patient samples (Zhi et al., 2015).

CDC73 is an essential factor of the PAF1c (Bahrampour and Thor, 2016; Mosimann et al., 2006). The PAF1c is found at actively transcribed genes and is interacting with the core of the RNAPII (see figure 1.7). For this interaction the CDC73 subunit is necessary (Amrich et al., 2012). Parafibromin, the human orthologue of CDC73, is directly interacting with β-catenin and Gli1 to stimulate Wnt and Notch signalling pathways (Kikuchi et al., 2016; Mosimann et al., 2006). But this interaction might be independent of the total assembly of the PAF1c (Takahashi et al., 2011; Yang et al., 2016). Furthermore, CDC73 is classified as a tumor suppressor. When parafibromin is mutated, it can lead to hyperparathyroidism/jaw tumor syndrom (Wang et al., 2005). Additionally, CDC73 is important for hematopoesis and it plays a direct role

in regulating Hoxa9 and Meis1 which are drivers for acute myeloid leukemia (AML) (Saha et al., 2019).

RTF1 is the subunit which is loosely attached to the PAF1c and therefore found the last to be associated with the complex. It is involved in many PAF1c-related processes but has additional other functions independent of the PAF1c (Cao et al., 2015; Mbogning et al., 2013; Yang et al., 2016). The PAF1c is not only directly interacting with the RNAPII but also with other elongation factors. Thus, RTF1 interacts with SPT5 on the core of the RNAPII but RTF1 itself is not necessary for the assembly of a PAF1c-RNAPII complex (Qiu et al., 2012). Nevertheless, it is involved in the integrity of a PAF1c-RNAPII complex (Cao et al., 2015; Mueller et al., 2004; Qiu et al., 2006). RTF1 is also important for H3K4me3 - a marker for transcriptional activity (Warner et al., 2007). Additionally, RTF1 interacts with the viral transactivator E1A protein to induce both, viral and host genes (Fonseca et al., 2014, 2013) to promote transcriptional activation.

SKI8 (WDR61) is the subunit which is only found in humans. This subunit is one component of the SKI complex, which is important for 3'-5' mRNA degradation (Zhu et al., 2005).

1.6.2 PAF1c and the transcriptional cycle

In yeast, the PAF1c is transferred onto the RNAPII 50-70 bp downstream of the TSS, after SPT5 is transferred on the RNAPII (Mayer et al., 2010; Oss et al., 2017), but the pattern of the PAF1c transfer is quite variable in eukaryotic systems where it was also observed to accumulate at TSS and TES of the gene (Chen et al., 2015; Yang et al., 2016; Yu et al., 2015). Vos et al. (2018a) and Vos et al. (2018b) could show when and how the PAF1c is transferred onto the mammalian RNAPII. First, NELF and DSIF assemble onto the RNAPII and promote promoter-proximal pausing. As soon as CDK9 phosphorylates NELF and DSIF, NELF dissociates from the RNAPII and frees the binding site for PAF1c. In addition, the transfer of SPT6 converts the RNAPII-SPT5-SPT6-PAF1c complex into an activated elongation complex to promote productive elongation. A subsequent study from Aoi et al. (2020) could show that in a mammalian system CDK9 activity and NELF dissociation alone is

not sufficient to promote elongation. They show that there is a second pausing site independent of NELF dissociation by P-TEFb. This indicates that PAF1c transfer on the RNAPII might need an additional factor. In general, the role of the PAF1c into promoter-proximal pausing has been very controversial: On the one side, PAF1c was reported to control promoter-proximal pausing as PAF1 depletion resulted in enhanced recruitment of the super elongation complex (SEC) and therefore leading to an increase of nascent and mature mRNA (Chen et al., 2015). Additionally, it was shown that PAF1 regulation of the promoter proximal pausing is regulated via enhancer activation (Chen et al., 2017a). On the other side, it was shown, that P-TEFb is recruited via different effectors (Lu et al., 2016): PAF1c and Med26 recruit SEC which stimulates P-TEFb to phosphorylate NELF to free the binding site for PAF1c. PAF1c is transferred onto the RNAPII to promote elongation. Taken together, this data show that the PAF1c is either preventing SEC recruitment onto the RNAPII or enhancing its recruitment resulting in enhanced or reduced promoter-proximal pausing. This step usually gets dissolved by P-TEFB (CDK9). These controversial observiations in turn lead to the conclusion that tha PAF1c-dependent outcome on pausing might be depending on more than only CDK9 activity *in vivo*.

From structural analysis it is clear when the PAF1c is transferred onto the RNAPII but the key function of PAF1c remains still unclear. Nevertheless, several studies showed that the PAF1c is involved in co- and post-transcriptional processing of the mRNA. Knockdown of components of the PAF1c leads to usage of alternate pA sites and direct interaction of PAF1c with RNA processing factors such as CPSF and CstF (Nagaike et al., 2011; Nordick et al., 2008; Rozenblatt-Rosen et al., 2009). In mouse myoblasts, PAF1c serves as a guard to repress the usage of alternate pA sites in introns as well as internal exons (Yang et al., 2016). Therefore PAF1c prevents premature termination of the RNAPII which results in full-length transcription of genes.

Transcription is dependent on chromatin remodelling. The PAF1c controls some of the histone modifications to make transcription more efficient. PAF1c is required for H2B monoubiquitylation (H2Bub) at lysine 120 (K120) which then recruits COMPASS and Dot1p to promote H3K4 and K79 methylation (Krogan et al., 2003; Ng et al., 2003a,b; Wood et al., 2003). PAF1c is additionally required for H3K36 trimethylation (Chu et al., 2007) which is repressing acetylation of H3 or H4 within the gene body (Venkatesh and Workman, 2013). CHD1, which is recruited by PAF1c, is establishing

the pattern of H3K36 trimethylation in gene bodies as well as H3K4 trimethylation at the 5' end of genes (Lee et al., 2017; Smolle and Workman, 2013).
In yeast, the human orthologues of UBE2A/2B and RNF20/40 directly interact with RTF1 (Piro et al., 2012; Van Oss et al., 2016; Warner et al., 2007), showing that the PAF1c is linking the ubiquitin system with transcription-related processes. Depletion of PAF1 in HeLa cells led to reduced ubiquitylation of H2B at K120 as well as K34 and also reduced association of the two E3 ligases RNF20/40 and MSL1/2 (Wu et al., 2014). Besides of reduction of H2Bub, H4 K16 acetylation was also reduced. H4 K16ac is found at boundaries of heterochromatin and it was shown that -at least in yeast - this is a boundary for heterochromatin spreading (Allshire and Ekwall, 2015). These data suggest, the PAF1c is not only involved in remodelling the chromatin for transcription but also in maintaining existing chromatin structures. Taken together, the PAF1c plays an important role during transcription of the RNAPII and is involved in chromatin remodelling to keep the chromatin open for transcription.

1.7 DNA damage repair

Maintaining genomic integrity is important for cellular functions., even though DNA is very stable. There are different causes for DNA damage, including reactive oxygen species (ROS), ionizing radiation (IR), ultraviolet (UV) radiation as well as chemical agents. A tightly regulated DNA damage response in cells is necessary to react to those genomic threats and to prevent age-related diseases and cancer (Chatterjee and Walker, 2017; Giglia-Mari et al., 2011).
DNA damage responses (DDR) are phosphorylation-dependent cascades to maintain genomic integrity. Different DDR pathways are triggered depending on the occurring DNA damage. Best characterized pathways are O6-methylguanine-DNA methyltransferase (MGMT), base excision repair (BER) nucleotide excision repair (NER) mismatch repair (MMR), DNA single-strand break (SSBR) and DNA double-strand break (DSB) repair. DSB repair can occur through two pathways: the homologous recombination (HR) or non-homologous end-joining (NHEJ) (Costa et al., 2003; Giglia-Mari et al., 2011; Iyama and Wilson, 2013; Jiricny, 2006; Mullins et al., 2019; Xiao and Samson, 1993). Upon DNA damage, the cell cycle usually arrests for

proper DNA repair. Different pathways upon different DNA damage are highlighted in figure 1.8. Proteins regulating those checkpoints are kinases such as ATM, ATR, CHK (checkpoint kinase), CDK (cyclin-dependent kinase) as well as p53. Those proteins regulate the cell cycle arrest as well as proper DNA repair. If the damage is too severe, cells undergo apoptosis (Barnum and O'Connell, 2014). The histone H2A variant H2AX plays a crucial role in DDR. When H2AX is phosphorylated at serine 138, also termed as γH2AX, it is accumulating around DSBs and is a sign for general DNA damage (Rogakou et al., 1998; Smith et al., 2020; Ward and Chen, 2001). Then the DNA repair proteins DNA-PK, ATM and ATR are recruited to the DNA damage site (Stiff et al., 2004; Ward and Chen, 2001; Yang et al., 2003). DSB induced by IR usually get recognized by ATM whereas UV or stalled replication forks are getting mainly recognized by ATR (Yang et al., 2003). When CHK2 is activated by phosphorylation, it promotes cell cycle arrest via CDKs (Smith et al., 2020) until the DNA damage is resolved (Barnum and O'Connell, 2014). S and G2/M checkpoints are under control of ATR, CHK1 and Wee1 whereas the G1 checkpoint is controlled by the ATM, CHK2 and p53 pathways (Smith et al., 2020; Vera et al., 2015).

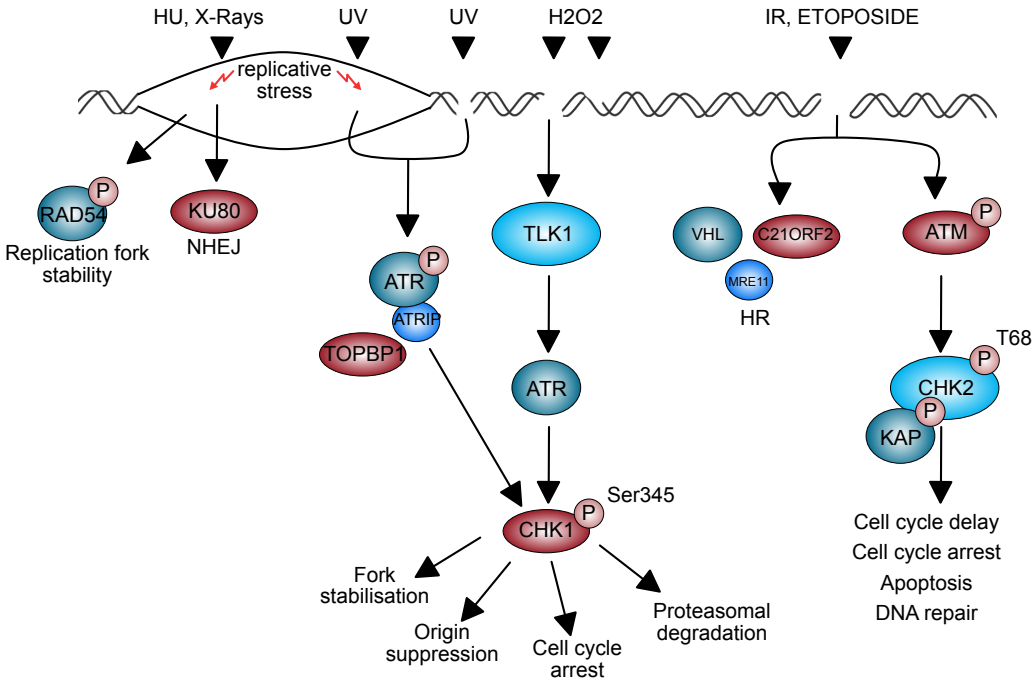

Figure 1.8: DNA Damage and DNA Damage Repair.
Different resources of DNA damage lead to different signalling pathways to deal with DNA damage and promote DNA damage repair. To prevent further DNA damage, phosphorylation of the effector protein leads to fork stabilisation, origin suppression, cell cycle arrest, proteasomal degradation or apoptosis as well as DNA repair. For DSB the DNA is repaired either through non-homologous end joining (NHEJ) or homologous recombination (HR).

1.8 Objective of the thesis

MYC is an oncogene and drives tumorigenesis in many entities. Therefore, it is important to understand basic mechanisms underlying MYC function on tumorigenesis.

The MYC protein interacts with a high variety of proteins. One of this interaction partners is the RNA Polymerase II associated factor 1 complex (PAF1c). The ubiquitin-dependent turnover of MYC is needed to transfer PAF1c onto the RNAPII and is important for transcriptional regulation.

The objective of this thesis is to investigate the function of this transfer in detail while manipulating protein levels of MYC or of subunits of PAF1c. Finally, the biological relevance of the MYC-PAF1c interaction and the subsequent transfer of PAF1c from MYC onto the RNAPII will be elucidated.

2 Material

2.1 Strains and cell lines

2.1.1 Bacterial strains

DH5α

Escherichia coli (E.coli) F-, Φ80dlacZΔM15 Δ(lacZYA-argF)U169 deoR recA1 endA1 hsdR17 (rk-,mk+) phoA supE44 λ- thi-1 gyrA96 relA1;
for plasmid amplification

XL1 blue

E. coli, recA1 gyrA96, thi-1 hsdR17 supE44 relA1 lac[F'proAB lacIqZΔM15Tn10 (Tetr)];
for plasmid amplification and generation

BL21

E. coli, F-, ompT gal dcm lon hsdSB (rB- mB) λDE3 lacI lacUV5-T7 gene 1 ind1 sam7 nin5;
for overexpression of GST fusion proteins

2.1.2 Human cell lines

HEK293TN

Human embryonic kidney cell line (ATCC).

U2OS

Human osteosarcoma cell line (ATCC).

K562

Human erythroleukemia cell line (Provided by Johannes Zuber).

NIH 3T3

murine embryonic fibroblast cell line (ATCC)

2.2 Cultivation media and supplements

2.2.1 Media and antibiotics for bacterial cell culture

LB-medium

10 % (w/v) bacto tryptone

0.5 % (w/v) yeast extract

1 % (w/v) NaCl

LB-agar

LB-medium containing 1.2 % Bacto agar was autoclaved, heated until 50 °C was reached, then antibiotics were added and poured in 10 cm dishes.

LB-antibiotics

The following antibiotics were added to either LB-media or LB-agar:

Antibiotic	**Concentration**
Ampicillin	100 µg/ml
Carbenicillin	100 µg/ml
Kanamycin	30 µg/ml
Chloramphenicol	25 µg/ml

2.2.2 Media for mammalian cell culture

Basal medium DMEM and RPMI-1640 containing 10 mM L-glutamine was purchased by Thermo Fisher Scientific. Fetal bovine serum (FBS, purchased from Capricorn Scientific and Sigma) was heat inactivated for 30 min at 56 ℃. Penicillin/streptomycin and L-glutamine were purchased from Sigma.
HEK293TN and U2OS were cultured in DMEM containing 4.5 g/l glucose and 0.584 g/l L-glutamine. 10 % (v/v) FBS and 1 % (v/v) penicillin/streptomycin were added. K562 cells were cultured in RPMI-1640 containing 14 mM L-glutamine as well as 10 % (v/v) FBS and 1 % (v/v) penicillin/streptomycin.
Opti-MEM was used for transfection of cells.

2.2.3 Antibiotics for mammalian cell culture

To select stably infected cells, the following antibiotics with the indicated concentrations were used:

Antibiolotic	**Source**	**Concentration**
Puromycin	InvivoGen	1-2 µg/ml
Hygromycin	InvivoGen	80 µg/ml

2.2.4 Additional supplements

Supplements additionally necessary are listed below.

Name	**Company**	**Stock**	**Final**
Doxycycline	Sigma	1 mg/ml	1 µg/ml
Protamine suflate	Sigma	4 mg/ml in ddH_2O	5 µg/ml
NVP-2	Tocris/Bio-Techne	10 mM in DMSO	1 µM
LDC4297	Selleckchem/Biozol	10 mM in DMSO	0.5 µM
5-EdU	Jena Bioscience	10 mM	10 µM
BrdU	Sigma	25 mM in H_2O	10 µM
IAA	Sigma	500 mM in DMSO	100 µM
Etoposide	Sigma	50 mM in DMSO	25 µM

Name	Company	Stock	Final
4-Hydroxytamoxifen	Sigma	1 mM in EtOH	200 nM

2.3 Consumables

Consumables such as disposable plastic items for cell culture or reaction tubes were purchased from the companies Applied Biosystems, Eppendorf, Greiner, Nunc, Sarstedt and VWR.

2.4 Consumables for immunoblot

Application	Name	Source
Whatman filter paper	Gel Blotting Paper	Schleicher and Schuell
PVDF transfer membrane	Immobilon-P transfer membrane	Millipore

2.5 Equipment

Application	Name	Source
Automated Electrophoresis	5200 Fragment Analyzer	Agilent
	Experion™	Bio-Rad
Chemiluminescence imaging system	LAS-4000 mini	Fujifim
Imaging system	Odyssey® CLx	Li-Cor
Cell Counter	Casy® cell counter	Innovatis
	Countess® Automated Cell Counter	Thermo Fisher Scientific
Cell culture incubator	BBD 6220	Heraeus

Application	Name	Source
Centrifuges	Avanti J-26 XP	Beckman Coulter
	Eppendorf 5417 R	Eppendorf
	Eppendorf 5425	Eppendorf
	Eppendorf 5430	Eppendorf
	Galaxy MiniStar	VWR
	Multifuge 1S-R	Heraeus
Deep-sequencer	NextSeq 500	Illumina
Flow cytometer	BD FACS Canto™ II	BD Biosciences
	BD FACS Aria III	BD Biosciences
Power supply	Power Pac	Bio-Rad
	Consort EV231/EV243	Roth
Photometer	Ultrospec™ 3100 pro UV/Visible	Amersham Biosciences
	Spectrofluorometer NanoDrop 1000	Thermo Fisher Scientific
	Multiscan Ascent	Thermo Labsystems
PCR thermal cycler	Mastercycler pro S	Eppendorf
	C1000 Thermal cycler	Bio-Rad
Microscopes	Axiovert 40CFL	Zeiss
	SP8 (DM6000)	Leica
	Operetta High Content Imaging System	Perkin Elmer
Incubator shaker	Model G25	New Brunswick Scientific
Heating block	Dry Bath System	Starlab
	Thermomixer®comfort	Eppendorf
Vortex mixer	Vortex-Genie	Scientific Industries
Ultrasonifier	Digital Sonifier W-250 D	Branson
	M220 Focused-ultrasonicator	Covaris
Water bath	Julabo ED-5M water bath	Julabo
	Memmert waterbath	Memmert

Application	Name	Source
UV fluorescent table	Maxi UV fluorescent table	Peqlab
Sterile bench	HeraSafe	Heraeus
Quantitative RT-PCR machine	StepOne plus	Applied Biosystem
SDS-PAGE	System Minigel	Bio-Rad
	Mini-PROTEAN Tetra Cell	Bio-Rad
Immunoblot transfer chamber	PerfectBlue Tank Electro Blotter Web S	Peqlab

2.6 Programs

Program	Source
Image Studio™ Lite 5.2.5	Li-Cor
Adobe Acrobat DC	Adobe Inc.
ApE plasmid editor	by M. Wayne Davis
MikTex	by Christian Schenk
TexMaker 5.0.4	by Pascal Brachet
GraphPad Prism v5/6.0 for Mac	Graph Pad Software Inc.
Microsoft Office	Microsoft
FASTQ Generation software v1.0.0	http://illumina.com
FastQC v0.11.3	
Tophat v2.1.0	Kim et al. (2013)
Bowtie v1.2	Langmead et al., 2009
Bowtie v2.3.2	Langmead and Salzberg (2012)
MACS v1.4.1	Zhang et al. (2008)
BEDtools v2.26.0	Quinlan and Hall (2010)
SAMtools v1.3	Li et al. (2009)
NGSplot v2.61	Shen et al. (2014)
Integrated Genome Browser v9.0.0	Freese et al. (2016)

Program	Source
Harmony High Content Imaging and Analysis Software	Perkin Elmer
StepOne software v2.3	Applied Biosystems
BD FACSDIVA Software v6.1.2	BD Biosciences
EdgeR	Robinson et al., 2010
R version 3.6.3	The R Foundation
UMI-tools v1.0.0	
DeepTools	Smith et al., 2017
Mac OS X	Apple Inc.
Affinity Designer	Serif
MultiGauge	Fujifilm Corporation

2.7 Enzymes, inhibitors and antibodies

Antibody	Host	Company, cat#	Application
Pol II (A-10)	Mouse monoclonal	Santa Cruz Biotechnology, sc-17798	IB, ChIP
Pol II (F-12)	Mouse monoclonal	Santa Cruz Biotechnology, sc-55492	IB, IF
MYC (Y69)	Rabbit monoclonal	Abcam, ab320728	ChIP, IB, IF
Ser2-RNAPII (phospho)	Rabbit polyclonal	Abcam, ab5095	ChIP, IB
RNAPII	Mouse monoclonal	MBL International, MABI0601	IB
H2B	Rabbit polyclonal	Abcam, ab1790	ChIP, IB
HUWE1	Rabbit polyclonal	Abcam, ab70161	IB
CTR9	Rabbit polyclonal	Novus Biologicals, NB100-68205	IF

Antibody	Host	Company, cat#	Application
CTR9	Rabbit polyclonal	Bethyl Laboratories, A301-395	IB, ChIP
Parafibromin	Rabbit polyclonal	Bethyl Laboratories, A300-171A	IB, ChIP
PAF1	Rabbit polyclonal	Abcam, Ab20662	IB
LEO1	Rabbit polyclonal	Novus Biologicals, NB600-276	IB
GST	Goat polyclonal	GE Healthcare, GE27-4577-01	IB
Ubiquityl-H2B (Lys120, D11)	Rabbit monoclonal	Cell Signaling Technology, 5546	IB,ChIP
VCL	Mouse monoclonal	Sigma-Aldrich, V9131	IB
Ser5-RNAPII (phospho)	Mouse monoclonal	Biolegend, 904001	IB
CDK2	Rabbit polyclonal	Santa Cruz Biotechnology, sc-163	IB
CHK1(FL-476)	Rabbit polyclonal	Santa Cruz Biotechnology, sc-7898	IB, IF
Chk1 (phospho, Ser345, 133D3)	Rabbit polyclonal	Cell Signaling Technology, 2348	IB, IF
H2A.X (phospho, Ser139)	Rabbit polyclonal	Cell Signaling Technology, 2577	IB, IF
KAP1 (phospho, S824)	Rabbit polyclonal	Abcam, ab70369	IB; IF
KAP1	Rabbit polyclonal	Bethyl Laboratories, A300-274A	IB, IF
TH1L (D5G6W)	Rabbit monoclonal	Cell Signaling Technology, 12265S	IB, ChIP

Antibody	Host	Company, cat#	Application
FITC-BrdU (3D4)	Mouse monoclonal	BioLegend, 364104	FACS
MIZ1 (10E2)	Mouse monoclonal	produced by AG Eilers	IB

IB: Immunoblot; ChIP: Chromatin immunoprecipitation; IF: Immunofluoresence; FACS: Fluorescence activated cell sorting

Antibody	Host	Company, cat#	Application
ECL-α-goat IgG-HRP	Donkey	Santa Cruz Biotechnology, sc-2020	IB
ECL-α-rabbit IgG-HRP	Goat	GE Healthcare, 1079-4347	IB
ECL-α-mouse IgG-HRP	Goat	GE Healthcare, 1019-6124	IB
IRDye 800CW α-Rabbit IgG	Donkey	LI-COR Biosciences, 926-32213	IB
IRDye 680RD α-Mouse IgG	Donkey	LI-COR Biosciences, 926-68072	IB
Alexa Fluor® 488 α-Mouse IgG	Goat	Thermo Fisher Scientific, A-11029	IF
Alexa Fluor® 568 α-Mouse IgG	Goat	Thermo Fisher Scientific, A-11004	IF

α: anti; IB: Immunoblot; IF: Immunofluoresence

Enzymes	Company
NotI	Thermo Fisher Scientific
MluI	Thermo Fisher Scientific
XhoI	Thermo Fisher Scientific
AsiSI	New England Biolabs
T4 DNA Ligase, concentrated	New England Biolabs
T4 RNA Ligase 2, truncated	New England Biolabs
DNase-free RNaseA	Qiagen
M-MLV reverse transcriptase	Promega
Proteinase K	Roth

Enzymes	Company
RNase A	Roth

Inhibitor	Company
RNaseOUT Recombinant Ribonuclease Inhibitor	Thermo Fisher Scientific
Protease inhibitor cocktail	Sigma-Aldrich
Phosphatase inhibitor cocktail 2	Sigma-Aldrich
Phosphatase inhibitor cocktail 3	Sigma-Aldrich

2.8 Beads

Beads	Company	Application
Glutathione Sepharose 4B	GE Healthcare	Purification
Dynabeads Protein A	Thermo Fisher Scientific	ChIP/ IP
Dynabeads Protein G	Thermo Fisher Scientific	ChIP/ IP
SPRI select reagent	Beckman Coulter	Library prep (ChIP, BLISS)
Agencourt RNAClean XP	Beckman Coulter	Library prep (RNA, BLISS)

IP: Immunoprecipitation; ChIP: Chromatin immunoprecipitation; BLISS: Breaks Labeling *In Situ* and Sequencing

2.9 Dyes

Dye	Company
Propidium iodide	Sigma-Aldrich
PowerUp™ SYBR® Green Master Mix	Thermo Fisher Scientific
Quant-iT Pico Green	Thermo Fischer Scientific
InstantBlue™ Safe Coomassie Stain	Sigma-Aldrich
AFDye 647 Azide	Jena Bioscience

Dye	Company
Hoechst 33342	Sigma-Aldrich

2.10 Ready-made kits

Kit	Company
NGS Fragment High Sensitivity Analysis Kit, 1-6,000 bp, 500 samples	Agilent
Standard Sensitivity RNA Analysis Kit (15 nt), 500 samples	Agilent
RNeasy Mini Kit	Qiagen
MinElute PCR Purification Kit	Qiagen
QIAquick® PCR Purification Kit	Qiagen
QIAquick® Gel Extraction Kit	Qiagen
NEBNext® Ultra RNA Library Prep Kit for Illumina	New England Biolabs
NEBNext® Poly(A) mRNA Magnetic Isolation Module	New England Biolabs
NEBNext ®ChIP-Seq Prep Master Mix Set for Illumina	Illumina
NEBNext® Ultra II DNA Library Prep	New England Biolabs
NEBNext® Multiplex Small RNA Library Prep Kit	New England Biolabs
NextSeq 500/550 High Output Kit v2 (75cycles)	New England Biolabs
MEGAscript T7 Transcription Kit	Thermo Fisher Scientific
SuperScript III Reverse Transcriptase	Thermo Fisher Scientific
Quick Blunting Kit	New England Biolabs
GeneJET Gel Extraction Kit	Thermo Fisher Scientific
Kit for MAXiprep	Invitrogen
NEBNext® mRNA-Seq Library	New England Biolabs

2.11 EdU labelling reagents

For EdU labelling reagents were prepared as follows:

Component	Stock	Final concentration
5'EdU	100 mM	10 µM
Tris pH 8.0	116.8 mM	100 mM
CuSO4	100 mM	4 mM
AF647-Picolyl-Azide	2.5 mM	10 µM
L-Ascorbic Acid	100 mM	10 mM

2.12 Protein and DNA Ladders

Ladder	Company
HiMark pre-stained HMW STD	Thermo Fisher Scientific
PageRuler™ Prestained Protein Ladder	Thermo Fisher Scientific
DNA marker Gene Ruler 1 kb Plus DNA ladder	Thermo Scientific

2.13 Chemicals

All chemicals used for this thesis were purchased from the companies Sigma-Aldrich, Invitrogen, Thermo Fisher Scientific, Applichem, Merck, Roth, Calbiochem. If not otherwise declared solutions and buffers listed below were prepared in ddH_2O.

2.14 Buffers and solutions

Buffer	Composition	Storage
Ammonium persulfate (10 %)	5 g ammonium persulfate (APS) dissolved in 50 ml ddH_2O and aliquoted	-20 °C
Ampicillin stock solution	10 g ampicillin solubilized in 100 ml ddH_2O and sterile filtered and aliquoted	-20 °C
Blocking solution for PVDF membrane	5 % (w/v) BSA in TBS-T	-20 °C
Blocking solution for ChIP	5 mg/ml BSA in PBS; sterile filtered	4 /-20 °C
BCA buffer A	1 % BCA-Na_2 2 % Na_2CO_3 x ddH_2O	RT
BCA buffer B	4 % $CuSO_4$ x 5 ddH_2O 0.16 % Na-tartrate 0.4 % NaOH 0.95 % $NaHCO_3$	RT
Bis-Tris (3.5 x)	1.25 M Bis-Tris	RT
Bis-Tris stacking gel	4 % (v/v) acrylamide/ bisacrylamide 1 x Bis-Tris 0.03 % (v/v) APS 0.05 % (v/v) TEMED	RT

Buffer	Composition	Storage
Bis-Tris separation gel	8-15 % (v/v) acrylamide/ bisacrylamide 1 x Bis-Tris 0.03 % (v/v) APS 0.05 % (v/v) TEMED	RT
Crystal violet solution	0.1 % (w/v) crystal violet 20 % (v/v) ethanol	RT
ChIP elution buffer	1 % (v/v) SDS 0.1 M $NaHCO_3$ prepared fresh in aqua dest	RT
ChIP lysis buffer I	5 mM PIPES pH 8.0 85 mM KCl 0.5 % (v/v) NP40 protease inhibitor mix (1:1000, add fresh)	4 °C
ChIP lysis buffer II	50 mM HEPES pH 7.9 140 mM NaCl 1 mM EDTA 1 % (v/v)TritonX-100 0.1 % (w/v) deoxycholic acid sodium salt 0.1 % (v/v) SDS protease inhibitor mix (1:1000, add fresh)	4 °C
ChIP wash buffer I	20 mM Tris HCl pH 8.1 150 mM NaCl 2 mM EDTA	4 °C

Buffer	Composition	Storage
	0.1 % (v/v) SDS 1 % (v/v) TritonX-100	
ChIP wash buffer II	20 mM Tris HCl pH 8.1 500 mM NaCl 2 mM EDTA 0.1 % (v/v) SDS 1 % (v/v) TritonX-100	4 °C
ChIP wash buffer III	10 mM Tris HCl pH 8.1 250 mM LiCl 1 mM EDTA 1 % (v/v) NP40 1 % (v/v) deoxycholic acid sodium salt	4 °C
Coomassie solution	50 % (v/v) methanol 10 %(v/v) acetic acid 0.5 % (w/v) Coomassie Brilliant Blue R-250	RT
Coomassie destain	20 %(v/v) methanol 10 % (v/v) acetic acid	RT
Crystal violet solution	0.1 % (w/v) crystal violet 20 % (v/v) ethanol	RT
DNA loading buffer (6 x)	10 mM EDTA, pH 8.0 0.2 % (w/v) Orange G 40 % (w/v) sucrose	-20 °C
EDTA 0.5 M	0.5 M EDTA	RT

Buffer	Composition	Storage
	adjusted to pH 8.0 using 10 M NaOH autoclaved	
Miniprep resuspension buffer	TE with RNaseA (1:1000, add fresh)	RT
Miniprep lysis buffer	0.2 N NaOH 1 % SDS	RT
Miniprep precipitation buffer	3 M KOAc, pH 5.2	RT
NETN-Puffer	20 mM Tris, pH 8 100 mM NaCl 1 mM EDTA 0.5 % NP40	4 °C
NuPAGE transfer buffer (20 x)	500 mM Bis-Tris 500 mM Bicine 20.5 mM EDTA 0.1 mM chlorobutanol	4 °C
NuPAGE transfer buffer (ready to use)	1x NuPAGE transfer buffer with 20 % methanol	4 °C
MOPS running buffer (20 x)	1 M MOPS 1 M Tris 20 mM EDTA 2 % SDS	4 °C

Buffer	Composition	Storage
MOPS running buffer (ready to use)	1x MOPS running buffer with 5 mM sodium bisulfite	4 °C
PBS	137 mM NaCl 2.7 mM KCl 10.1 mM Na_2HPO_4 1.76 mM KH_2PO_4 autoclaved	RT
Phenylmethylsulfonylfluorid (PMSF)	150 mM in isopropanol	RT
Propidium Iodide (PI)	1 mg/ml in PBS	4 °C
Pulldown buffer	100 mM NaCl 4 °C 20 mM Na HEPES, pH 7.4 4 % glycerol 1 mM DTT 3 mM $MgCl_2$	
RIPA lysis buffer	50 mM HEPES, pH 7.9 140 mM NaCl 1 mM EDTA 1 % Triton X-100 0.1 % Na-deoxycholate 0.1 % SDS 1 mM PMSF (add fresh) protease and phosphatase inhibitors (1:1000, add fresh)	4 °C
RNase A (10 mg/ml)	100 mg RNase A	-20 °C

Buffer	Composition	Storage
	27 µl 3 M sodium acetate, pH 5.2 9 ml ddH_2O boiled for 30 min at 100°C to inactivate DNases 50 µl 1 M Tris, pH 7.4 added per aliquot	
Sample buffer (6 x)	1.2 g SDS 6 mg bromophenol blue 4.7 ml 100 % glycerol 1.2 ml 0.5 M Tris, pH 6.8 2.1 ml ddH_2O the solution was heated up 0.93 g DTT was dissolved	-20 °C
Silver gel fixing solution	40 % (v/v) methanol 10 %(v/v) acetic acid	RT
Silver gel staining solution	0.2 % (w/v) $AgNO_3$ light-sensitive	RT
Silver gel washing solution	50 % (v/v) ethanol	RT
Silver gel developing solution	27.5 g/l Na_2CO_3 0.2 % formaldehyde (add fresh) pH<11.5 (titrate with $NaHCO_3$)	RT
Silver gel stopping solution	10 % (v/v) acetic acid	RT
STET-Puffer	8 % (w/v) sucrose 0.5 % (v/v) Triton X-100	4 °C

Buffer	Composition	Storage
	50 mM EDTA 50 mM Tris-HCl, pH 8.0	
TBS (20 x)	500 mM Tris base 2.8 M NaCl adjusted to pH 7.4 with concentrated HCl	RT
TBS-T	1 x TBS 0.2 % Tween-20	4 °C
TE	10 mM Tris, pH 7.4 1 mM EDTA, pH 8.0	RT
Trypsin solution	0.25 % trypsin 5 mM EDTA 22.3 mM Tris, pH 7.4 125 mM NaCl	-20/4 °C

2.15 Nucleic acids

2.15.1 Plasmids

Name	Description
pGIPZ	Lentiviral expression vector, CMV-promoter, tGFP marker
pINDUCER10	Dox inducible lentiviral expression vector, CMV-promoter, tGFP marker

Name	Description
pRRL-SFFV-IRES (hygromycin)	Lentiviral expression vector, SFFV-promoter, hygromycin resistance
pGEX4T3	Bacterial expression vector, tac-promoter, for expression of GST-tagged recombinant proteins
pcDNA3.1	Eukaryotic expression vector, CMV-promoter

Name	Description
psAX.2	Plasmid for lentivirus production, encoding for virion packaging system
pMD2.G	Plasmid for lentivirus production, encoding for virion envelope

Name	Description
pRRL-SFFV-IRES-MYC (hygromycin)	Lentiviral expression vector with CDS of human WT MYC
pGEX4T3 MYC wt	pGEX4T3 with CDS of human *MYC* wt (AA1-162)
pGEX4T3 MYC ΔMBI	pGEX4T3 with CDS of human *MYC* wt (AA1-162) lacking MBI
pGEX4T3 MYC ΔMBII	pGEX4T3 with CDS of human *MYC* wt (AA1-162) lacking MBII

Name	Description
pGIPZ shCDC73-1	Lentiviral vector for shRNA-mediated depletion of human CDC73
pGIPZ shCDC73-2	Lentiviral vector for shRNA-mediated depletion of human CDC73

Name	Description
pGIPZ shCDC73-3	Lentiviral vector for shRNA-mediated depletion of human CDC73
pGIPZ shCDC73-4	Lentiviral vector for shRNA-mediated depletion of human CDC73
pGIPZ shCDC73-5	Lentiviral vector for shRNA-mediated depletion of human CDC73
pGIPZ shCTR9-1	Lentiviral vector for shRNA-mediated depletion of human CTR9
pGIPZ shCTR9-2	Lentiviral vector for shRNA-mediated depletion of human CTR9
pGIPZ shCTR9-3	Lentiviral vector for shRNA-mediated depletion of human CTR9
pGIPZ shCTR9-4	Lentiviral vector for shRNA-mediated depletion of human CTR9
pGIPZ shCTR9-5	Lentiviral vector for shRNA-mediated depletion of human CTR9
pGIPZ shPAF1-1	Lentiviral vector for shRNA-mediated depletion of human PAF1
pGIPZ shPAF1-2	Lentiviral vector for shRNA-mediated depletion of human PAF1
pGIPZ shPAF1-3	Lentiviral vector for shRNA-mediated depletion of human PAF1
pGIPZ shPAF1-4	Lentiviral vector for shRNA-mediated depletion of human PAF1
pGIPZ shPAF1-5	Lentiviral vector for shRNA-mediated depletion of human PAF1
pINDUCER10 shCDC73-1	Lentiviral vector for Dox inducible shRNA-mediated depletion of human CDC73
pINDUCER10 shCDC73-2	Lentiviral vector for Dox inducible shRNA-mediated depletion of human CDC73

Name	Description
pINDUCER10 shCDC73-3	Lentiviral vector for Dox inducible shRNA-mediated depletion of human CDC73
pINDUCER10 shCDC73-4	Lentiviral vector for Dox inducible shRNA-mediated depletion of human CDC73
pINDUCER10 shCDC73-5	Lentiviral vector for Dox inducible shRNA-mediated depletion of human CDC73
pINDUCER10 shCTR9-1	Lentiviral vector for Dox inducible shRNA-mediated depletion of human CTR9
pINDUCER10 shCTR9-2	Lentiviral vector for Dox inducible shRNA-mediated depletion of human CTR9
pINDUCER10 shCTR9-3	Lentiviral vector for Dox inducible shRNA-mediated depletion of human CTR9
pINDUCER10 shCTR9-4	Lentiviral vector for Dox inducible shRNA-mediated depletion of human CTR9
pINDUCER10 shCTR9-5	Lentiviral vector for Dox inducible shRNA-mediated depletion of human CTR9
pcDNA3.1 HA-CTR9	Eukaryotic expression vector with CDS of human WT *CTR9* and HA-tag (N-terminal)
pcDNA3.1 HA-CDC73	Eukaryotic expression vector with CDS of human WT *CDC73* and HA-tag (N-terminal)
pcDNA3.1 HA-SKI8	Eukaryotic expression vector with CDS of human WT *SKI8* and HA-tag (N-terminal)
pcDNA3.1 HA-RTF1	Eukaryotic expression vector with CDS of human WT *RTF1* and HA-tag (N-terminal)

2.15.2 Primer

The following subsection describes primers used for PCR, cloning or BLISS(8).

Name	Application	Sequence (5' -> 3')
NCL for	ChIP qPCR	CTACCACCCTCATCTGAATCC
NCL rev	ChIP qPCR	TTGTCTCGCTGGGAAAGG
Negative Region for	ChIP qPCR	TTTTCTCACATTGCCCCTGT
Negative Region rev	ChIP qPCR	TCAATGCTGTACCAGGCAAA
GNL3 for	ChIP qPCR	GTGACGCTCGTCAGTGG
GNL3 rev	ChIP qPCR	CATATTGGCTGTAGAAGGAAGC
NPM1 for	ChIP qPCR	TTCACCGGGAAGCATGG
NPM1 rev	ChIP qPCR	CACGCGAGGTAAGTCTACG
IFRD1 for	ChIP qPCR	CCTGTCCCGACACACTCTC
IFRD1 rev	ChIP qPCR	CGTGGTTTGGCTACTGAACT
CHMP2A for	ChIP qPCR	GGGGATCCCAGAAAGAGAAG
CHMP2A rev	ChIP qPCR	CAAGGTGGTGTTGGAGACCT

Name	Application	Sequence (5' -> 3')
shCDC73 human mirE3	cloning	TGCTGTTGACAGTGAGCGCCAGCGATCTACTC AAGTCAAATAGTGAAGCCACAGATGTATTTGA CTTGAGTAGATCGCTGATGCCTACTGCCTC GGA
shCDC73 human mirE4	cloning	TGCTGTTGACAGTGAGCGCCAGGTACATGGTA AAGCATAATAGTGAAGCCACAGATGTATTATGC TTTACCATGTACCTGTTGCCTACTGCCTCGGA
shCTR9 human mirE3	cloning	TGCTGTTGACAGTGAGCGCTCGGATGAGGAT AAACTTAAATAGTGAAGCCACAGATGTATTTA AGTTTATCCTCATCCGAATGCCTACTGCCTC GGA

Name	Application	Sequence (5' -> 3')
shCTR9 human mirE5	cloning	TGCTGTTGACAGTGAGCGAAAGCAACAAAAGAGAAGAAAATAGTGAAGCCACAGATGTATTTTCTTCTCTTTTGTTGCTTCTGCCTACTGCCTCGGA
MYC for (pGex4T3)	cloning	CCCGAATTCGCCCCTCAACGTTAGCTTC
MYC rev (pGex4T3)	cloning	GGGCTCGAGTCAGTTCGGGCTGCCGCTGTCT
pInducer10 sequencing primer	cloning	cgcaagccttgttaagtgct
pGIPZ sequencing primer	cloning	GCATTAAAGCAGCGTATC
pLT3 GEPIR sequencing primer	cloning	TGTTTGAATGAGGCTTCAGTAC
mirE XhoI PCR for	cloning	TACAATACTCGAGAAGGTATATTGCTGTTGACAGTGAGCG
mirE EcoRI PCR rev	cloning	TTAGATGAATTCTAGCCCCTTGAAGTCCGAGGCAGTAGGCA

Name	Application	Sequence (5' -> 3')
A1 Bottom	Adapter	[P]GCGTGATGNNNNNNNNGATCGTCGGACTGTAGAACTCTGAACCCCTATAGTGAGTCGTATTACCGGCCTCAATCGAA
A1 Top	Adapter	CGATTGAGGCCGGTAATACGACTCACTATAGGGGTTCAGAGTTCTACAGTCCGACGATCNNNNNNNNNCATCACGC

Name	Application	Sequence (5' -> 3')
A2 Bottom	Adapter	[P]GGAACGACNNNNNNNNGATCGTCGGACTG TAGAACTCTGAACCCCTATAGTGAGTCGTAT TACCGGCCTCAATCGAA
A2 Top	Adapter	CGATTGAGGCCGGTAATACGACTCACTATAGG GGTTCAGAGTTCTACAGTCCGACGATCNNNN NNNNGTCGTTCC
A3 Bottom	Adapter	[P]GATCATCANNNNNNNNGATCGTCGGACTG TAGAACTCTGAACCCCTATAGTGAGTCGTATT ACCGGCCTCAATCGAA
A3 Top	Adapter	CGATTGAGGCCGGTAATACGACTCACTATAGG GGTTCAGAGTTCTACAGTCCGACGATCNNNN NNNNTGATGATC
A4 Bottom	Adapter	[P]GATGTCGTNNNNNNNNGATCGTCGGACTG TAGAACTCTGAACCCCTATAGTGAGTCGTAT TACCGGCCTCAATCGAA
A5 Bottom	Adapter	[P]GGATGATGNNNNNNNNGATCGTCGGACTG TAGAACTCTGAACCCCTATAGTGAGTCGTAT TACCGGCCTCAATCGAA
A5 Top	Adapter	CGATTGAGGCCGGTAATACGACTCACTATAGG GGTTCAGAGTTCTACAGTCCGACGATCNNNN NNNNCATCATCC
A6 Bottom	Adapter	[P]GCGGTCGTNNNNNNNNGATCGTCGGACTG TAGAACTCTGAACCCCTATAGTGAGTCGTATT ACCGGCCTCAATCGAA
A6 Top	Adapter	CGATTGAGGCCGGTAATACGACTCACTATAGG G GTTCAGAGTTCTACAGTCCGACGATCNNNN NNNNACGACCGC
RPI 01	Index Primer	CAAGCAGAAGACGGCATACGAGATCGAGTAA TGTGACTGGAGTTCCTTGGCACCCGAGAATT CCA

Name	Application	Sequence (5' -> 3')
RPI 02	Index	CAAGCAGAAGACGGCATACGAGATTCTCCGG
	Primer	AGTGACTGGAGTTCCTTGGCACCCGAGAATT
		CCA
RPI 03	Index	CAAGCAGAAGACGGCATACGAGATAATGAGC
	Primer	GGTGACTGGAGTTCCTTGGCACCCGAGAATT
		CCA
RPI 04	Index	CAAGCAGAAGACGGCATACGAGATGGAATCT
	Primer	CGTGACTGGAGTTCCTTGGCACCCGAGAATT
		CCA
RPI 05	Index	CAAGCAGAAGACGGCATACGAGATTTCTGAA
	Primer	TGTGACTGGAGTTCCTTGGCACCCGAGAATT
		CCA
RPI 06	Index	CAAGCAGAAGACGGCATACGAGATACGAATT
	Primer	CGTGACTGGAGTTCCTTGGCACCCGAGAATT
		CCA
RPI 07	Index	CAAGCAGAAGACGGCATACGAGATAGCTTCA
	Primer	GGTGACTGGAGTTCCTTGGCACCCGAGAATT
		CCA
RPI 08	Index	CAAGCAGAAGACGGCATACGAGATGCGCATT
	Primer	AGTGACTGGAGTTCCTTGGCACCCGAGAATT
		CCA
RPI 09	Index	CAAGCAGAAGACGGCATACGAGATCATAGCC
	Primer	GGTGACTGGAGTTCCTTGGCACCCGAGAATT
		CCA
RPI 10	Index	CAAGCAGAAGACGGCATACGAGATTTCGCGG
	Primer	AGTGACTGGAGTTCCTTGGCACCCGAGAATT
		CCA
RPI 11	Index	CAAGCAGAAGACGGCATACGAGATGCGCGAG
	Primer	AGTGACTGGAGTTCCTTGGCACCCGAGAATT
		CCA

Name	**Application**	**Sequence (5' -> 3')**
RPI 12	Index Primer	CAAGCAGAAGACGGCATACGAGATCTATCGC TGTGACTGGAGTTCCTTGGCACCCGAGAATT CCA
RP1	Index Primer	AATGATACGGCGACCACCGAGATCTACACGTT CAGAGTTCTACAGTCCGA
RA3	Adapter	TGGAATTCTCGGGTGCCAAGG
RTP	RT Primer	GCCTTGGCACCCGAGAATTCCA

3 Methods

3.1 Cell biology methods

3.1.1 Cultivation of eukaryotic cells

HEK 293TN, U2OS, K562 or NIH-3T3 cells were cultured in a cell incubator at 37 °C, 5 % CO_2 and a relative humidity of 95 %.

Passaging of cells

For passaging of adherent eukaryotic cells, the medium was removed from the cells, washed once with warm PBS and trypsinized until the cells detached from the plate. The enzymatic reaction of trypsinization was stopped by adding serum containing media. Afterwards, the cell suspension was transferred in a Falcon tube and centrifuged for 4 min at 1,000 rpm to remove cell debris. The media was removed and the cell pellet resuspended. A portion of the cell suspension was transferred on a cell culture dish of appropriate size. For maintaining the cell culture, this procedure was repeated every two to three days. To plate the cells for experiments with a specific cell density, cells were counted using the Neubauer counting chamber, the Casy or the Countess cell counter.

Freezing and thawing of cells

To freeze cells, media was removed, cells were once washed with PBS and adherent cells trypsinized. Afterwards, cells were centrifuged for 4 min at 1,000 rpm. Medium was removed and cells were resuspended in 1 ml freezing media, consisting of 90 % adequate media and 10 % DMSO, per one 10 cm dish. This cell suspensiuon was transferred in

cryo tubes which were placed in Mr. Frosty™ containers and shortly stored at -80 °C. These containers contain isopropanol as intermediate phase to ensure slow freezing (-1 °C per minute) of the cells. For long storage, frozen cells were transferred in a liquid nitrogen tank.
To thaw cells stored in liquid nitrogen, cell suspension was quickly thawed and resuspended in 10 ml adequate media, transferred in a 15 ml Falcon tube and centrifuged for 4 min at 1,000 rpm. Medium was removed and cell pellet resuspended in 5 to 10 ml fresh full media. Adherent cells were transferred on a 10 cm dish, suspension cells such as K562 were placed in a small cell culture flask (25 cm^2), placed in a cell incubator and controlled after 24 h for further passaging.

3.1.2 Transfection of plasmid DNA

The following subsection describes different methods to transfect eukaryotic cells with plasmid DNA.

Transfection with polyethilenimine (PEI)

Cells were seeded 24 h before transfection in a specific cell density on a 10 cm dish. Usually this cell density varied between 500,000 to 800,000 cells per dish. Full media was replaced with 5 ml transfection media containing 2 % FBS in DMEM. Two solutions, solution A and B, were prepared. Solution A constists of 250 µl OptiMEM and 10 µg of plasmid DNA. Solution B contains 250 µl OptiMEM and 20 µl PEI. Both solutions were individually incubated for 5 min, then mixed together. The mixture of solution A and B was incubated for 15 min and equally distributed on the plate. After 5 to 7 h of incubation in the cell incubator, cells were once washed with PBS and fresh full media was added.

Production of lentiviruses

HEK 293TN cells were freshly thawed, passaged 2 to 3 times and 5 M cells per 10 cm cell culture dish were seeded 24 h before transfection. For lentiviral production different plasmids are necessary: the packaging vector psPAX2, the envelope vector

pMD2.G and a lentiviral expression plasmid such as pRRL, pGIPZ or pINDUCER10. To produce lentiviruses, two solutions were prepared: Solution A consisting of 250 µl OptiMEM, 10 µg of psPAX2, 2.5 µg pMD2.G and 10 µg of the desired expression plasmid. Solution B contains 250 µl OptiMEM and 30 µl PEI. The two solutions were incubated for 5 min before mixing. The mixture was incubated for another 15 min before dropping them on the cell culture dish containing 5 ml transfection medium. After 5 to 7 h of incubation in a S2 cell incubator, the medium was changed to 10 ml fresh full medium.
Supernatant containing virus particles was harvested for the first time (10 ml) 24 h after transfection followed by every 12 h (5 ml) up to four times. The supernatant was pooled, sterile filtered using a syringe with 0.45 µm filter and either stored for several days at 4 °C or for long time storage at -80 °C.

3.1.3 Lentiviral infection of cells

Cells were seeded 24 h before lentiviral infection. For example, 600,000 or 1,500,000 U2OS cells were seeded either on a 10 cm or 15 cm dish. Cell number was determined using one of the two cell counter systems (see 3.1.1). Medium was changed to either 2.5 ml or 5 ml full medium. The same amount of viral supernatant was added together with a final 1:750 dilution of protamine sulfate (4 µg/µl). 24 h post infection 5 ml or 10 ml fresh full media were added to the 10 cm or 15 cm dish. All expression vectors used in this study contained either a puromycin or hygromycin resistance. Selection against appropriate antibiotics was started 48 h post infection. To determine a successful selection, a control plate of uninfected cells was treated with the same concentration of the appropriate antibiotic as the infected cells.

3.1.4 Colony formation assay (Crystal violet staining)

Cells were seeded on a 6-well dish and cultured for at least 24 h depending on the experiment. Medium was removed, cells washed with PBS and crystal violet solution (see 2.14) added for 1 h at room temperature. Afterwards, the staining solution was removed and carefully washed with desalted water. The plates were air dried at room temperature and photographed for documentation.

3.1.5 BrdU Propidium iodide staining for flow cytometry (BrdU-PI FACS)

Cells were seeded on a 6 cm dish at least 24 h prior harvesting. 30 min prior harvesting, cells were treated with the thymidine analogue bromodeoxyuridine (10 µM, BrdU). BrdU is incorporating into DNA during S-phase and therefore can be identified using a fluorescent coupled anti-BrdU antibody.
Supernatant of the cells was transferred into a new Falcon tube. Cells were trypsinized as described in 3.1.1. The enzymatic reaction was stopped by adding media which was transferred into a Falcon tube. Cell suspension was centrifuged for 4 min at 1,000 rpm. Cell pellet was washed once with cold PBS, pellet was resuspended in 1 ml cold PBS and dropped in 4 ml ice cold 100 % ethanol while vortexing for fixation. The ice cold ethanol was before transferred into a low affinity binding 15 ml Falcon tube. The fixed cells were incubated for at least 1 h at -20 °C.
Cells were pelleted for 10 min at 1,500 rpm at 4 °C, respsuended in 1 ml 2 M HCl containing 0.5 % TritonX-100 and incubated for 30 min at RT. Afterwards, the cells were pelleted for 5 min at 1,500 rpm and resuspended in 1 ml 0.1 M $Na_2B_4O_7$ (pH 8.5). After another centrifugation step, the cell pellet was resuspended in 100 µl 1 % BSA in PBS-T containing 10 µl anti-BrdU FITC, incubated for another 30 min at room temperature in the dark and the pellet was once washed with 1 % BSA in PBS-T. Finally, cells were pelleted for 4 min at 2,000 rpm at 4 °C, the pellet was resuspended in 400 µl PBS containing 54 µM PI and 24 µg/ml RNase A and incubated for 30 min at room temperature or over night at 4 °C. Cells were analyzed using flow cytometry.

3.2 Molecular biology methods

3.2.1 Transformation of competent cells with plasmid DNA followed by plasmid amplification

Chemically competent bacteria were thawed on ice, mixed either with 20 µl ligation mix or 1 µg plasmid DNA and incubated for 20 min on ice. After incubation, heat shock was performed by placing the mixture for 45 s in a 42 °C water bath. The

mixture was incubated for 5 min on ice, 1 ml LB media was added and incubated for another 60 min at 37 °C und smooth shaking. For amplification of plasmid DNA 50 µl were plated on LB agar plates with a selection antibiotic of the DNA plasmid. For ligation, the bacteria were spun down, resuspended in 50 µl and as well plated on LB agar plates with an adequate selection antibiotic. The plates were incubated at 37 °C overnight.

3.2.2 Overexpression and isolation of recombinant proteins in *E.coli*

E. coli BL21 were used for transformation of the overexpression plasmid pGEX4T3. Transformation was performed as described in 3.2.1. Single colonies were picked, inoculated in 10 ml LB media and incubated at 37 °C overnight. After incubation, 200 ml LB media containing antibiotics were measured until an OD600 between 0.4-0.6 nm was reached. Overexpression of the protein was started by adding 100 µM IPTG (isopropyl β-d-1-thiogalactopyranoside) for 6 h at 37 °C. The pGEX4T3 overexpression plasmid contains a *lac* operon. By adding the inductor IPTG the *lac*-repressor is removed from the promoter and expression of the gene of interest started.

Overexpressed proteins of the pGEX4T3 plasmid contain a GST tag to use for purification of the protein of interest. The bacteria were pelleted at 4000 rpm for 10 min at 4 °C and stored at -20 °C until further procedure. The bacteria pellet was resuspended in STET buffer containing freshly added TCEP (Tris(2-carboxyethyl)phosphin-hydrochlorid) and protease inhibitors. To lyse the cells, the cell suspension was sonified three times for 60 s at an amplitude of 30 % with a pulse and pause of 1 s. The lysed cells were transferred into 2 ml reaction tubes and centrifuged at 14,000 rpm for 15 min at 4 °C. Supernatant contaning the overexpressed protein was transferred into a 15 ml Falcon tube. Glutathion sepharose beads were washed with STET buffer, 80 µl beads were added to the supernatant of the lysed cells and incubated for at least 1 h at 4 °C under smooth rotation. The beads were washed three times with STET buffer, resuspended in 80 µl STET buffer and stored for a short time at 4 °C until *in vitro* pulldown was performed.

3.2.3 Analytical preparation of plasmid DNA from bacteria (Miniprep)

The analytical preparation of plasmid DNA, also termed as Miniprep, was performed using alkaline lysis. 1.5 ml overnight culture was spun down and the bacteria pellet was resuspended in 150 µl E1 which consists of TE buffer containing 1.5 µl RNase A (10 mg/ml stock solution). 150 µl lysis buffer E2 were added and incubated for 5 min at room temperature. The samples were centrifuged for 10 min at 14,000 rpm prior stopping lysis by adding 150 µl precipitation buffer E3. The supernatant was transferred into a new reaction tube and mixed with 1 ml 100 % EtOH, incubated for 20 min at -20 °C and the plasmid DNA was pelleted by centrifugation for 10 min at 14,000 rpm at 4 °C. The DNA pellet was washed at least once with 70 % EtOH, air dried and solubilized in 50 µl ddH_2O.

3.2.4 Preparative isolation of plasmid DNA (Maxiprep)

Bacteria were transformed as described in 3.2.1. 200 ml overnight culture was processed according to the manufacturer's protocol (PureLink® HiPure Plasmid Maxiprep Kit, Thermo Fisher) for the preparative isolation of plasmid DNA. The purified plasmid DNA was solubilized in ddH_2O and adjusted to a final concentration of 1 µg/µl.

3.2.5 Restriction analysis of DNA

Restriction enzymes from New England Biolabs were used to hydrolyse DNA sequence-specifically. Restriction buffers and enzyme amounts were used as recommended from the manufacturer. The reaction was incubated for at least 1 h usually at 37 °C and set up according to the following table

Substance	
DNA	1 (µg)
Restriction Endonuclease 1	0.3 µl
Restriction Endonuclease 2	0.3 µl
5x Reaction Buffer	2.0 µl
ddH_2O	to 10 µl
Σ Volume	10 µl

3.2.6 Gel electrophoretic separation of DNA fragments

Gel electrophoresis was used to visualize the size of specific fragmented DNA. The negatively charged DNA is separating towards the positively charged anode. The smaller the DNA fragment, the faster it migrates through the agarose gel. To determine the specific size, a DNA ladder (Thermo Scientific) of known fragmented sizes is loaded on the gel with the samples.
Depending on the expected DNA fragment size, a 1-2 % agarose gel in 1x TAE buffer supplemented with 0.3 µg/ml ethidium bromide (EtBr, a DNA intercalator), was prepared. Therefore, the agarose was boiled in 1x TAE buffer and, after cooling down, supplemented with EtBr and poured into a gel chamber with combs. The samples were mixed with 6x DNA loading buffer and loaded on the gel. The separation was performed applying 120-180 V for 30 to 50 min. The DNA fragments were visualized on an UV transilluminator. For analytical purposes, a picture was taken and for preparative purpose the DNA fragment of expected size was cut out and further processed.

3.2.7 Extraction and purification of DNA fragments and PCR products

As described in 3.2.6, the DNA fragments of specific size were cut out from the agarose gel and purified and extracted with the gel extraction kit according to the manufacturer's protocol (GeneJET Gel Extraction Kit, Thermo Scientific). The

purification of PCR products was performed using the GeneJET Gel Extraction Kit from Thermo Scientific but following the manufacturer's protocol of the GeneJET PCR Extraction Kit.

3.2.8 Ligation of DNA fragments

Ligation of DNA fragments with a backbone vector was performed using T4 DNA ligase (Thermo Scientific). The insert (DNA fragment) was used in equimolar ratio as calculated with the following formula:

$$amount\ of\ insert = \frac{amount\ of\ backbone\ (ng) * size\ of\ insert\ (kB)}{size\ of\ vector\ (kB)} \tag{3.1}$$

$$\tag{3.2}$$

The mix was pipetted as follows, incubated for at least 1 h at room temperature and transformed into competent bacteria as described in 3.2.1.

Substance	
linearized vector	60 ng
digested DNA fragment	x ng
T4 DNA Ligase	1 µl
10x Ligase Buffer	1 µl
ddH_2O	to 10 µl
Σ Volume	10 µl

3.2.9 Nucleic acid quantification

There are different methods to determine amount and quality of different kinds of nucleic acids such as DNA or RNA. In the following subsection different methods to determine quantity and quality of nucleic acid for different methods are described.

Nanodrop

To determine RNA and DNA concentration, the NanoDrop 1000 (Thermo Fisher) was used. The absorbance was measured at 260 nm. To determine purity of the sample, the ratio of absorbance at 260 nm and 280 nm was measured. A ratio of around 2.1 for pure RNA and 1.8 for pure DNA was expected.

PicoGreen

In contrast to the Nanodrop, the QuantiT™ PicoGreen® dsDNA reagent (Invitrogen) can distinguish between single stranded DNA (ssDNA) or double stranded DNA (dsDNA). The determination of the amount of dsDNA is necessary for a ChIP sequencing library preparation. PicoGreen is a dsDNA intercalator with an excitation/emission of 485/535 nm that can be measured according to the manufacturer's protocol.

Experion

RNA or DNA, which was used for library preparation or DNA libraries were quantified with the Experion™ Automated Electrophoresis System (Biorad) following the manfucaturer's protocols.

Fragment Analyzer

The Fragment Analyzer is an HPLC based method to quantify very small amounts of nucleic acid by applying a voltage to use molecular amounts of the sample. This method is used to determine the quality and amount of RNA as well as DNA before starting library preparations.
Additionally, the Fragment Analyzer is used to determine concentration, purity and size of libraries for next generation sequencing. This measurement is necessary to make an equimolar mix of the individual libraries as well as for the final mix which will get loaded on the flow cell for final deep sequencing.
For measuring the RNA a 2 µl sample within a range of 25 ng/µl - 500 ng/µl was

heated at 70 °C for 2 min to melt secondary structures. The sample was placed on ice and mixed with 22 µl diluent marker, mixed well by pipetting up and down and 24 µl were transferred into a well of a low affinity 96-well plate. The plate was shortly spun down to remove any air bubbles and measured according to the manufacturer's protocol (Fragment Analyzer RNA (15 NT) Kit).
To measure DNA, mostly final libraries, 2 µl samples within 5-500 pg/µl were mixed with 22 µl diluent marker and the same procedure was followed as for RNA determination. The samples were measured according to the manufacturer's protocol (HS NGS Fragment Kit (1-6,000 bp), 500)

3.2.10 RNA Isolation

RNA isolation with TriFAST

For cDNA synthesis, total RNA was usually isolated with peqGOLD TriFast (Peqlab). The cell culture medium was aspirated and the cells directly lysed by adding 1 ml TriFast on the plate. The lysed cells were transferred into a 1.5 ml reaction tube, 200 µl chloroform were added and the suspension vortexed for 30 s. The reactions were centrifuged for 10 min at 14,000 rpm at room temperature to separate phases. The upper aqueous phase contains RNA (ca. 500 µl) and was transferred into a new 1.5 ml reaction tube containing glycoblue. To precipitate RNA, an equal amount of 100 % isopropanol was added, incubated for 30 min at -20 °C and centrifuged for 30 min at 14,000 rpm at 4 °C. The RNA pellet was washed twice with 75 % EtOH, air dried, solubilized in 30-100 µl RNase-free ddH_2O and adjusted to 500 ng/µl-1,000 ng/µl. RNA was stored at -80 °C until further used.

RNA Isolation with RNeasy ® Mini Columns and DNase digestion (Qiagen)

For RNA sequencing RNA was isolated using the RNeasy® Mini Columns and DNase I digestion according to the manufacturer's protocol.

3.2.11 cDNA Synthesis

To analyse expression levels of individual genes, extracted RNA was reverse transcribed into complementary DNA (cDNA) by using random hexanucleotide primers. 0.5 - 1 µg RNA was diluted with RNAse-free ddH_2O up to 20 µl, incubated at 65 °C to dissolve secondary structures and cooled down on ice. 30 µl of cDNA synthesis master mix was added per reaction:

Substance	
5x First strand reaction buffer (Promega)	10 µl
dNTPs (10 mM stock, Roth)	1.25 µl
random primers (2 µg/ml Stock, Roche)	2.00 µl
RiboLock RNase Inhibitor (40 U/µl, Thermo Fisher)	0.20 µl
M-MLV reverse transcriptase (200 U/µl, Promega)	1.00 µl
ddH_2O	to 30 µl
Σ Volume	30 µl

The reaction was incubated as follows:

- 25 °C for 10 min
- 37 °C for 50 min
- 70 °C for 15 min

The cDNA was diluted up to 250 µl with ddH_2O and 2.5-5 µl of diluted cDNA was used per quantitative reverse transcriptase PCR reaction (see 3.2.13).

3.2.12 Polymerase chain reaction (PCR)

PCR to amplify DNA for cloning

To generate new expression vectors of a gene of interest, DNA was amplified either from DNA or an already existing expression vector. This amplification step allows to

insert tags, mutations or additional restriction sites to a gene of interest. To amplify the gene of interest, the following reagents were mixed together:

Substance	
DNA template	5 ng
10x Phusion High-Fidelity (HF) reaction buffer	5.00 µl
dNTPs (10 mM stock, Roth)	1.00 µl
forward primer (10 µM stock)	1.25 µl
reverse primer (10 µM stock)	1.25 µl
DMSO (3 % final concentration)	1.50 µl
Phusion HF DNA polymerase (Thermo Scientific)	0.50 µl
ddH_2O	to 50 µl
Σ Volume	50 µl

After mixing the components together, the mix was placed in a thermo cycler and the following program started:

Cycle step	**Temperature**	**Time**	**Cycles**
Initial denaturation	98 °C	30 s	1 x
Denaturation	98 °C	10 s	
Annealing	55 - 62 °C	30 s	30 x
Extension	72 °C	15 - 30 s per kb	
Final extension	72 °C	8 min	1 x

3.2.13 Quantitative real-time PCR (qPCR)

To analyze the enrichment of DNA fragments after chromatin immunoprecipitation as described in 3.3.8 or to measure expression levels of specific genes by analyzing mRNA (see 3.2.10), quantitative PCR (qPCR) was performed. During the amplification of DNA from a template DNA, a fluorescent dye intercalates into the freshly

synthesized DNA which can be measured and quantified in real-time. To measure this amplification, the following components were mixed together in triplicates on a 96-well plate:

Substance	
diluted cDNA (see 3.2.10) or chromatin (see 3.3.8)	2.5 µl
SYBRGreen Mix (Thermo Scientific)	5.00 µl
forward primer (10 µM Stock)	0.25 µl
reverse primer (10 µM Stock)	0.25 µl
ddH_2O	to 10 µl
Σ Volume	10 µl

The plate was covered with a adhesive film, shortly spun down, placed into a real time PCR instrument (Applied Biosystems) and the following program was started:

Cycle step	**Temperature**	**Time**	**Cycles**
Initial denaturation	95 °C	15 min	1 x
Denaturation	95 °C	30 s	
Annealing	60 °C	20 s	38 x
Extension	72 °C	15 s	
	95 °C	1 min	
Melting curve	60 °C	30 s	1 x
	95 °C	30 s	

To analyze the data, the fold induction relative to a control such as untreated cells for quantitative reverse transcriptase PCR (analysis of cDNA) was calculated. A housekeeping gene (e.g. β-Microtubulin) was used for normalization. The threshold cycle (CT), the cycle number at which the fluorescence signal exceeds a set "threshold"

value, was calculated:

$$\Delta CT = CT_{B2M} - CT_{Gene\ of\ interes} \tag{3.3}$$

$$\Delta\Delta CT = \Delta CT_{control} - \Delta CT_{sample} \tag{3.4}$$

$$relative\ expression = 2^{-\Delta\Delta CT} \tag{3.5}$$

The ChIP results were presented as % of input. If 1 % input was used, the calculation was as follows:

$$\%\ of\ input = 2^{CT_{1\%input} - CT_{IP}} \tag{3.6}$$

As described above (see 3.2.13), the measurements were performed in triplicates. To calculate the average and the standard deviation (SD), the following formula was used:

$$SD = \sqrt{\frac{(X - \bar{X})^2}{(n-1)}} \tag{3.7}$$

3.3 Biochemical methods

3.3.1 Preparation of whole cell protein extracts

To isolate proteins from cell lines, full medium was aspirated from the cells, cells were washed twice with ice cold PBS. Afterwards, RIPA lysis buffer containing proteinase and phosphatase inhibitors was added to the cell culture dish. Cells were scraped off the plate and transferred into a 1.5 ml reaction tube. The resuspended cells were either shock frozen in liquid nitrogen and stored at -80 °C or further processed. Cells were lysed by incubating on ice for 20 min by vortexing every 2-3 min. Cell debris were pelleted by centrifugation for 30 min at 14,000 rpm at 4 °C. Supernatant containing the lysate was transferred into a new 1.5 ml reaction tube and whole protein concentration was determined as described in the following subsection 3.3.2.

3.3.2 Total protein quantification by bicinchoninic acid assay (BCA)

To quantify total protein concentration via BCA assay, the BCA ready-to-use solution was prepared consisting of buffer A and buffer B in a ratio of 50 to 1 (see 2.14). 4 µl protein lysate were pipetted in duplicates into a flat bottom 96-well plate (Thermo Scientific) and 150 µl BCA solution were added. The reaction was incubated for 20 min at 37 °C. The absorbance was measured at 550 nm. The protein concentration was determined by comparing the outcome of the measurement with a standard curve of known protein standards, which was measured in parallel on the 96-well plate.

3.3.3 SDS Polyacrylamide gel electrophoresis (SDS-PAGE)

To separate proteins according to their molecular weight, SDS polyacrylamide gel electrophoresis was used. Proteins are positively charged and migrate towards the negatively charged anode. Proteins which have a small molecular weight migrate faster towards the anode than large proteins. To determine the size of the loaded protein samples, a protein ladder (PageRuler™ Pre-Stained Protein Ladder, Thermo Scientific) of known molecular weight was loaded.
Protein lysates were boiled at 95 °C for 5 min, and shortly spun down. Equal amounts of protein were loaded on a Bis-Tris polyacrylamide gel consisting of a 4 % stacking gel and a 8-12 % separating gel. Separation of protein samples and protein ladder was performed by using SDS-PAGE chambers (Biorad) filled with 1x ready-to-use MOPS running buffer (see 2.14) at 80-140 V.

3.3.4 Immunoblot

After complete separation of the protein lysates by SDS-PAGE, proteins were transferred on a PVDF membrane prior to activation in 100 % methanol for 1 min. Membrane, gel, Whatman filter papers and sponges were equilibrated in 1x ready-to-use NuPAGE transfer buffer (see 2.14) . A sandwich consisting of sponge, Whatman filters, membrane, gel, Whatman filters and sponge was built, placed in a tank blot transfer chamber (Peqlab) filled with 1x ready-to-use NuPAGE™ Transfer

Buffer. The proteins were transferred for 2-3 h at 300 mA at 4 °C. The membrane was blocked in blocking buffer (see 2.14) for 30 min at room temperature and incubated overnight at 4 °C. The membrane was washed three times in 1x TBS-T, incubated for 1 h at room temperature with a secondary antibody either coupled with HRP (dilution 1:5,000) or with a fluorescent dye (dilution 1:15,000) followed by washing three more times in 1x TBS-T. Bound antibodies were either visualized by chemiluminscence using Immobilon™ Western Chemiluminescent HRP Substrate (Millipore) according to the manufacturer's protocol and detected with LAS-4000 imager (Fujifilm Global) or with the fluorescence based Odyssey® CLx imaging system (LI-COR). Protein signals were quanified relative to a loading control by using the ImageStudio (LI-Cor) software.

3.3.5 Coomassie staining of proteins in polyacrylamide gels

Beyond the detection of specific proteins as described in subsection 3.3.4, Bis-Tris gels were also used to visualize the expression of recombinant proteins (see 3.2.2). After complete separation of samples on a SDS-PAGE, the Bis-Tris gel was stained with Coomassie solution (see 2.14) for at least 1 h upon smooth shaking. After incubation, the gel was placed in Coomassie destain solution (see 2.14) with gentle shaking until a clear background was obtained.
Alternately, InstantBlue™ (Sigma-Adrich), a water-based Coomassie staining alternative, was used according to the manufacturer's protocol.

3.3.6 Silver staining of proteins in in polyacrylamide gels

Compared to coomassie staining as described in subsection 3.3.5, silver staining is more sensitive. All reagents necessary to perform silver staining are described in 2.14. After separation of proteins via SDS-PAGE, the Bis-Tris gel was washed three times with Washing Solution for 20 min. The gel was incubated for 60 s in 1x Reducing Solution (dilution from stock, 1:100) followed by a three times washing step with ddH_2O for 20 s. After that, the gel was incubated with 1x Silver Solution (dilution from stock, 1:100) for 20 min and developed with Developing Solution, to which 0.2 % formaldehyde was freshly added, until the desired staining intensity of protein

bands was reached. The developing was stopped by incubating with Stopping Solution for 10 min and the stained Bis-Tris gel was stored in ddH_2O until a photo for documentation was taken.

3.3.7 *In vitro* pulldown assay

The recombinant proteins tagged with GST were overexpressed and purified as described in 3.2.2. Per immunoprecipitation 10 µl sepharose beads coupled with the GST-tagged protein were used. The beads were washed three times with Pulldown Buffer containing freshly added 1 mM 1,4-dithiothreitol (DTT) and 300 ng/ml BSA. After washing, the beads were resuspended in 500 µl Pulldown buffer. Recombinant purified PAF1c was resuspended in 100 µl Pulldown buffer: 10 µl were taken as input sample, the remaining solution added to the sepharose beads and incubated overnight at 4 °C. The beads were washed four times with Pulldown Buffer, two times with NETN Buffer and once again with Pulldown Buffer.
To elute the pulldown from the beads, the beads were incubated in 30 µl 2x sample buffer for 5 min at 95 °C, shortly spun down, and 15 µl loaded on a 8-10 % Bis-Tris gel by using a Hamilton syringe. After SDS-PAGE, pulldown was either visualized by performing an immunoblot (see 3.3.4) or a silver staining (see 3.3.6).

3.3.8 Chromatin immunoprecipitation (ChIP)

Chromatin immunoprecipitation (ChIP) is used to detect the binding of a protein of interest to a specific region of DNA. ChIP constist of five steps: fixation, fragmentation, enrichment (IP), crosslink reversion and qPCR. The different steps are described in detail below.

Formaldehyde fixation

To fix proteins to the DNA, cells were incubated with 1 % formaldehyde for different times depending on the employed fragmentation method: 5 min for fragmentation with the Ultrasonicator (Covaris) or 10 min with sonication. Therefore 405 µl 37 % formaldehyde were added directly to 15 ml cell culture medium on a 15 cm cell

culture dish and incubated under smooth shaking. The fixation was stopped with 2 ml 1 M Glycine (5 min, RT) and cells were washed twice with ice cold 1x PBS. Cells were scraped off the plate in 2 ml PBS containing protease, phosphatase inhibitors and 1 mM PMSF and transferred into a 15 ml Falcon tube. The cells were pelleted for 20 min at 1,500 rpm at 4 °C. Supernatant was aspirated and either shock frozen in liquid nitrogen to store at -80 °C or to further proceed as described below.

Chromatin isolation and Fragmentation

To isolate chromatin, a two-step lysis was performed. First, the cells were lysed in Lysis Buffer I (see 2.14) to isolate the nuclei, incubated for 20 min on ice and centrifuged for 15 min at 1,500 rpm at 4 °C. Second, the chromatin was isolated by using Lysis Buffer II for at least 10 min on ice. Both buffers contained freshly added protease and phosphatase inhibitors. Afterwards the chromatin was fragmented to obtain a fragment size between 150-300 bp by using either a probe sonicator (total duration, 20 min with 10 s pulses and 45 s pausing) or the ultrasonicator (20 min). After fragmentation the chromatin size was determined as described below (see 3.3.8).

Chromatin size control

To control fragmentation efficiency, 20 µl chromatin was mixed with 280 µl TE buffer containing 160 mM NaCl and 20 µg/ml RNase A, incubated for 1 h at 37 °C followed by the de-chrosslinking step at 65 °C overnight. Subsequently, 5 mM EDTA and 200 µg/µl Proteinase K were added and chromatin was purified by phenol chloroform extraction followed by precipitation with 100 % EtOH and 30 µl NaAc (stock: 3 M, pH 5.2), and washed with 70 % EtOH. The pellet was air dried and resuspended in 20 µl ddH_2O. 10 µl chromatin were mixed with 6x DNA loading dye and loaded on a 2 % agarose gel. After chromatin size control, the chromatin was centrifuged for 30 min at 14,000 rpm at 4 °C. The supernatant was either shock frozen in liquid nitrogen to store at -80 °C or further processed as described below.

Coupling of antibodies to Dynabeads

30 µl magnetic Dynabeads (protein A and protein G, 1:1) were coupled with an antibody against the protein of interest. Beads were washed three times with 1 ml ChIP Blocking solution (5 mg/ml BSA in PBS). Beads were resuspended in 500 µl ChIP Blocking solution and 3 µg antibody was added. The mixture was placed on a rotating wheel and incubated for at least 6 h at 4 °C. The beads were washed three times with ChIP Blocking Solution and resuspended in 30 µl ChIP Blocking Solution per IP.

Immunoprecipitation

Before starting the IP, 1 % input was collected. The washed and antibody-coupled Dynabeads were added to the chromatin and the IP was incubated on a rotating wheel for at least 6 h at 4 °C.

Washing and elution of chromatin

Beads were transferred into a fresh reaction tube and washed three times first, with Wash Buffer I, second, with Wash Buffer II, and third, with Wash Buffer III. These buffers contain different salt concentrations. To remove the salt-containing buffers completely, the beads were washed once with TE buffer and the reaction tube was changed.
The chromatin was eluted twice with 150 µl Elution Buffer by incubating for 15 min on the rotating wheel at room temperature.

Decrosslinking and DNA purification

To the eluted samples 9.6 µl 5 M NaCl, 13 µl Tris (pH 8) and 2 µl RNaseA (stock 10 µg/ µl) were added. The reaction was incubated for 1 h at 37 °C followed by 65 °C overnight while smooth shaking. 5 µl proteinase K (stock 10 µg/ µl) were added and incubated for 2 h at 45 °C. The DNA was purified by phenol chloroform extraction. 300 µl phenol-chloroform-isoamyl-alcohol was added to each sample, the samples were

vortexed for 5 min and centrifuged for 10 min at 14,000 rpm at room temperature. The upper phase (300 µl) was transferred into a new reaction tube containing 1 µl GlycoBlue. 900 µl 100 % EtOH and 3 µl 30 M NaAc (pH 5.2) was added, mixed and incubated for at least 30 min at -20 °C. To pellet DNA, samples were centrifuged for at least 30 min at 14,000 rpm at 4 °C. The DNA pellet was washed twice using 70 % EtOH, air dried and solubilized in 250 µl. For quantitative real time PCR, 2.5 µl or 5 µl of chromatin were used per reaction as described in 3.2.13.

3.4 Next generation sequencing

3.4.1 ChIP for deep sequencing

For ChIP sequencing the protocol was performed as described in 3.3.8 but some changes were made. For cell culture 50 M cells per IP were used. For the IP step 100 µl Dynabeads and 10-15 µg antibody were used and the DNA pellet was solubilized in 30 µl ddH_2O. 3 µl of this DNA was mixed with 130 µl ddH_2O, to test efficiency of the ChIP as described in 3.2.13. 1 µl was used to determine dsDNA content of the IP as described in 3.2.9. Resulting from the PicoGreen measurment 1.5-10 ng DNA were used to perform library prep as described in 3.4.4. To perform spike-in ChIP sequencing, also termed as ChIP-Rx, 10 % fixed mouse cells (see 3.3.8), such as NIH-3T3 for ultrasonication or T-cells for sonication, were added to the human cells at the step of Lysis Buffer I.

3.4.2 mRNA Isolation, fragmentatiuon and cDNA synthesis for RNA sequencing

To isolate RNA for RNA sequencing, total RNA was isolated using RLT buffer containg 10 µl β-mercaptoethanol per ml. Afterwards, RNeasy® Mini Columns as described in 3.2.10 were used. RNA concentration was determined using Nanodrop1000. Quality of RNA was measured using either Experion™ Automated Electrophoresis System (Biorad) (see 3.2.9) with the RNA standard sense Chips according to the manufacturer's protocols were used or the Fragment Analyzer using

the standard sensitivity RNA kit following the manfucaturer's protocol (Agilent, 3.2.9). 1 µg of RNA with a RNA quality indicator (RQI) of at least 9.5 was used for library preparation. RQI can vary between 1 (degraded RNA) and 10 (intact, high quality RNA). To further isolate mRNA from total RNA, the NEBNext® Poly(A) mRNA Magnetic Isolation Module according to the manufacturer's instructions was used. The first step of this protocol is an oligo$(dT)_{15}$ purification step which selects for non degraded, intact, full length mRNA as those beads bind the poly-A tail of the mRNA. For further purification steps during RNA library preparation (see 3.4.4), Agencourt AMPure XP Beads (Beckman Coulter) were used after cDNA preparation.

3.4.3 BLISS and BLISS8

In this section Breaks Labeling *In-situ* and sequencing (BLISS) is described. The library preparation was performed as described in 3.4.4. BLISS was performed in triplicates.

Seeding and fixation of cells in a 24-well plate

For BLISS or BLISS8 sequencing, an adequate number of cells, depending on the experiment, was plated on a 24-well plate, so that at the time of fixation the cell density was around 80 %. Cells were fixed for 10 min at room temperature by adding a final concentration of 4 % Paraformaldehyde. For non-adherent K562 cells, shortly before fixation, cells were centrifuged for 3 min at 400 rpm . The plate was fixed while centrifuging for 10 min at 400 rpm at room temperature. Cells were washed three times with 1x PBS. Fixed cells could either be kept for several weeks at 4 °C, the plate edges covered with parafilm, or further processed as described below.

Cell lysis

Cells were lysed in two steps. First, cells were washed with 1x PBS and lysis buffer 1 (LB1) was added for 1 h at 4 °C to isolate the nuclei. Second, the cells were washed once with 1x PBS to remove the buffer, and LB2 was added for 1 h at 37 °C

to permeabilize the nuclei. Afterwards, the nuclei were washed twice with 1x PBS, either directly continued with blunting or followed with AsiSI digestion for double strand break (DSB) normalization (BLISS8).

In-situ AsiSI digestion for BLISS8

AsiSi digestion was performed for normalization of the DSB. The restriction enzyme AsiSI cuts DNA at a known sequence introducing DSB. Samples were covered with 1x CutSmart® buffer at room temperature. To equilibrate the buffer, this step was repeated twice. 150 µl of the following digestion master mix were added to one 24-well of the plate containing the isolated and permibilized nuclei:

Substance	**1x [µl]**
CutSmart® 10x	15
AsiSI	3
ddH_2O	132
Σ Volume	150

After adding the mix, the 24-well plate was sealed with parafilm and incubated for 1-2 h at 37 °C.

In-situ double strand break blunting

To blunt the DSB, in order to make the subsequent ligation possible, the NEB Quick Blunting™ Kit was used. To wash off the AsiSI mix the wells were washed three times with CutSmart® buffer. 150 µl of the following blunting master mix were added to the 24-well:

Substance	1x [µl]
Blunting buffer 10x	15
BSA (50 mg/ml)	0.3
dNTPs (1 mM)	15
Blunting enzyme mix	6
ddH_2O	112.7
Σ Volume	150

The plate was sealed with parafilm and incubated for 1 h at room temperature.

In-situ ligation

To prepare the adapters which will be ligated to label the double strand breaks, 10 µM concentrated oligo pairs were annealed. Therefore, the oligos were incubated for 5 min at 95 °C followed by gradual cool down to 25 °C within 45 min (1.55 °C per min) in a PCR thermal cycler.
After incubation time, blunting mix was removed from the wells and washed three times with 1x CutSmart® buffer. The buffer was exchanged to 1x T4 Ligase Buffer and incubated for 5 min at room temperature. 144 µl of the following ligation master mix were added to the wells:

Substance	1x [µl]
T4 ligase buffer 10x	15
BSA (50 mg/ml)	3
T4 ligase	1.5
ddH_2O	124.5
Σ Volume	144

6 µl of the annealed adapters were added. Per condition one specific adapter was used (e. g. adaper A1 in three wells of the control condition). The ligation was incubated for 16-18 h at 16 °C.

Removal of unligated adapters and extraction of genomic DNA

After ligation, the unligated adapters were removed by washing three times with high salt wash buffer (HSW) for 1 h at 37 °C. To remove the high salt concentration, the wells were washed with 1x PBS followed by a washing step with nuclease-free water. The genomic DNA was extracted by adding 100 µl DNA extraction buffer containing 10 µl proteinase K (10 mg/ml) to the wells. The nuclei were collected in a reaction tube by scraping them directly from the well. As the different conditions were ligated with different adapters containing a sample bar code, they were pooled in one reaction tube. From this step onwards three technical library preps of the same conditions were performed. The reaction tubes were placed in a thermo shaker and incubated at 55 °C while shaking overnight.

Fragmentation and concentration of DNA

The genomic DNA was extracted by using phenol chloroform extraction followed by isopropanol precipitation. 1:1 volume of phenol-chloroform-isoamyl alcohol was added to the genomic DNA, vortexed and centrifuged for 10 min at 14,000 rpm at room temperature. The upper phase, containing the DNA, was transferred into a new reaction tube containing 1 µl GlycoBlue. 100 % isopropanol was added in a ratio of 3 to 1 (v/v). To precipitate DNA, the sample was placed at -20 °C for at least 30 min. The DNA was pelleted for 30 min at 14,000 rpm at 4 °C. After aspiration and discarding the supernatant, the DNA pellet was washed twice with 70 % EtOH, air dried and solubilized in 50 µl nuclease-free water. The DNA was fragmented for 1-2 min with the ultrasonicator (Covaris) to obtain a fragment size between 300-500 bp.
To concentrate the fragmented DNA, Ampure XP beads (Beckman Coulter) or SPRI (Beckman Coulter) beads were used. A ratio of 0.8x beads was added to the suspension at room temperature and mixed by pipetting up and down for ten times. The beads were incubated at room temperature for 5 min and placed on a magnetic rack for 5 min until the beads were completely attached to the magnet. Supernatant was aspirated and discarded to wash the beads twice with ice cold 80 % EtOH. After complete removal of the EtOH, beads were air dried for 5 min at room temperature.

The sample was removed from the magnetic rack, the beads resuspended in 10 µl nuclease-free water and incubated for 5 min at room temperature. The sample was placed in the magnetic rack for 5 min until the beads were attached to the magnet. 8 µl supernatant containing the concentrated DNA were transferred into a new reaction tube. 0.5 µl DNA were diluted with 4 µl nuclease-free water and measured on the Fragment Analyzer following the manufacturer's protocol (HS NGS Fragment Kit (1-6,000bp)).

In vitro transcription

After quality control run on the Fragment Analyzer, *in vitro* transcription (IVT) was performed. To enrich the DSB sequence from the total genomic DNA, the ligated adaper contains a T7 promoter. Thanks to the T7 promoter sequence contained in the adaptors, IVT was performed to selectively convert the DSB sequences to RNA , therefore enriching them over the total genomic DNA. The MEGAscript® kit (Invitrogen) was used preparing the following reaction mix:

Substance	**1x [µl]**
concentrated gDNA	7.5
rNTP mix	8
T7 polymerase buffer 10x	2
T7 polymerase	2
RiboLock RNase Inhibitor	0.5
Σ Volume	20

The mix was incubated for 14 h at 37 °C in a thermo cycler with the lid set to 70 °C. After incubation, the DNA template was degraded adding 1 µl TURBO™ for 15 min at 37 °C. The remaining RNA product was purified as described in 3.4.3.

RNA clean up

The RNA containing the sequence of the DSB DNA as well as the sequences of the adapters, UMIs and the sample barcode, were purified using Agencourt RNAClean

XP beads (Beckman Coulter) for two-sided size selection. The volume of the IVT product was adjusted to 50 µl with nuclease-free water and beads were added with a ratio of 0.4x by pipetting up and down for ten times. The mixture was incubated for 10 min at room temperature and placed for 5 min on a magnetic rack. The supernatant was transferred into a new reaction tube and the beads were discarded. 0.2x beads were added to the supernatant, incubated for 10 min and placed on the magnetic rack until the beads were attached to the magnet. The supernatant was aspirated and removed. The beads were washed twice with ice cold 70 % EtOH. After complete removal of the EtOH, the beads were air dried for 10 min and the RNA was eluted by resuspending the beads in 5.7 µl nuclease-free water, incubating for 5 min at room temperature and placing the sample on a magnetic rack until all beads were attached to the magnet. 5.5 µl were transferred into a new reaction tube. 1.7 µl nuclease-free water were mixed with 0.5 µl to determine the RNA concentration by using the Fragment Analyzer following the manufacturer's protocol as described in 3.2.9.

3.4.4 Library Preparation

This section describes the different library preparations of the different sequencing experiment. As sequencing was performed on the NextSeq500 from Illumina®, all kits and protocols were purchased from NEB®.

NEBNext® Ultra RNA Library Prep Kit for Illumina®

RNA library preparation was performed according to the manufacturer's protocol. To summarize, mRNA was isolated using NEBNext Oligo $d(T)_{25}$, and total RNA was fragmented and primed. RNA was transcribed into cDNA using ProtoScript II Reverse Transcriptase and double stranded cDNA was purified using Agencourt AMPure XP beads. Before performing Adapter ligation (1:10 diluted) and bead-based size selection, an end preparation step was included. Libraries were enriched using PCR with 12 cycles of amplification. Libraries were purified using beads. Final DNA library quantification and size was determined using the Experion as described in 3.2.9.

NEBNext® ChIP-Seq Prep Master Mix Set for Illumina®

Input material was ranging between 0.5 ng to 10 ng per IP and condition. Libraries were prepared using the instruction manual of NEBNext® ChIP-Seq Prep Master Mix Set. In short, 3' end of DNA were repaired followed by dA tailing and Adapter ligation (1:30 diluted). After each step a column based purification was performed using MinElute® PCR Purification kit (Qiagen®). Before final library PCR enrichment, DNA was size selected on an agarose gel and purified with the MinElute® Gel Extraction kit (Qiagen®). Libraries were amplified with PCR with a range of 14-18 cycles depending on the input material and the antibody used. Final libraries were purified using MinElute® PCR Purification kit by eluting in 20 µl 0.3x EB buffer (Qiagen). 1-2 µl of final libraries were used to quantifiy and determine the size either with the Experion or the Fragment Analyzer as described in 3.2.9.

NEBNext® Ultra II DNA Library Prep for Illumina®

If the ChIP seq libraries were not described as above, they were prepared as described in this subsection following the manufacturer's instructions. The single steps remained the same, but a two sided size selection was performed using SPRI beads before PCR enrichment of the libraries. A beads ratio of 0.5x followed by 0.25x aiming for an expected final library size of 270 bp (including insert, adapter and primer) when starting with an input size of around 150 bp was used. Number of cycles used for the final library PCR amplification was determined using qPCR. 9 µl of the 50 µl final PCR mix were aliquoted and pipetted together with 1 µl 10x SYBRGreen on a 96-well plate. Standard qPCR program was started and number of cycles was determined empirically. The turning point towards the exponential phase of the curve from the multiple component plot determined the number of cycles. After final PCR enrichment, libraries were purified using SPRI beads and eluted in 30 µl nuclease-free water. Libraries were usually diluted 1:4 (v/v) in nuclease-free water and size distribution and quality of the libraries were determined using Fragment Analyzer as described in 3.2.9.

NEBNext® Multiplex Small RNA Library Prep Kit for Illumina®

The following steps describe the library preparation steps for BLISS and BLISS8. It is based on the Small RNA Library Prep Kit for Illumina® with some adaptations.

RA3 adapter ligation The RA3 adapter was freshly diluted from 15 µM to 3 µM, 1 µl added to the 5 µl purified RNA as described in 3.4.3 and placed for 2 min at 70 °C with the lid set at 70 °C in a thermo cycler. The reaction was placed on ice and the following mix was prepared:

Substance	**1x [µl]**
RNA including RA3 adapter	6
T4 RNA ligase buffer 10x	2
T4 RNA ligase 2, truncated	1
RNaseOUT™	1
Σ Volume	10

The reaction was incubated for 1 h at 28 °C in a thermo cycler with the lid set at 30 °C.

Reverse Transcription After RA3 adapter ligation, the mix was placed on ice, 3.5 µl nuclease-free water were added to the mix as well as 1 µl of RTP primer and the reaction was placed for 2 min at 70 °C on a thermo cycler as described in 3.4.4. After incubation, the following reaction was pipetted to start the reverse transcription (RT):

Substance	**1x [µl]**
RA3 ligated RNA including RTP	14.5
FS buffer 5x	2
12.5 mM dNTP mix	0.5
100 mM DTT	1
SuperScript® III	1
RNaseOUT™	1
Σ Volume	20

The RT reaction was incubated for 1 h at 50 °C in a thermo cycler with the lid set at 70 °C. To inactivate the enzyme, the reaction was incubated for 15 min at 30 °C. After incubation the sample were either stored at -20 °or further processed.

Library indexing and amplification After RT the following reaction was mixed for final library amplification:

Substance	**1x [µl]**
10 µM indicated RPI	2
10 µM RP1	2
NEBNext® 2X PCR Mix	25
Nuclease free water	1
Σ Volume	50

To determine the PCR cycle number, 9 µl of the final library amplification mix were mixed with 1 µl 10x SYBRGreen and transferred into a 96-well PCR plate. The qPCR was performed as described in 3.2.13. The turning point towards the exponential phase of the curve from the multiple component plot determined the number of cycles.
Before starting the PCR, 9 µl nuclease-free water were added to the library amplification mix to obtain 50 µl.

The PCR was performed as described below.

Cycle step	Temp.	Time	Cycles
Initial denaturation	98 °C	30 s	1 x
Denaturation	98 °C	30 s	
Annealing	60 °C	10 s	n x
Extension	72 °C	30 s	
Final extension	72 °C	10 min	1x
Hold	4 °C	∞	1x

Library clean up For cleaning up the cDNA library, the protocol was performed as described in 3.4.3. To elute library 20 µl nuclease-free water were added and after incubation on the magnetic rack 17-18 µl of library were transferred into a new reaction tube. 1 µl of final library was mixed 1:4 (v/v) with nuclease-free water and measured on the Fragment Analyzer as described in 3.2.9 following the manufacturer's protocol.

3.4.5 Sequencing data analysis

According to the manufacturers instructions, sequencing libraries were subjected to Illumina NextSeq 500 machine by Elmar Wolf, Carsten Ade or Apoorva Baluapuri. Illumina's FASTQ Generation software v1.0.0 (NEXTSeq500 sequencing) was used for base calling. High quality PF-clusters were selected to further analyse the data and quality control was measured using FastQC.

ChIP Sequencing analysis

ChIP sequencing samples were mapped to the human hg19 genome using Bowtie2 either with default parameters or allowing one mismatch ((Langmead and Salzberg, 2012). ChIP sequencing samples were normalized to the number of reads in the smallest sample. Input was merged of all different conditions from the experiment. For ChIP-Rx, sequencing samples were additionally mapped to the murine mm10 genome. Spike-in normalized reads were calculated as follows:

$$spike-in\ normalized\ reads = min(mapped\ reads_{mm10}) * \frac{mapped\ reads_{hg19}}{mapped\ reads_{mm10}} \tag{3.8}$$

Density and metagene plots were generated using ngs.plot.r (Shen et al., 2014). PlotProfile programm from the Deep Tools suite were used to produce non-scaled density plots (Ramírez et al., 2016). Read-normalized MYC ChIP-seq bam files were processed by using BEDtools intersectBed program to generate MYC-reads in promoter or enhancer regions (Quinlan and Hall, 2010). Enhancer regions were defined as previously described in Walz et al. (2014), promoter regions were defined as 1 kb before or after TSS and MYC-activated and -repressed genes were derived from Lorenzin et al. (2016). Analyses of ChIP-seq samples were either performed by Peter Gallant, Daniel Solvie or Theresa Endres.

RNA Sequencing analysis

RNA-seq samples were mapped to hg19 using Bowtie and the samples were normalized to the number of mapped reads on the smallest sample. The "summarizeOverlaps" function of R package "GenomicAlignments" was used to count the reads per gene. Thereby "union"- mode and Ensembl genes were used. All genes with a mean count smaller than 1 were removed to exclude unexpressed or weakly expressed genes. EdgeR was used to call differentially expressed genes. Benjamini-Hoechberg was used for calculating p-values adjusted to multiple testing. To generate bin plots in R, 13,337 genes with significant expression in U2OS cells were grouped into 23 bins each composed of 600 genes according to their inducibility upon MYC overexpression (Walz et al., 2014). RNA sequencing analysis was partly performed by Peter Gallant and Theresa Endres.

BLISS and BLISS8 Sequencing analysis

BLISS and BLISS8 analysis was performed by Daniel Solvie and Peter Gallant. BLISS or BLISS8 samples were multiplexed on the basis of their condition specific barcodes

using UMItools (Smith et al., 2017) allowing 1 mismatch in the barcode. Then the samples were separately mapped to hg19 as described above (Smith et al., 2017). Samples of biological triplicates were merged and collectively processed. To remove sites of high variance in mappability commonly found in specific regions (Amemiya et al., 2019), samples were filtered against an ENCODE Blacklist file using BEDtools intersectBed program (Quinlan and Hall, 2010). After filtering, absolute quantification of DSB was performed by removing artifacts introduced by PCR and duplicated reads were identified based on their UMI. Default parameters of UMItools (Smith et al., 2017) were used to group and deduplicate the reads. To normalize BLISS8 to the *in situ* AsiSI restriction sites as described in 3.4.3, hg19 genome was *in silico* digested and 1,123 predicited restriction sites were counted. Per sample, deduplicated reads (dedup reads) in AsiSI specific sites (AsiSI site) were counted using countBAMInGRange from the R package exomeCopy. AsiSI sites without mapped reads across all conditions in the respective experiment were dropped. The smallest read number of those AsiSI sites ($\min(\text{reads}_{\text{AsiSI site}})$) was used for normalization of each sample as follows:

$$BLISS8\ normalized\ reads = \frac{min(reads_{AsiS\ site})}{reads_{AsiSI\ site}} * reads_{DSB+AsiS\ site} \tag{3.9}$$

The samples were subsequently randomly subsampled to the calculated number of deduplicated reads. Density plots were generated using the R package metagene2 with the parameters 'ChIPseq', 150 bp read extension and 50 bins to smoothen the curve. ExomeCopy R package was used to generate promoter counts whithin +/- 500 bp of the TSS which were then divided by the total number of genes within the gene set used. Gene sets were generated from RNA sequencing data using RPKM (data set 'gene expression', top n=3,177, bottom n=1,814) and logCPM (data set 'MYC response', activated n=340, repressed n=296) or from RNAPII ChIP-Rx sequencing data using the Polymerase II occupancy within the gene body versus the corresponding promoter region (data set 'pausing', paused n=3,414, non-paused n=671). Heterochromatic regions in U2OS were defined for H3K9me3 (Tasselli et al., 2016), H3K4me3, H3K27me3 (Easwaran et al., 2012), H3K79me2 (Clouaire et al., 2018), H3K36me3 (Wen et al., 2014), H3K4me1, H3K27ac (Walz et al., 2014) by

using a 16-state model (Ho et al., 2014) with chromHMM.
Subsets of genes for U2OS data were derived from the RNA seq data from this thesis as well as published ChIP Seq data (Lorenzin et al., 2016):

- 3,000 most/least expressed genes passing the minimal expression threshold;
- MYC-bound: 7,684 genes that are expressed in U2OS according to the RNAseq data and contain a MYC-binding site in the region between -1,500 and +500 relative to the transcription start site, MYC-bound: 10,013 expressed genes lacking such a MYC binding site
- E box MYC bound: canonical "CACGTG" sequence within 100 nucleotides of their MYC-binding summit producing sub-groups of 1,169 and 6,515 genes.

4 Results

4.1 MYC is directly interacting with PAF1 complex and DSIF

MYC interacts with several proteins known to regulate different steps of the transcriptional cycle (Baluapuri et al., 2019; Büchel et al., 2017; Heidelberger et al., 2018; Kalkat et al., 2018). Two complexes identified in the interactomes are DSIF represented by SPT5 and the PAF1 complex (PAF1c) represented by the subunits CDC73 and CTR9. Co-IPs from HeLa cells in the presence of the proteasome inhibitor MG132 also revealed an interaction between MYC and the PAF1c subunits CTR9 and CDC73 (Jaenicke et al., 2016).

Since these assays were performed using cell lysates, an indirect interaction of those complexes with MYC could not been ruled out. To show a direct interaction between DSIF or PAF1c with MYC, *in vitro* pulldown assays of recombinant proteins were performed. A short version of MYC spanning from amino acid 1-163, and two different MYC mutants either lacking MYCBox I (ΔMBI) or MYCBox II (ΔMBII) were used. A scheme highlighting the different MYC constructs is shown in figure 4.1.

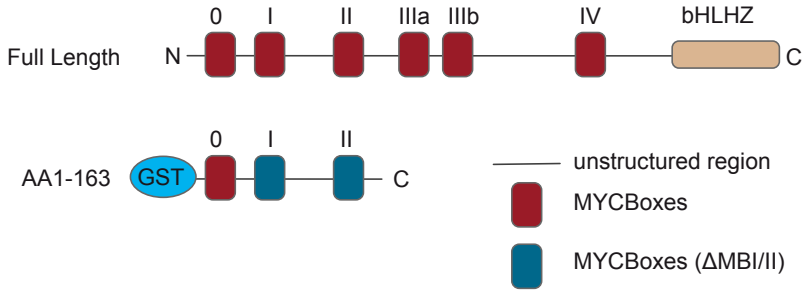

Figure 4.1: Diagram of MYC protein structure.
Top: Diagram of full lentgh MYC spanning from N-terminus (N) until C-terminus (C). MYCBoxes (MB) are highlighted as red boxes and labelled as 0, I, II, IIIa, IIIb and IV. Position of basic Helix-Loop-Helix Leucin Zipper (bHLHZ) is shown as a beige box. Unstructured regions are represented as black lines.
Bottom: Diagram shows the MYC construct used for pulldown experiments. Construct is spanning from amino acid 1-163 (AA1-163) and contains a GST-tag (GST) at the N-terminus. MYCBoxes deleted for the deletion mutants ΔMBI or ΔMBII are highlighted as dark blue boxes. This figure was published in similar form in Endres et al. (2021).

On the one side, a short version of MYC spanning from amino acid 1 till 163 or the two different MB mutants ΔMBI or ΔMBII containing a GST-tag and GST alone as a control were expressed in *E. coli*, purified and coupled to sepharose beads (see 4.2 A, lane "GST-MYC" and "GST"; 4.2 B, lane "GST-MYC" and "GST"). On the other side, recombinant DSIF and PAF1c, lacking the RTF1 subunit, expressed and isolated from insect cells, were kindly provided by Seychelle Vos (PAF1c see figure 4.2 A, lane "PAF1c"; DSIF see figure 4.2 B, lane "DSIF").

Purified GST-tagged MYC or GST alone were subjected on a SDS-PAGE and Coomassie staining (see figure 4.2 A, lane "GST-MYC" and "GST") or silver staining (see figure 4.2 B, lane "GST-MYC" and "GST") was performed. GST alone showed a band of the expected size and GST-MYC showed a double band of which the upper band was of the expected size and the lower band a degradation product. The recombinant PAF1c shown on the Coomassie staining of the SDS-PAGE of figure 4.2 A (lane "PAF1c") showed five distinct bands of the expected sizes of the different subunits of the complex: CTR9, LEO1, PAF1, CDC73 and SKI8. The silver staining of figure 4.2 B (lane "DSIF") revealed a clear band of the expected size of SPT5. The subunit SPT4 of DSIF expected to be visible at around 15 kDa was not detectable.

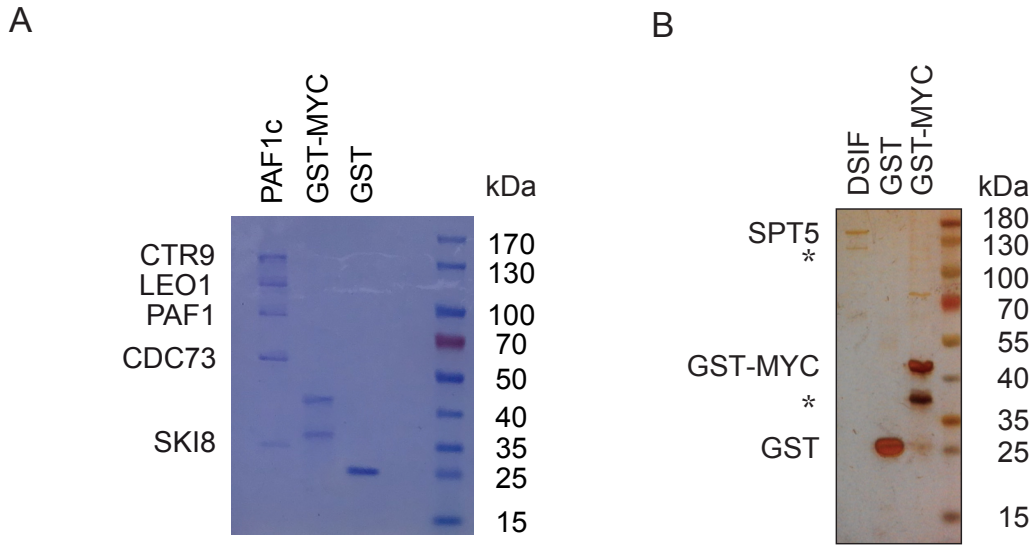

Figure 4.2: Input of *in vitro* pulldown experiments.
A) Coomassie staining showing 10 % input used for *in vitro* pulldown assay of GST-MYC and GST with PAF1c. Recombinant PAF1c consisting of the 5 subunits CTR9, LEO1, PAF1, CDC73, SKI8 but lacking RTF1 subunit was purifed by Seychelle Vos. GST-MYC and GST were overexpressed in *E. coli* and subsequently isolated by using glutathion sepharose beads.
B) Silver staining showing 10 % input used for *in vitro* pulldown assay of GST-MYC and GST with DSIF. Recombinant DSIF consisting of SPT4 and SPT5 was purified by Seychelle Vos. Silver staining of SDS-PAGE was performed by Julia Hofstetter. * represents a unspecific band. This figure was published in similar form in Endres et al. (2021) and Baluapuri et al. (2019).

GST pulldown of GST-tagged MYC with PAF1c or DSIF was performed and the eluate of the immunoprecipitation was subjected on a SDS-PAGE. The presence of GST-MYC or GST was confirmed with immunoblot analysis (see "Input", "GST-MYC" and "GST" of figure 4.3 A and B). The immunoblot analysis revealed that PAF1c subunits CTR9, LEO1, PAF1 and CDC73 as well as the DSIF subunit SPT5 were co-immunoprecipitated with GST-MYC but not GST alone (see figure 4.3 A,"IP PAF1c", "GST-MYC" and "GST" as well as figure 4.3 B,"IP DSIF", "GST-MYC" and "GST").

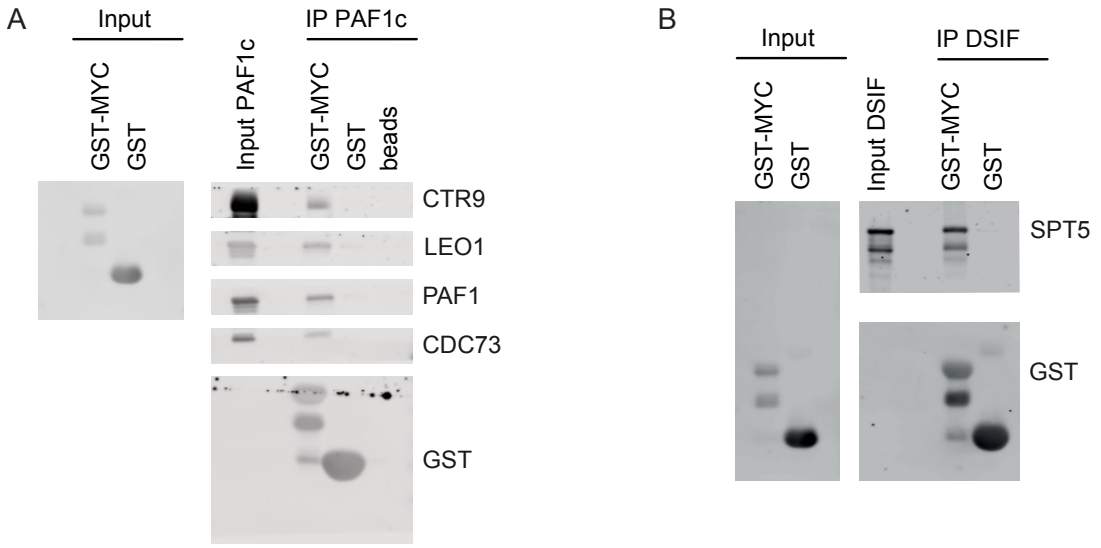

Figure 4.3: PAF1c and DSIF are interacting directly with MYC.
A) Immunoblot of *in vitro* pulldown assay of GST-MYC with PAF1c. Pulldown was eluted and subjected on a SDS PAGE. Shown is a representative experiment of biological triplicates.
B) Immunoblot of *in vitro* pulldown assay of GST-MYC with DSIF. Pulldown was performed as described in A. (n=1)
This figure was published in similar form in Baluapuri et al. (2019) and Endres et al. (2021).

Jaenicke et al. (2016) showed that phosphorylated MYCBox I of MYCN peptides leads to an enhanced transfer of PAF1c from MYC onto RNAPII.

To further analyse if MYCBox I or II play a role in the interaction between MYC and PAF1c, GST-pulldown assays were performed with MYC constructs of ΔMBI or ΔMBII.

The eluates of the immunoprecipitation were subjected to a SDS-PAGE and further analysed by immunoblotting or silver staining. Figure 4.4 A and B (lane "Input PAF1c", "Supernatant") show that same amounts of PAF1c were used for the immunoprecipitation. The immunoblot analysis revealed, that wt MYC and the two MYCBox deletion mutants ΔMBI and ΔMBII showed interaction with PAF1c subunits as shown in figure 4.4 A (lane "GST-MYC", "GST-ΔMBI" and "ΔMBIII") but not with GST alone (see figure 4.4 A, lane "GST"). Silver staining of a biological replicate revealed the same results as the immunoblot analysis (4.4 B).

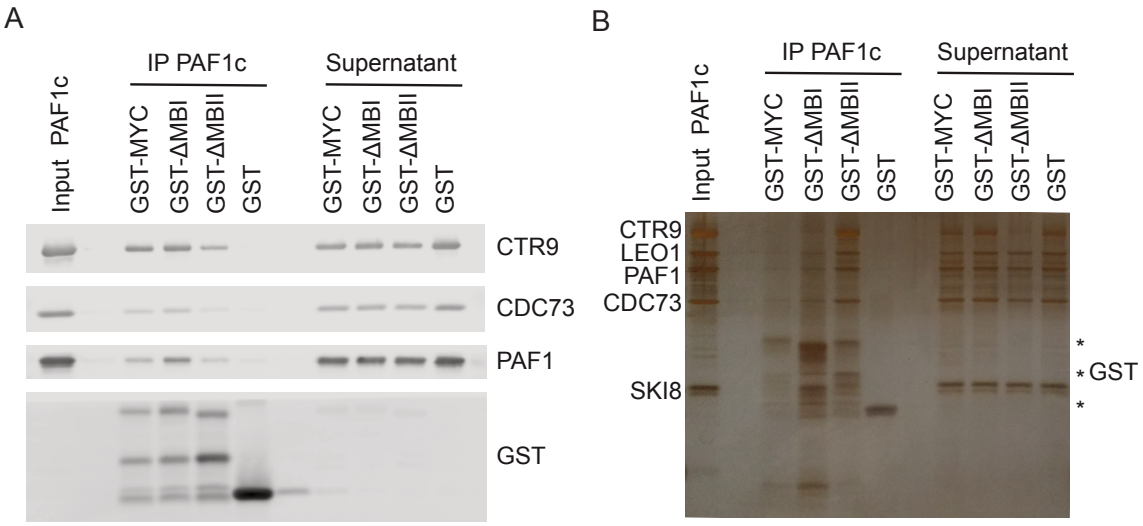

Figure 4.4: PAF1c interacts directly with MYC independent of MYCBox I or II.
A) Immunoblot of *in vitro* pulldown assay of GST-MYC and deletion mutants ΔMYCBox I and ΔMYCBox II with PAF1c. Pulldown was eluted, subjected on a SDS PAGE and visualized with immunoblot.
B) Silver staining of *in vitro* pulldown assay of GST-MYC and deletion mutants ΔMYCBox I and ΔMYCBox II with PAF1c. Pulldown was performed as described in A.
Shown are representative experiments of biological triplicates.
Panel A of this figure was published in similar form in Endres et al. (2021).

Taken together, the pulldown assays show a direct interaction of PAF1c and DSIF with MYC. Furthermore, MYCBox I or II do not appear to be necessary for the interaction with PAF1c.

4.2 PAF1c enhances association of MYC with active promoters

To further determine the role of the direct interaction between the elongation factor PAF1c and MYC, U2OS cells expressing a MYC Tet-ON system were used to introduce a constitutive active knockdown of the two subunits *CDC73* and *CTR9*. These subunits were also found in the MYC or MYCN interactome analysis of Baluapuri et al. (2019) and Büchel et al. (2017). To knockdown the subunits of the PAF1c, shRNAs bearing sequences predicted to target the named subunits in Fellmann et al. (2013) were used. The underlying mechanism is the post-transcriptional RNA interference (RNAi) (Fellmann et al., 2013).

Cells were infected with the pGIPZ vector containing either a non targeting control or sequences targeting either *CTR9* or *CDC73*. 48 h post-infection, the cells were selected for successful infection with puromycin for 24 h and cells were harvested 96 h post infection.

To determine knockdown efficiency, immunoblot analysis was performed. Upon knockdown of *CDC73*, CDC73 protein levels were reduced by 80 % but also CTR9 levels dropped by 20 % compared to the control (see figure 4.5 A lane "NTC", "shCDC73" and figure 4.5 B, "CDC73"). Induction of shCTR9 resulted in a 80 % reduced protein level of CTR9 and CDC73 also showed 20 % less protein compared to control (see figure 4.5 A lane "NTC", "shCTR9" and figure 4.5 B, "CTR9"). Both knockdowns of the subunits of the complex led to a MYC protein reduction by 20 % compared to the control cells (see figure 4.5 A and figure 4.5 B, "MYC").

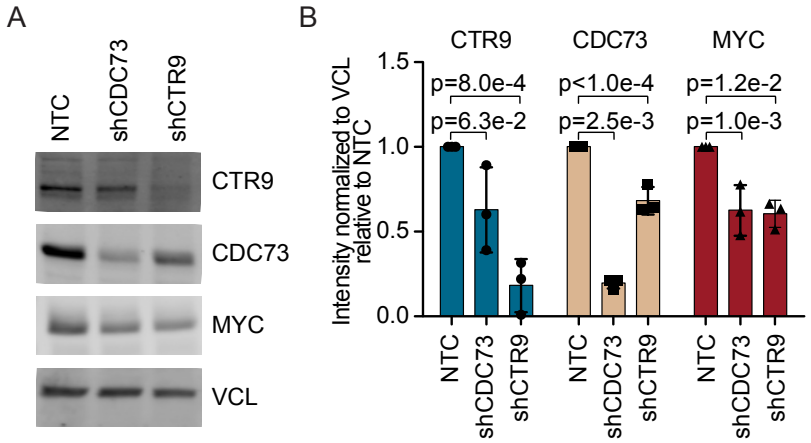

Figure 4.5: Knockdown efficiency of CDC73 or CTR9 in U2OS using constitutively active pGIPZ vector.
A) Immunoblot of lysates from U2OS MYC Tet-ON cells expressing the lentiviral pGIPZ vector including either a non targeting control (NTC) or shRNA sequences targeting *CDC73* (shCDC73) or *CTR9* (shCTR9). Cells were harvested 96 h post infection. Shown is a representative experiment of biological triplicates.
B) Quantification of the immunoblot shown in panel A. Shown is the mean of biological triplicates. Error bars show the S.D. of biological triplicates. P values were calculated using unpaired t-test.
This figure was published in similar form in Endres et al. (2021).

After successfull validation of the knockdown efficiency in this cell system, MYC ChIP with reference exogenous genome (ChIP-Rx) sequencing was performed (Orlando et al., 2014). MYC ChIP sequencing was used to analyze the changes MYC binding

on chromatin after PAF1c depletion. Therefore, the fragments of chromatin, after successfull pulldown with a specific MYC antibody followed by library preparation, were sequenced. Cells were treated as described for figure 4.5.

A density plot of a ChIP-Rx experiment revealed that knockdown of the PAF1c subunits *CTR9* or *CDC73* leads to a reduced binding of MYC at promoters (see figure 4.6 A, "shCTR9", "shCDC73", dark blue and red line) compared to control (see figure 4.6 A, "NTC", light blue line). Specific enrichment of DNA fragments bound by MYC was validated by comparing the different conditions with the input signal (see figure 4.6 A, "input", beige line). MYC binding at specific promoter region could be validated by inspection of different promoters. Figure 4.6 B shows occupancy at the *NPM1* locus. The MYC binding at the promoter region of the *NPM1* locus confirmed that MYC binding is reduced upon knockdown of either *CTR9* (figure 4.6 B, "shCTR9") or *CDC73* (figure 4.6 B, "shCDC73") compared to the control (figure 4.6 B, "NTC"). Specific enrichment is validated by comparing input signal with NTC or knockdown conditions (see figure 4.6 B, "Input" vs. "NTC", "shCTR9", "shCDC73").

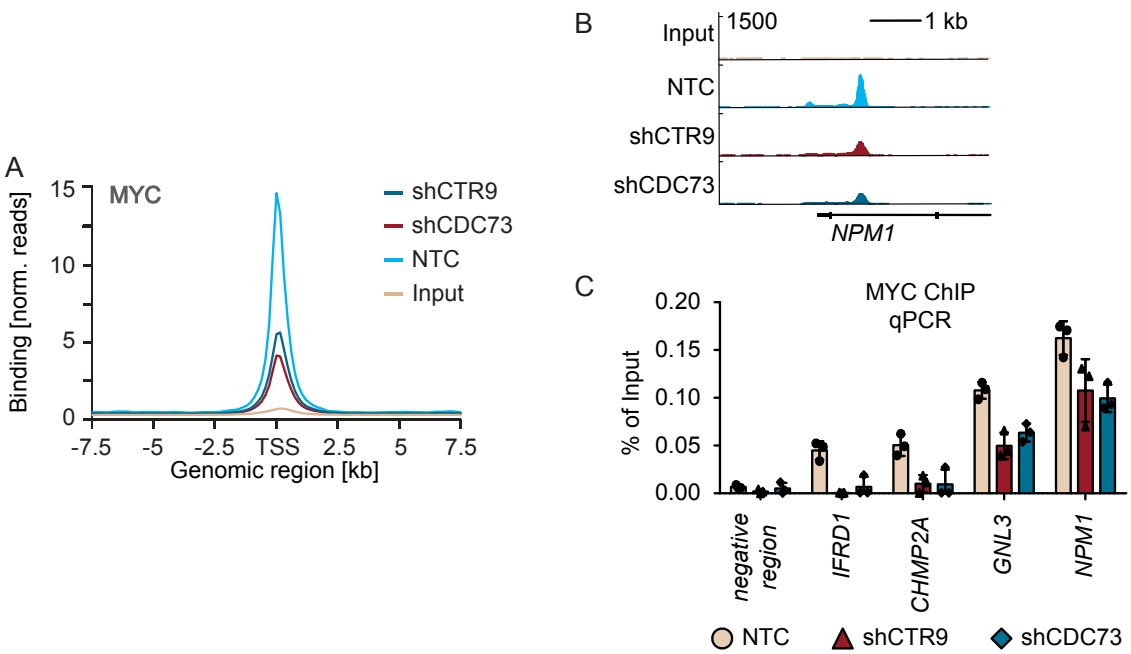

Figure 4.6: PAF1c knockdown reduces association of MYC on chromatin.
A) Density plot of MYC chromatin binding centered on the Transcription Start Site (TSS) of 8,437 promoters in a ChIP-Rx experiment in U2OS cells expressing the lentiviral pGIPZ vector including either a non targeting control (NTC) or shRNA sequences targeting *CDC73* (shCDC73) or *CTR9* (shCTR9).
B) Representative browser track of the *NPM1* locus of a MYC ChIP-Rx experiment from panel A.
C) MYC ChIP qPCR of several MYC-bound promoters. Experimental settings as described in panel A. Specific primers of known MYC-bound promoters were used for RT-qPCR. Shown are technical replicates representative of three independent experiments. Error bars represent the S.D. of technical replicates.
This figure was published in similar form in Endres et al. (2021).

MYC ChIP qPCR experiments further confirmed the ChIP-Rx experiment. Knockdown of either *CTR9* or *CDC73* led to a reduced MYC binding of promoter regions of different loci such as *IFRD1*, *CHMP2A*, *GNL3* or *NPM1* (see figure 4.6 C). Further bioinformatic analysis revealed that the reduced occupancy of MYC upon knockdown of the two different subunits of PAF1c is promoter-specific (figure 4.7, "Promoter") whereas known MYC binding sites at enhancers were not affected (figure 4.7, "Enhancer").

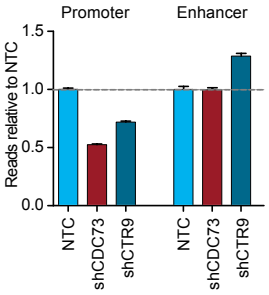

Figure 4.7: PAF1c knockdown reduces association of MYC at promoters but not enhancers.
Histogram of the ChIP-Rx experiment from figure 4.6 showing read number relative to control (NTC) for all MYC-bound promoters and enhancers in control cells or upon expression of either shCTR9 or shCDC73 in the lentiviral pGIPZ vector infected in U2OS. Shown are mean ±S.E.M. of 12,153 promoters and 2,321 enhancers. For promoters, both comparisons shCTR9 vs. shNTC or shCDC73 vs. shNTC have p-values below 0.0001.
Bioinformatic analysis was performed by Peter Gallant.
This figure was published in similar form in Endres et al. (2021).

The MYC ChIP-Rx experiment described in figure 4.6 and figure 4.7, had reduced MYC protein levels. To investigate whether the reduced MYC occupancy at promoters due to the absence of the PAF1c and not caused by the reduced MYC protein (compare immunoblot of figure 4.5 A and "MYC" in B with figure 4.8 B, top and bottom, "shCTR9", "shCDC73"), ChIP sequencing experiments were performed in U2OS control cells or cells ectopically expressing MYC upon an inducible knockdown of either *CTR9* or *CDC73* for 48 h.

Parallel to the harvest of chromatin, protein lysates of the same conditions were generated to test MYC protein levels and knockdown efficiency. Knockdown of *CTR9* led to a reduction of 50 % of the CTR9 protein and 40 % of the CDC73 protein (see figure 4.8 A, top, "shCTR9", lane "-" and "+" and figure 4.8 C top, "shCTR9"). Knockdown of *CDC73* resulted as well in a reduction by 50 % of the CDC73 protein but only a protein reduction of 10 % of the CTR9 protein was detectable (see figure 4.8 A, bottom, "shCDC73", lane "-" and "+", and figure 4.8 C, bottom, "shCDC73"). Stable ectopic expression of the *MYC* from a SFFV promoter resulted in a 3-5 times higher expression of the MYC protein (see figure 4.8 A, top and bottom, "shCTR9" and "shCDC73", lane "-" and "+" and figure 4.8 B, top and bottom, "shCTR9", "shCDC73").

More importantly, the knockdown of both subunits of the PAF1c for 48 h did not

result in a reduction of the MYC protein level (see figure 4.8 A, top and bottom, "shCTR9" and "shCDC73", lane "-" and "+" and figure 4.8 B, top and bottom, "shCTR9" and "shCDC73").

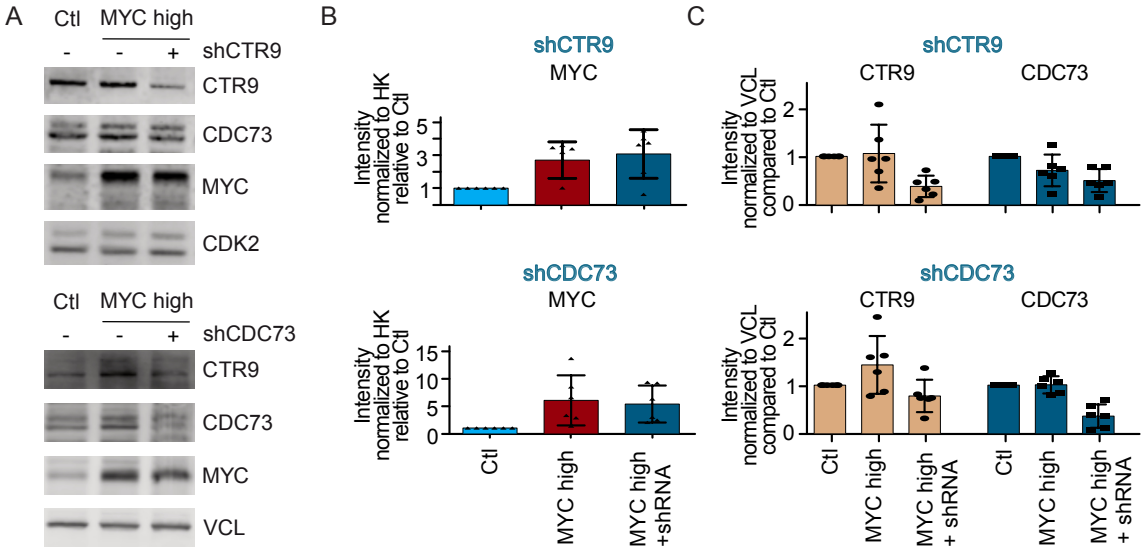

Figure 4.8: Knockdown efficiency of CDC73 or CTR9 in U2OS using doxycycline inducible pInducer10 vector.
A) Immunoblot of lysates from U2OS cells expressing a lentiviral pRRL MYC and the lentiviral pInducer10 vector including either a non targeting control (NTC) or shRNA sequences targeting *CDC73* (shCDC73) or *CTR9* (shCTR9). Cells were harvested 48 h after addition of doxycycline (1 µg/ml). (n=6)
B) Quantification of the immunoblot of MYC protein levels shown in panel A. P values were calculated using unpaired t-test. (n=6)
C) Quantification of the immunoblot of CDC73 and CTR9 protein levels shown in panel A. P values were calculated using unpaired t-test. (n=6)
This figure was published in similar form in Endres et al. (2021).

Density plot of a MYC ChIP sequencing experiment revealed that MYC occupancy on around 8,500 MYC-bound promoters was enhanced between 25 % and 40 % upon expression of ectopic MYC when comparing with the control condition (see figure 4.9 A, top and bottom, "Ctl", "MYC high", light blue and red line).

Comparing MYC occupancy in cells with ectopic MYC expression alone and cells with an additional knockdown of *CTR9* for 48 h, the MYC binding is reduced by around 50 % (shown in figure 4.9 A, top, "MYC high", "MYC high+shCTR9", red and dark blue line). Knockdown of *CDC73* also reduced MYC occupancy, but to a lesser extent as the *CTR9* knockdown (see figure 4.9 A, bottom, , "MYC high", "MYC high+shCDC73", red and dark blue line). Browser tracks shown in figure 4.9 B of the

NPM1 locus confirmed the observation that knockdown of the PAF1c subunits *CTR9* or *CDC73* reduces MYC binding at known promoters.

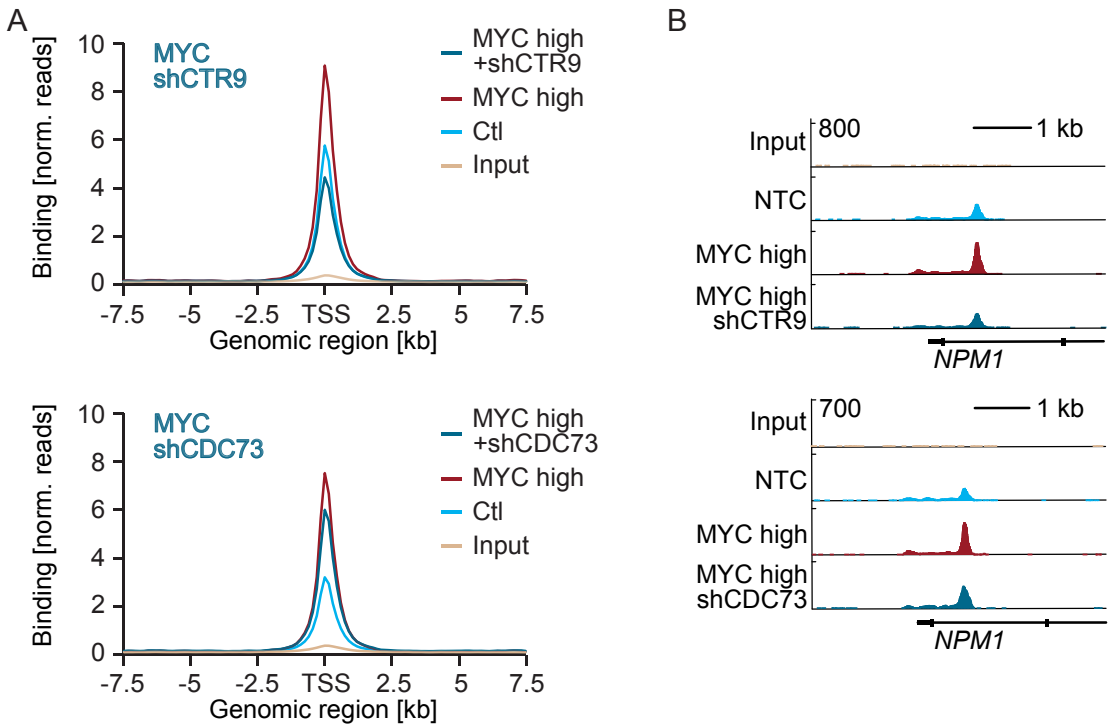

Figure 4.9: PAF1c knockdown reduces association of MYC on chromatin in a MYC oncogenic environment.
A) Density plot of MYC centered on the Transcription Start Site (TSS) of 8,437 promoters in a ChIP sequencing experiment in U2OS cells expressing a constitutive active pRRL MYC or control (Ctl) vector and a doxycycline-inducible pInducer10 vector including either a shRNA sequences targeting *CTR9* (shCTR9, top) or *CDC73* (shCDC73, bottom). Cells were harvested 48 h after doxycycline treatment (1 µg/ml).
B) Representative browser track of the *NPM1* locus of a MYC ChIP sequencing experiment from panel A. Top: MYC ChIP seq of U2OS expressing either pRRL ctl or pRRL MYC and pInducer10 shCTR9 (top panel) or shCDC73 (bottom panel).
This figure was published in similar form in Endres et al. (2021).

Classification into promoter and enhancer regions in the MYC ChIP sequencing showed that ectopic MYC expression leads to a fold increase of MYC binding at promoter regions by half (see figure 4.10 A, "Promoter", "Ctl", "MYC high") or double (see figure 4.10 B, "Promoter", "Ctl", "MYC high") and that addition of *CTR9* knockdown (see figure 4.10 A, "Promoter", "MYC high", "MYC high+shCTR9") and to a lesser extent of *CDC73* knockdown (see 4.10 B, "Promoter", "MYC high", "MYC high+shCDC73"), reduced this binding significantly. Enhancer regions showed similar tendencies as the promoter regions, (see 4.10 A and B, "Enhancer"), but the

effects were not as prominent as the effects on promoter regions.

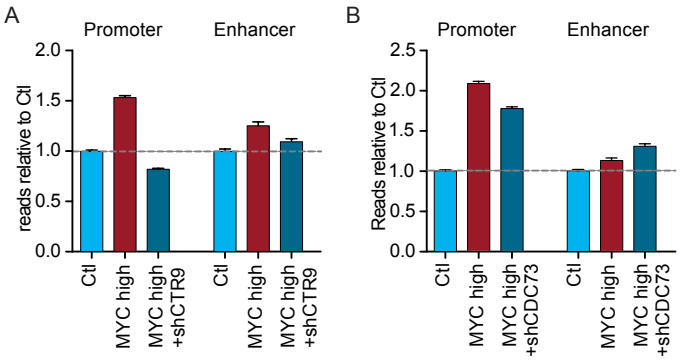

Figure 4.10: PAF1c knockdown reduces MYC promoter association in a MYC oncogenic environment.
A) Histogram showing read number relative to control (Ctl) for all MYC-bound promoters and enhancers in control cells or upon constitutive active expression of ectopic MYC and doxycycline-inducible pInducer10 shCTR9 in U2OS. Where indicated, U2OS cells were treated for 48 h with 1 µg/ml doxycycline prior harvesting. Shown are mean ±S.E.M. of 12,153 promoters and 2,321 enhancers. For promoters, all pairwise comparisons between "MYC high" and "Ctl" or "MYC high+shCTR9" have p <0.0001.
B) Same as panel A but U2OS infected with pInducer10 shCDC73.
Bioinformatic analysis was performed by Peter Gallant.
This figure was published in similar form in Endres et al. (2021).

Taken together, these data sets show that PAF1c levels affect MYC occupancy and that the binding of MYC is reduced upon PAF1c subunit knockdown at promoters but not enhancers.

4.3 MYC-mediated transfer of SPT5 is required to maintain RNA Polymerase II processivity

Section 4.1 showed, that MYC and SPT5 are interacting directly. Baluapuri et al. (2019) suggested based on SPT5 ChIP-Rx and proximity ligation assay (PLA) data, that SPT5 is transferred from MYC onto RNAPII. To further investigate the function of this transfer, total RNAPII ChIP-Rx was performed in U2OS control cells and cells expressing a doxycycline inducible knockdown of *SPT5* for 48 h.
Additionally, protein levels were analysed by immunoblotting shown in figure 4.11 A. Comparing lysates from control cells (figure 4.11 A,"Ctl") with doxycycline treated

cells, a clear decrease in SPT5 protein levels was visible (figure 4.11 A,"shSPT5"). Density plots shown in figure 4.11 B and C show a clear enrichment of the RNAPII signal ("Ctl", "shSPT5", light and dark blue line) compared to input ("Input", beige line). Whereas the total RNAPII occupancy was enriched shortly downstream of the TSS upon SPT5 knockdown compared to the control (see figure 4.11 B) this effect was successively inverted towards the TES (see figure 4.11 C). To visualize the effect further, a processivity score was calculated as described in formula (4.1) and Baluapuri et al. (2019).

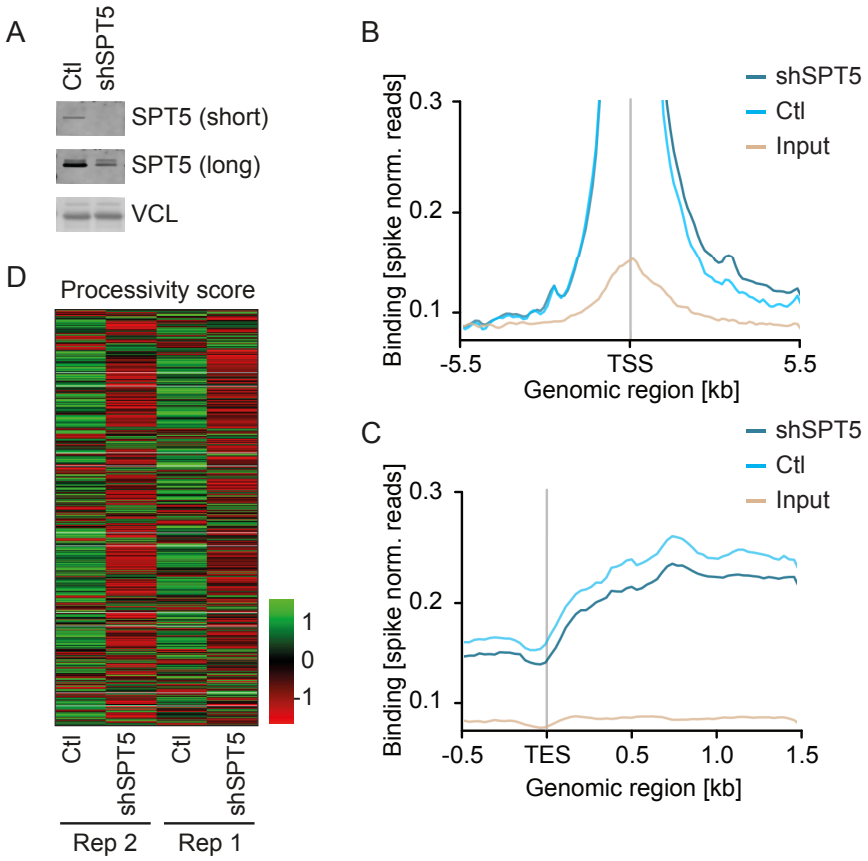

Figure 4.11: MYC-mediated transfer of SPT5 is required to maintain RNA Polymerase II processivity.
A) Comparison of SPT5 protein levels in control and *SPT5*-depleted U2OS. Cells were either treated with EtOH (Ctl) or doxycylin (1 µg/ml) for 48 h prior to cell lysis. Specific antibodies targeting SPT5 or vinculin ("VCL") were used. VCL served as loading control.
B) Density plot of total RNA polymerase II (RNAPII) around the Transcription Start Site (TSS). RNAPII ChIP-Rx experiment was performed with U2OS cells as described in A. Plot representative of two independent biological replicates.
C) Density plot of RNAPII around Transcriptional End Site. (TES). ChIP-Rx experiment was performed with U2OS cells as described in A. Plot representative of two independent biological replicates.
D) Processivity Score calculated from two independent RNAPII ChIP-Rx replicates as described in B) and C).
Bioinformatic analysis was performed by Apoorva Baluapuri.
This figure was published in similar form in Baluapuri et al. (2019).

$$processivity\ score = log_2 \frac{[(TSS - 0.5\ kb) - (TSS + 1.5\ kb)]}{[(TES - 1\ kb) - (TES + 2\ kb)]} \tag{4.1}$$

In both replicates of the total RNAPII ChIP-Rx, the processivity score comparing the distal read density and the proximal read density, was reduced at most genes upon depletion of SPT5 compared to control cells (see figure 4.11 D). This suggests that SPT5 depletion leads to less efficient travelling of the RNAPII along the genes.

These data conclude that MYC affects the transcriptional elongation of the RNAPII downstream of the TSS by promoting the assembly of RNAPII and SPT5.

4.4 MYC-mediated transfer of PAF1c is required to maintain elongation of RNA Polymerase II

Since PAF1c and MYC are directly interacting (section 4.1) and PAF1c enhances binding of MYC at promoters (section 4.2) the effect of the PAF1c transfer from MYC onto RNAPII was determined by performing RNAPII ChIP sequencing.
To discriminate the specific step of transcription influenced by PAF1c depletion in cells with oncogenic levels of MYC, two different antibodies specific for total RNAPII and elongating RNAPII (pS2) were used. Ectopic MYC expression led to an increase of the total RNAPII occupancy at the transcription start site (TSS) but also led to a successive decrease towards the body of the gene (see figure 4.12 A, "Ctl", "MYC high", light blue and red line). Knockdown of *CTR9* reverted the MYC effect on intiation of total RNAPII (see figure 4.12 A, "MYC high", "MYC high+shCTR9", red and dark blue line). Ectopic expression of MYC led to an increase in pS2 RNAPII downstream of the TSS but also in the gene body (see figure 4.12 C, "Ctl", "MYC high", light blue and red line). Strikingly, knockdown of *CTR9* nearly completely abolished the MYC effect on the elongating form of the RNAPII (see figure 4.12 B). Browser tracks from individual loci confirmed this obervation. Figure 4.12 C and D show exemplarily the *RPL13* locus for total RNAPII (C) or pS2 RNAPII (D). Total RNAPII was mainly unaffected by ectopic MYC expression (see figure 4.12 C, light blue and red browser track) or additional knockdown of *CTR9* (see figure 4.12 C, dark blue and red browser track). Knockdown of the PAF1c subunit *CTR9* reduced

the MYC based enhanced binding of pS2 RNAPII downstream of the promoter region towards the end (see figure 4.12 D).

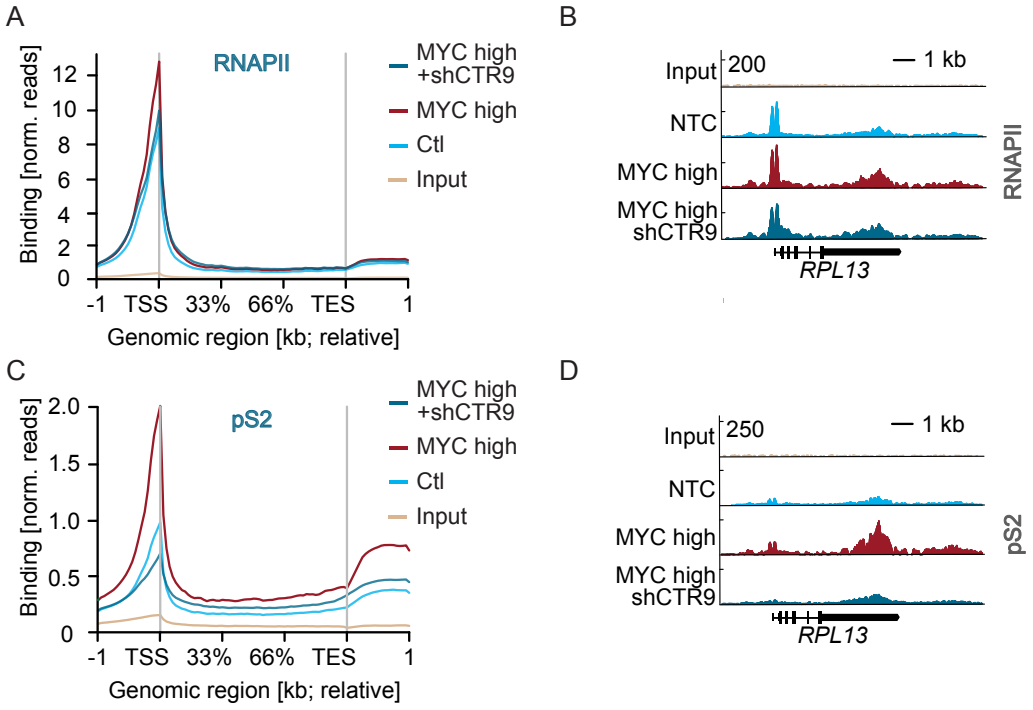

Figure 4.12: MYC mediated transfer of PAF1c is required to maintain RNA Polymerase II elongation.
A) Metagene plot showing total RNA Polymerase II (RNAPII) ChIP sequencing in U2OS upon inducible knockdown of *CTR9*. Shown are the top 4000 MYC-bound genes. ChIP sequencing was performed with control U2OS cells or upon constitutive active expression of ectopic MYC and doxycycline-inducible pInducer10 shCTR9 in U2OS (48 h, 1 µg/ml).
B) Representative browser track of the *RPL13* locus of a RNAPII ChIP sequencing experiment from panel A.
C) Metagene plot showing phosphorylation of Ser2 RNAPII (pS2) ChIP sequencing in U2OS upon inducible knockdown of *CTR9*. Shown are the top 4000 MYC-bound genes. ChIP sequencing was performed with control U2OS cells or upon constitutive active expression of ectopic MYC and doxycycline-inducible pInducer10 shCTR9 in U2OS (48 h, 1 µg/ml).
D) Representative browser track of the *RPL13* locus of a pS2 ChIP sequencing experiment from panel C.
Similar results were obtained upon knockdown of *CDC73* (Data not shown).
This figure was published in similar form in Endres et al. (2021).

4.5 MYC squelches SPT5 from chromatin at oncogenic MYC levels

Since the direct interaction between MYC and the DSIF subunit SPT5 was confirmed (see section 4.1) and in section 4.4 the transfer of SPT5 from MYC onto RNAPII

suggests increased processivity of RNAPII the role of SPT5 at oncogenic MYC levels was elucidated.

Therefore, SPT5 ChIP-Rx was performed in control cells or cells expressing high MYC levels after addition of doxycycline in U2OS MYC Tet-ON cells.

Lysates of these cells were generated subjected on an SDS-PAGE and analysed via immunoblot. While the induction of MYC led as expected to a high abundance of the MYC protein, SPT5 protein levels remained unaffected (see figure 4.13 A).

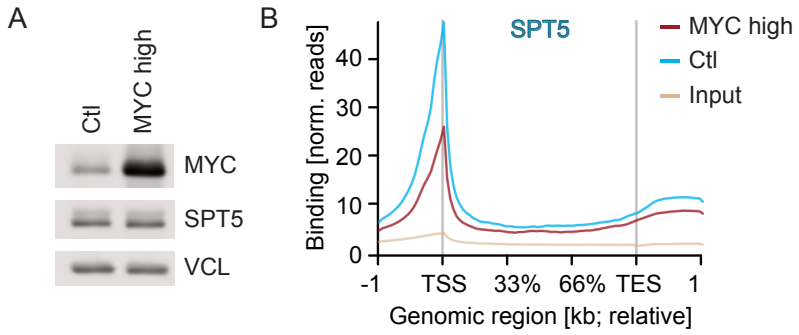

Figure 4.13: MYC squelches SPT5 from chromatin.
A) Comparison of MYC protein levels in control cells ("Ctl") and doxycyline treated U2OS MYC-Tet-ON (1 µg/ml, 12 h, "MYC high").Specific antibodies targeting MYC, SPT5 or vinculin ("VCL") were used. VCL served as loading control.
B) Metagene plot of SPT5. ChIP-Rx experiment was performed with U2OS MYC-Tet-On cells as described in A. Occupancy of SPT5 in U2OS MYC Tet-ON cells as described in A. Bioinformatic analysis was performed by Apoorva Baluapuri
This figure was published in similar form in Baluapuri et al. (2019).

SPT5 chromatin immunoprecipitation showed a clear enrichment over input (see figure 4.13 B, "Input" vs. "MYC high", "Ctl", beige line compared with red and blue line). In contrast to ectopic MYC expression, which led to an overal increase in pS2 RNAPII (see figure 4.12 C), SPT5 binding was reduced in cells expressing MYC high levels compared to control cells (see figure 4.13 B, "MYC high", "Ctl", red line compared with blue).

In combination with results shown in section 4.4 this suggests, that high levels of MYC remove SPT5 from RNAPII, an event hereafter usually referred to as "squelching".

4.6 PAF1c is rapidly transferred from MYC onto RNA Polymerase II

Since PAF1c and MYC are directly interacting (section 4.1) and PAF1c enhances binding of MYC at promoters (section 4.2) resulting in a reduction of MYC-induced elongation of the RNAPII (see section 4.4) the behaviour of PAF1c upon MYC protein level manipulation was investigated.

First, CTR9 and CDC73 ChIP sequencing were performed in U2OS cells expressing ectopic MYC and a doxycycline inducible shRNA targeting *CTR9* or *CDC73*. CTR9 and CDC73 ChIP sequencing revealed that PAF1c occupancy mirrors MYC binding. Top MYC-bound genes are also highly bound by CTR9 or CDC73 whereas weakly bound genes present with a low occupancy (see figure 4.14 compare A , "top" and B, "bottom"). Ectopic MYC expression led to a higher CTR9 occupancy at highly MYC-bound genes (see figure 4.14 A, "Ctl", "MYC high", light blue line and red line). The CTR9 protein reduction by 50 % (see figure 4.8) upon inducible knockdown of *CTR9*, also reverted the MYC effect on the CTR9 occpancy in gene bodies (see figure 4.14 A, left, "MYC high" and "MYC high+shCTR9", red line and dark blue line). Similar effects were observed for the CDC73 occupancy: Ectopic MYC expression enhanced the occupancy of CDC73 in gene bodies, which was abolished upon knockdown of *CDC73* (see figure 4.14 A, right). Note, that CDC73 only showed significant enrichement after the TSS, which is in line with published literature (Vos et al., 2018a), arguing that PAF1c is transferred onto the RNAPII at the transition to positive elongation between 30 and 50 bp downstream the TSS.

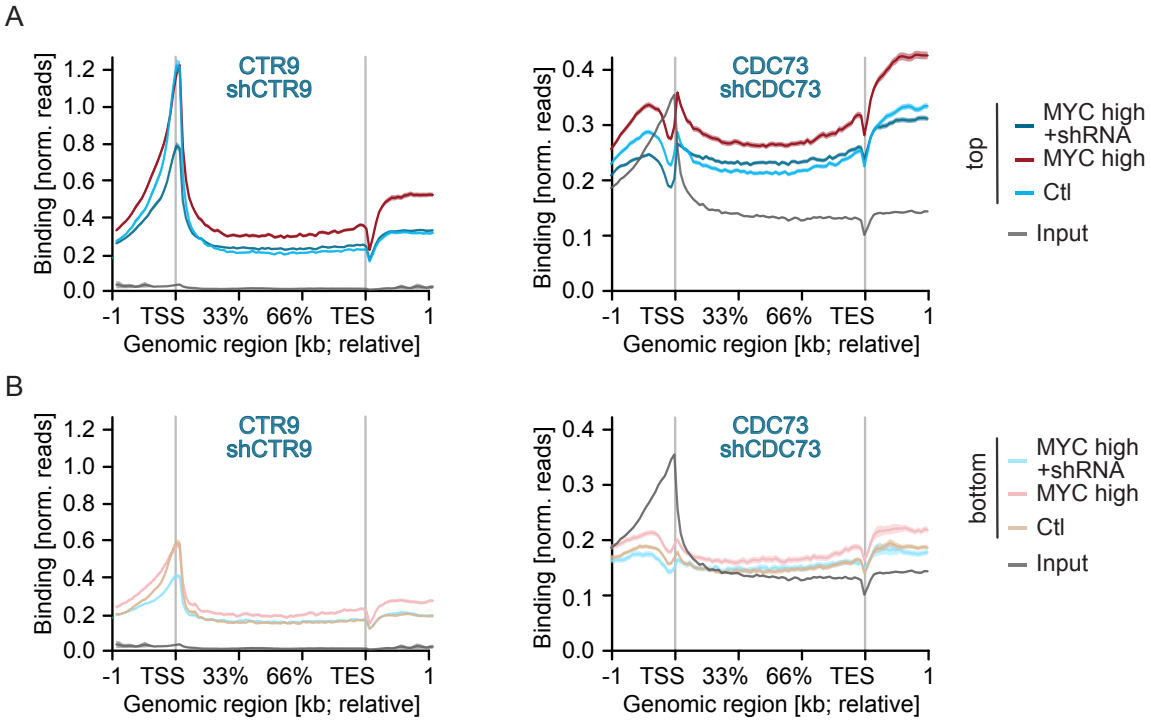

Figure 4.14: Overexpression of MYC enhances occupancy of PAF1c on chromatin.
A) Left: Metagene plot showing CTR9 ChIP sequencing in U2OS control cells or cells expressing ectopic MYC and a doxycycline inducible shRNA targeting *CTR9* (1 µg/ml, 48 h). Shown are 7,479 strongly MYC-bound genes ("top").
Right Metagene plot showing CDC73 ChIP sequencing in U2OS control cells or cells expressing ectopic MYC and a doxycycline inducible shRNA targeting *CDC73* (1 µg/ml, 48 h). Shown are 7,479 strongly MYC-bound genes ("top").
B) Left: Metagene plot showing CTR9 ChIP sequencing in U2OS control cells or cells expressing ectopic MYC and a doxycycline inducible shRNA targeting *CTR9* (1 µg/ml, 48 h). Shown are 5,768 weakly MYC-bound genes ("bottom").
Right Metagene plot showing CDC73 ChIP sequencing in U2OS control cells or cells expressing ectopic MYC and a doxycycline inducible shRNA targeting *CDC73* (1 µg/ml, 48 h). Shown are 5,768 weakly MYC-bound genes ("bottom").
This figure was published in similar form in Endres et al. (2021).

To further study, how fast PAF1c is transferred from MYC onto the RNAPII, cells expressing a MYC-ER system were used. Once 4-OHT is added to the cells, the MYC-ER is translocated from the cytoplasm into the nucleus so that MYC can bind the chromatin. To test how fast this system is working, cells were harvested at different timepoints between 5 min and 4 h after 4-OHT addition. ChIP was performed and analysed via qPCR with primers of promoter regions known to be enriched for MYC. As shown in figure panel 4.15 A and B of different promoters bound by MYC, a clear induction of MYC chromatin binding was observed already after 15 min and stayed substantially stable until the latest timepoint. To get a

higher resolution of the MYC chromatin binding before the 15 min timepoint, cells were harvested for ChIP between 0 and 15 min after 4-OHT addition. 5 min of MYC activation did not result in a clear enhanced MYC occupancy, for all promoters analysed but between 10 and 15 min the strongest binding of MYC onto chromatin was observed (see figure 4.15 C and D).

For the subsequent ChIP-Rx experiments, U2OS MYC-ER were treated for 10 min with 4-OHT to evaluate direct effects of MYC binding on chromatin association of PAF1c and the RNAPII. Additionally, cells were harvested after 30 min to compare when MYC occupancy at promoters is saturated within a short activation period of the MYC-ER system.

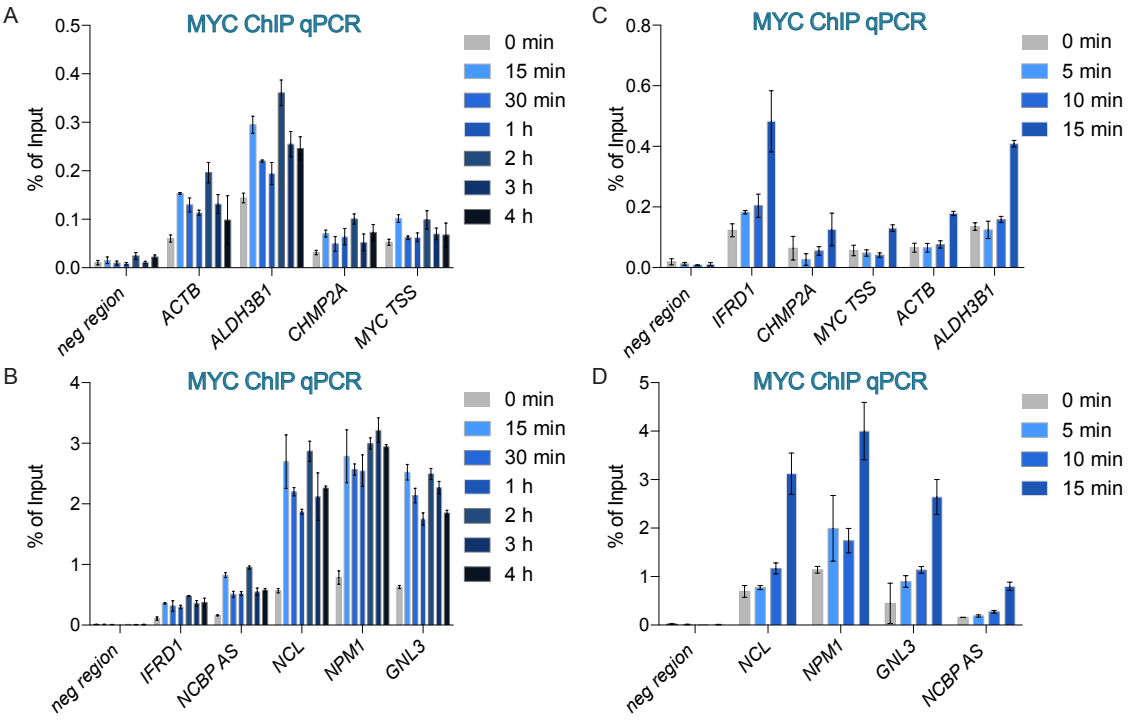

Figure 4.15: Acute activation of MYC enhances MYC occupancy at promoters. A-D) MYC binding at promoters. MYC ChIP qPCR of U2OS cells expressing a chimeric MYC-ER protein, which were treated for indicated timepoints with 200 nM 4-OHT. Primers which amplify the transcription start site (TSS) of the indicated genes or an unspecific intergenic control region ("neg region") were used. IgG served as control (Data not shown). Shown is the mean ± SD. Shown are replicates of two independent biological experiments.

As shown in the immunoblot of figure 4.16 A, MYC-ER activation did not chance protein levels of RNAPII, CTR9, CDC73 or MYC.

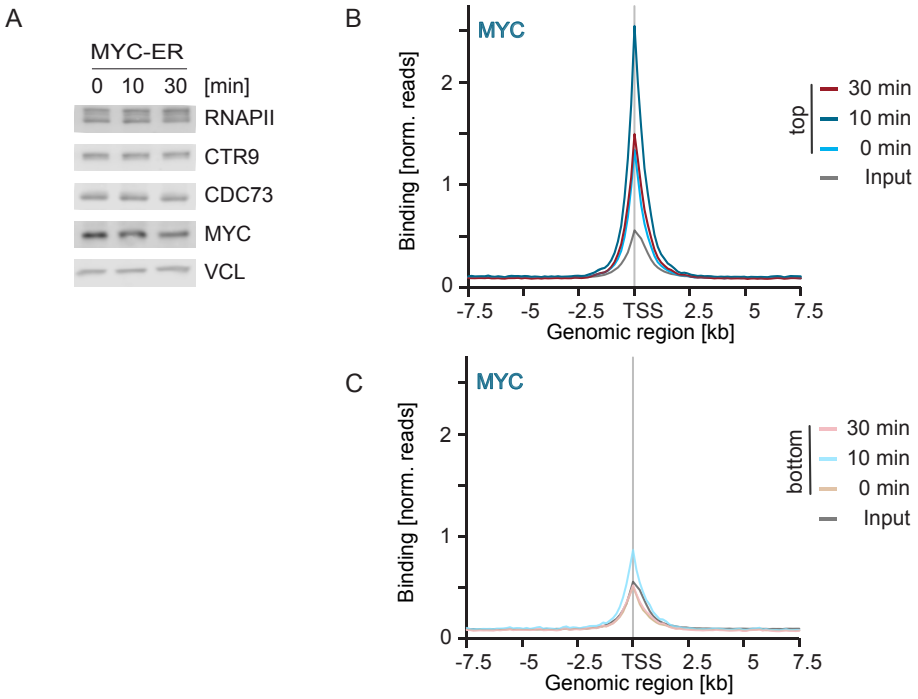

Figure 4.16: Acute activation of MYC enhances MYC occupancy globally.
A) Comparison of protein levels in control cells and 4-OHT treated U2OS MYC-ER (200 nM, 10 or 30 min) on an immunoblot. Protein lysates of U2OS MYC-ER cells. Specific antibodies targeting total RNAPII, CTR9, CDC73, MYC or vinculin ("VCL") were used. VCL served as loading control.
B) Density plot of a MYC ChIP-Rx experiment. Shown are 7,479 strongly MYC-bound genes ("top"). ChIP-Rx sequencing was performed with control U2OS cells or cells treated with 200 nm 4-OHT for 10 or 30 min. Shown is a representative experiment of biological replicates (0 and 10 min 4-OHT).
C) Density plot of a MYC ChIP-Rx experiment. Shown are 5,768 weakly MYC-bound genes ("bottom"). ChIP-Rx sequencing was performed with control U2OS cells or cells treated with 200 nm 4-OHT for 10 or 30 min. Shown is a representative experiment of biological replicates (0 and 10 min 4-OHT).
This figure was published in similar form in Endres et al. (2021).

ChIP-Rx sequencing of MYC revealed that MYC-ER activation by 4-OHT led to an increase in MYC occupancy at top MYC-bound promoters and to a less extent to bottom MYC-bound promoters (see figure 4.16 B and C, "top" and "bottom").

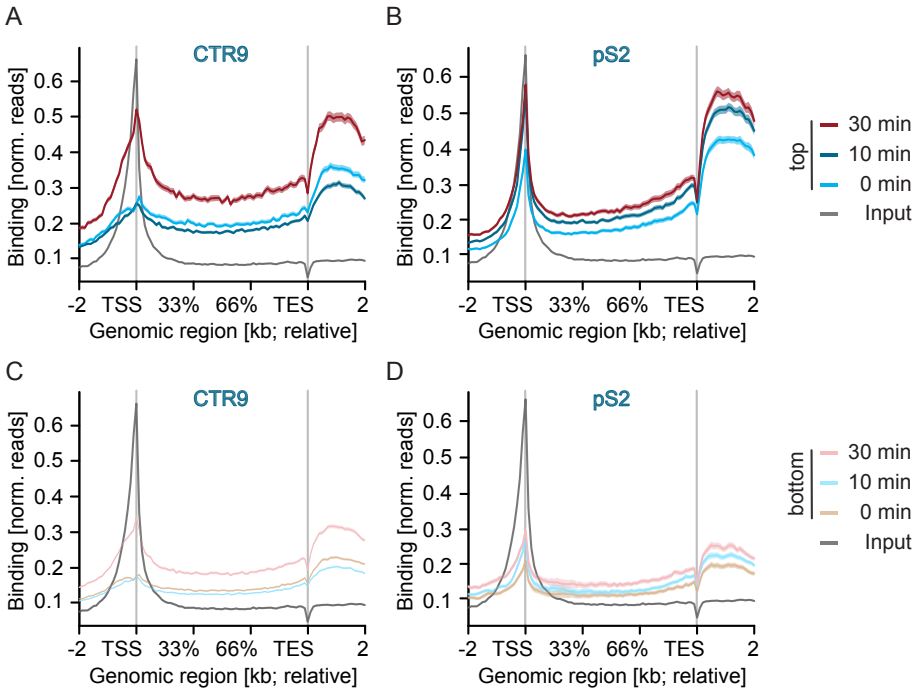

Figure 4.17: Acute activation of MYC enhances PAF1c and pSer2 RNAPII occupancy on chromatin.
A) Metagene plot or a CTR9 ChIP-Rx experiment. Shown are 7,479 strongly MYC-bound genes ("top"). ChIP-Rx sequencing was performed with control U2OS cells or cells treated with 200 nm 4-OHT for 10 or 30 min. Shown is a representative experiment of biological replicates (0 and 10 min 4-OHT).
B) Metagene plot or a pS2 RNAPII ChIP-Rx experiment. Shown are 7,479 strongly MYC-bound genes ("top"). ChIP-Rx sequencing was performed with control U2OS cells or cells treated with 200 nm 4-OHT for 10 or 30 min. Shown is a representative experiment of biological replicates (0 and 10 min 4-OHT).
C) and D) Metagene plot of CTR9 and pS2 RNAPII. Shown are 5,768 weakly MYC-bound genes ("bottom"). Cells were treated as described in A) and B).
ChIP-Rx sequencing experiments were performed in collaboration with with Daniel Solvie. Bioinformatic analysis was performed by Peter Gallant and Daniel Solvie.
This figure was published in similar form in Endres et al. (2021).

CTR9 ChIP-Rx revealed that 10 min were not sufficient to increase MYC dependent CTR9 occupancy in the body of MYC-bound genes, but that 30 min led to an increase of CTR9 occupancy in the body of the genes (see figure 4.17 A and C). This increase was more prominent on highly MYC-bound promoters compared to weakly MYC-bound promoters (see figure 4.17 A and C, "top" and "bottom"). pS2 RNAPII lead to a steady increase already after 10 min or 30 min 4-OHT addition to the cells (see figure 4.17 B and D, "top" and "bottom").

The data from figure 4.17 showed that the occupancy of the elongating RNAPII is already increasing after 10 min of MYC activation, whereas MYC-dependent PAF1c

transfer on the RNAPII takes 30 min of MYC activation.

The experiments showed so far suggest that MYC activation (MYC-ER) or ectopic expression in U2OS cells which express moderate levels of endogenous MYC induce PAF1c transfer onto RNAPII.
To corroborate these results using both a loss-of-function approach and a system more closely resembling the setting of MYC-deregulated tumors, K562 erythroleukemia cells were used. In particular, K562 cells engineered to express auxin-inducible-degron (AID) allowing a fast degradation of the MYC protein were used (Muhar et al., 2018).
Two clones of the K562 MYC-AID cells, C3 or D10, were freshly infected with osTIR and treated for 30 min with 100 µl IAA or DMSO. Cells were used to perfrom ChIP qPCR or ChIP-Rx sequencing (see figure 4.19).

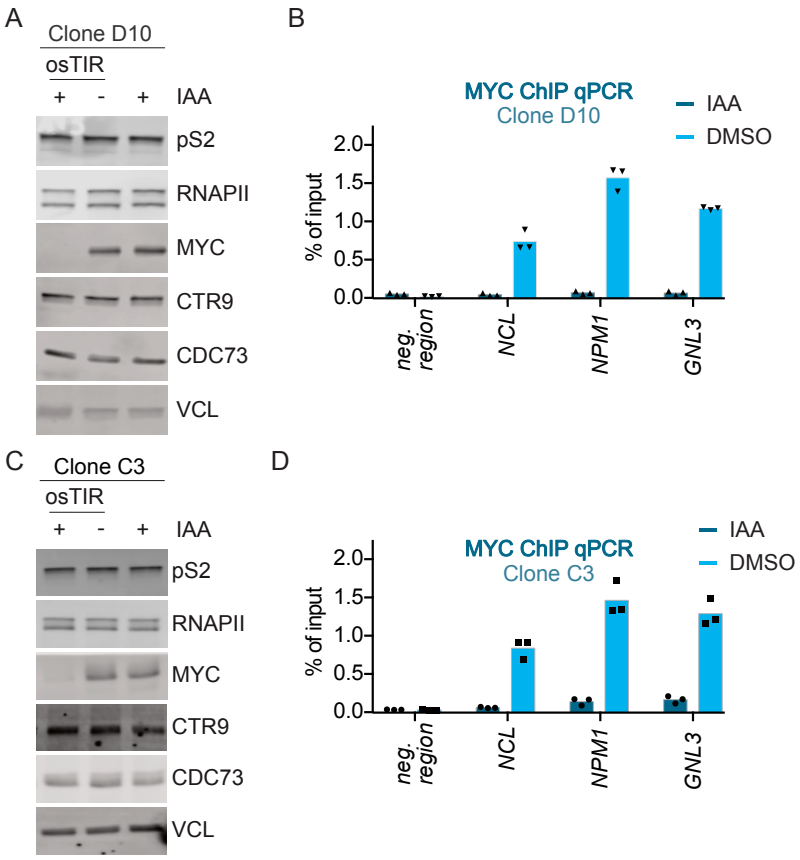

Figure 4.18: Acute depletion of MYC abolishes MYC occupancy at promoters.
A) Comparison of MYC protein levels in control and MYC-depleted K562 cells (clone D10). Cells were either treated with DMSO or 100 µM IAA for 30 min prior to cell lysis. Specific antibodies targeting MYC, pS2, RNAPII, CTR9, CDC73 or vinculin ("VCL") were used. VCL served as loading control.
B) MYC binding at promoters. MYC ChIP of a clone D10 of K562 cells expressing a MYC-AID protein, which were treated for 0 or 30 min with 100 µM IAA. ChIP qPCR was performed with primers which amplify the transcription start site (TSS) of the indicated genes or an unspecific intergenic control region ("neg. region"). Shown is the mean ± SD.
C) Comparison of MYC protein levels in control and MYC-depleted K562 cells (clone C3). Immunoblot was performed as described in A.
D) MYC binding at promoters. ChIP was performed as described in B with the clone C3.
Figure panel A and B were published in similar form in Endres et al. (2021).

The immunoblots from figure 4.18 A and C show that MYC was degraded already 30 min after IAA treatment. Total RNAPII, and the PAF1c subunits CTR9 and CDC73 were unaffected by the MYC depletion for 30 min in both clones. To further validate, that no MYC is bound to chromatin after 30 min of IAA treatment, MYC ChIP-qPCR was performed with primers of known MYC-bound promoters. MYC occupancy after MYC depletion was reduced to the occupancy of MYC at the negative region in both clones (see figure 4.18 B and D).

These results show that treatment of IAA for 30 min in K562 MYC AID cells leads to a nearly complete MYC protein degradation and to a loss of MYC-bound chromatin.

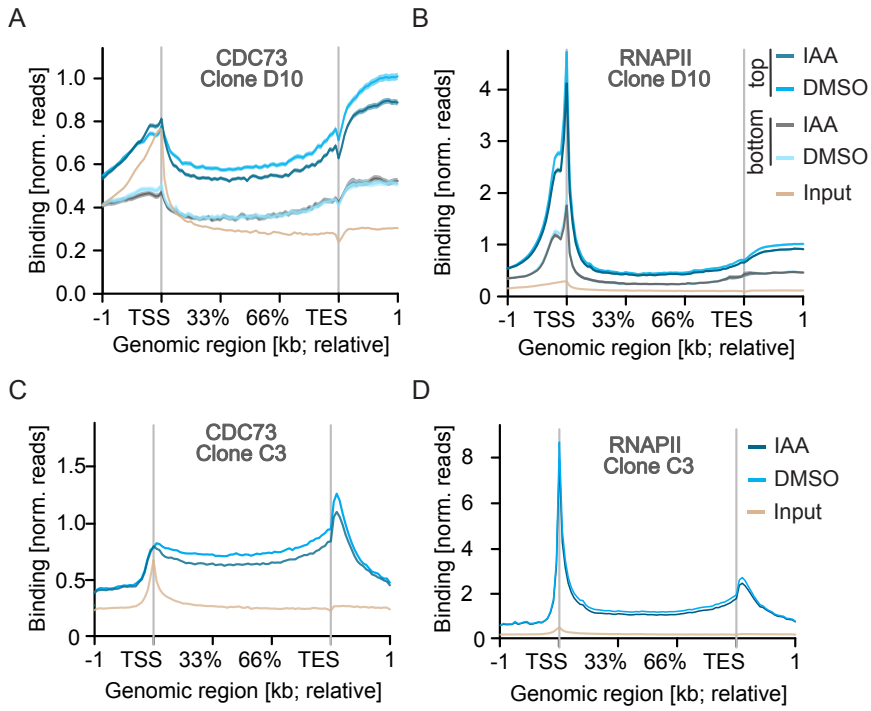

Figure 4.19: Acute depletion of MYC reduces PAF1c occupancy on chromatin.
A) Metagene plot of a CDC73 ChIP-Rx experiment. Shown are the 7,684 most strongly MYC-bound ("top") or 10,013 weakly MYC-bound ("bottom") genes. Input shows 17,697 genes. Where indicated K562 cells (clone D10), engineered to express a MYC-AID knock-in allele and an osTIR delivery vector, were treated for 30 min with 100 µM IAA.
B) Metagene plot of a RNAPII ChIP-Rx experiment. Preparation and analysis of cells of clone D10 was done like described in A.
C) Metagene plot of a CDC73 ChIP-Rx experiment. Shown are the 4,000 most strongly MYC-bound genes. Where indicated K562 cells (clone C3), engineered to express a MYC-AID knock-in allele and an osTIR delivery vector, were treated for 30 min with 100 µM IAA.
D) Metagene plot of a RNAPII ChIP-Rx experiment. Preparation and analysis of cells of clone D10 was done like described in C.
This figure was published in similar form in Endres et al. (2021).

To analyze the effects of MYC depletion on RNAPII and PAF1c, ChIP-Rx was performed in two K562 MYC AID cell clones constitutively expressing osTIR. Cells were either treated with IAA or DMSO for 30 min.

Metagenes were generated and analysed with gene lists stratifying for the occupancy of MYC at the promoter. CDC73 and RNAPII showed less enrichment over input on weakly MYC-bound genes compared to strongly MYC-bound genes (see figure 4.19

A and B, "top" vs "bottom"). A metagene analysis of CDC73 ChIP-Rx (see figure 4.19 A and C) revealed that in MYC-depleted cells ("IAA"), the occupancy of CDC73 was reduced in the gene body of usually strongly MYC-bound genes (see figure 4.19 A and C, "top", "IAA" vs "DMSO", light blue line vs. dark blue line). Total RNAPII occupancy was unaffected by loss of MYC (see figure 4.19 B and D). The same effect was obseved when the experiment was repeated using the C3 clone (see figure 4.19 C and D).

Taken together, the shown functional studies indicate that the enhanced PAF1c occupancy in the body of mainly highly MYC-bound genes happens within minutes after MYC activation, suggesting a model by which PAF1c and MYC are getting cooperatively recruited to the promoter region.

4.7 HUWE1 drives the transfer of PAF1c from MYC onto RNAPII

Shown results (see figures 4.14, 4.19 and 4.12) suggest that MYC serves as a platform for PAF1c to get transferred onto the RNAPII to promote elongation. Jaenicke et al. (2016) proposed a model, that MYC proteasomal turnover is important for the MYC dependent elongation of RNAPII. E3 ligases ubiquitinate proteins to prime them for further degradation via the proteasome. This was suggested by the fact that mutation of all lysine residues of MYC to arginine was not able to promote efficient elongation of the RNAPII and that in the presence of the proteasome inhibitor MG132, MYC and PAF1c form a complex.

To study which E3 ligase might be involved in the process of turning over MYC to transfer PAF1c onto the RNAPII, a siRNA based Proximity Ligation Assay (PLA) screen was performed by Daniel Solvie. siRNAs targeting different E3 ligases known to have a role in MYC regulation were used for this screen. Proximity between the PAF1c subunit PAF1 and MYC as well as pS5 RNAPII and PAF1 was screened with a high throughput microscope to identify the E3 ligase involved in the handover of PAF1c from MYC onto RNAPII.

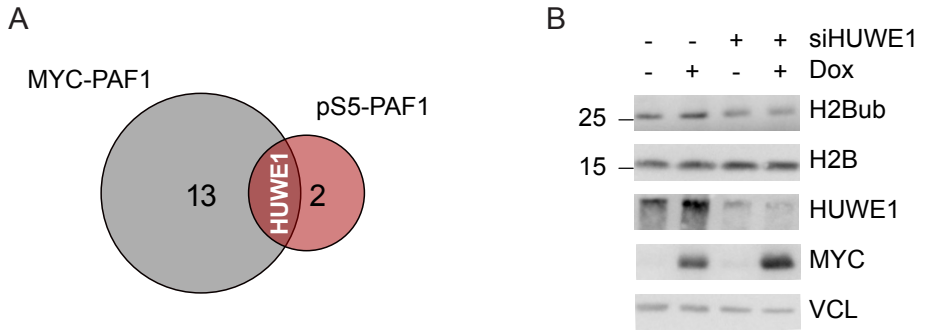

Figure 4.20: HUWE1 drives the transfer of PAF1c from MYC onto RNAPII and recruits histone modifiers.
A) Venn diagram of siRNAs significantly enhancing the proximity between MYC and PAF1c subunit PAF1 and pS5 RNAPII and PAF1. U2OS cells expressing a MYC Tet-On system were transfected with a total of 31 siRNAs targeting different E3 ligases. 16 h after transfection cells were treated for 24 h with 1 µg/ml doxycycline. Proximity ligation assays (PLAs) between MYC and PAF1 or pS5 RNAPII and PAF1 were performed. Statistical significance was calculated using Wilcoxon rank sum test (n=10). Daniel Solvie performed and analyzed the screen.
B) Comparison of ubiquitylated H2B (H2Bub) protein levels in control cells and cells treated with siHUWE1. Cells were either treated with a non targeting control siRNA or a siRNA targeting HUWE1. Where indicated, cells were treated 24 h after transfection with 1 µg/ml doxycycline for 24 h prior to cell lysis. Specific antibodies targeting H2B, HUWE1, MYC or or vinculin ("VCL") were used. VCL served as loading control.
This figure was published in similar form in Endres et al. (2021).

After statistical analysis of the proximity of PAF1c with MYC or with pS5 RNAPII and subsequent comparison of the 14 hits from the MYC-PAF1 PLA screen and 3 hits from the pS5-PAF1 PLA screen, HUWE1 turned out to be the top hit (see figure 4.20 A).

A subunit of the PAF1c, RTF1, is interacting with Bre1, also termed as RNF20/40 and known to monoubiquitinylate histone H2B (Van Oss et al., 2016).
To study if HUWE1 is affecting H2B monoubiquitinylation, U2OS MYC Tet-ON were treated with an siRNA targeting HUWE1. 24 h after transfection of the siRNA targeting either HUWE1 or a non targeting control, cells were treated for additional 24 h with doxycycline. 48 h after transfection a HUWE1 knockdown was visible (see figure 4.20 B, "siHUWE1", "+"). A high abundance of the MYC protein was visible 24 h post induction (see figure 4.20 B, "Dox", "+"). Total protein levels of H2B were unaffected by the different treatments (see figure 4.20 B). Interestingly, HUWE1 knockdown led to a clear reduction of the ubiquitylated H2B as shown in figure 4.20

B ("siHUWE1", "+").

These data in combination with data published in Endres et al. (2021) suggests that HUWE1 triggers the transfer of PAF1c from MYC onto the RNAPII and that MYC and HUWE1 enhance H2B ubiquitylation in a PAF1c-dependent manner.

4.8 MYC promotes Double Strand Break repair in a PAF1c-dependent manner

Monoubiquitylation of histone H2B has different functions. It is involved in elongation (Minsky et al., 2008), but it also opens the chromatin for double strand break repair (Moyal et al., 2011). To test the hypothesis that the handover of PAF1c from MYC onto the RNAPII is important for double strand break repair, Breaks labelling *in Situ* and Sequencing (BLISS) was used.
On the one side, MYC is enhancing the transcription by the RNAPII which leads to transcription induced stress but on the other side MYC is resolving this transcription induced stress by recruiting topoisomerases (Baranello et al., 2016).
To investigate how the absence of MYC is affecting the double strand break amount, K562 cells expressing a MYC-AID system and a osTIR (see section 4.6 figure 4.18) were treated with etoposide, a topoisomerase 2 inhibitor, to induce torsional stress in the cell. Cells were either treated with DMSO or with IAA for 30 min followed by addition of etoposide for 3 h to compare the amount of double strand breaks in either control cells, or cells with low MYC protein levels (see immunoblot in figure 4.18).

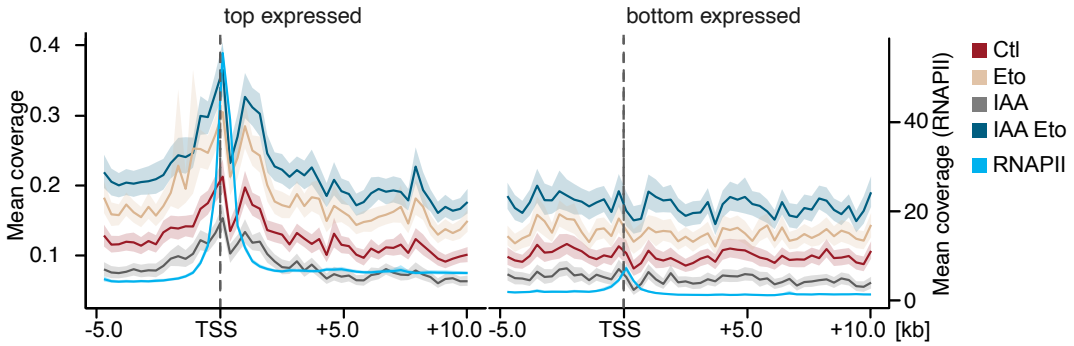

Figure 4.21: Depletion of MYC enhances accumulation of DSB.
Density plot showing mean coverage and estimated confidence interval of double-strand breaks (BLISS) and ocupancy of total RNAPII (ChIP-Rx) around the transcription start sites (TSS). Shown are the 3,954 mostly expressed ("top", left) or the 3,012 weakly expressed ("bottom", right) genes in K562 MYC-AID cells (n=2). Where indicated K562 cells, engineered to express a MYC-AID knock-in allele and an osTIR delivery vector, were treated for 3.5 h with 100 µM IAA and 25 µM etoposide for 3 h. Shown is the merge of biological triplicates.
Daniel Solvie performed the bioinformatic analysis.
This figure was published in similar form in Endres et al. (2021).

To visualize DSB density plot analysis was used to highlight the promoter region from 5 kb upstream to 10 kb downstream of the TSS in top and bottom expressed genes (see figure 4.21). To highlight the expression levels of the two groups of genes, the density plot of BLISS results was overlapped with the density plot of total RNAPII ChIP-Rx as already described in figure 4.19. Top expressed genes showed a higher overal RNAPII coverage most prominent at the TSS compared to the bottom expressed genes (see figure 4.21, "RNAPII", light blue line). BLISS density plot shows the highest signal in all conditions shortly after the TSS. Etoposide-treated cells showed a higher density of double strand breaks compared to control cells (see figure 4.21, "Ctl", "Eto", red vs. beige line). IAA-treated cells alone led to a reduction of overal double strand breaks (see figure 4.21, "IAA", grey line). Etoposide and IAA-treated cells showed the highest BLISS signal (see figure 4.21, "IAA Eto", dark blue line). The effect of the breaks at the promoter region was only present in top expressed genes but not in bottom expressed genes (see figure 4.21, left "top expressed" vs. right "bottom expressed"). The double strand breaks in the body of the gene remained unchanged between the two sets of genes.

Consistently, Endres et al. (2021) showed, that etoposide induced double strand breaks upstream of the TSS were rescued with MYC overexpression.

To investigate whether depletion of PAF1c is necessary for MYC-dependent induction of double strand break repair, BLISS8, a normalized BLISS, was perfomed in U2OS MYC Tet-ON cells upon *CTR9* knockdown. Cells were fixed for BLISS8 96 h after CTR9 knockdown, 24 h after MYC induction and 3 h after etoposide treatment. BLISS8 was performed as described for figure 4.21.

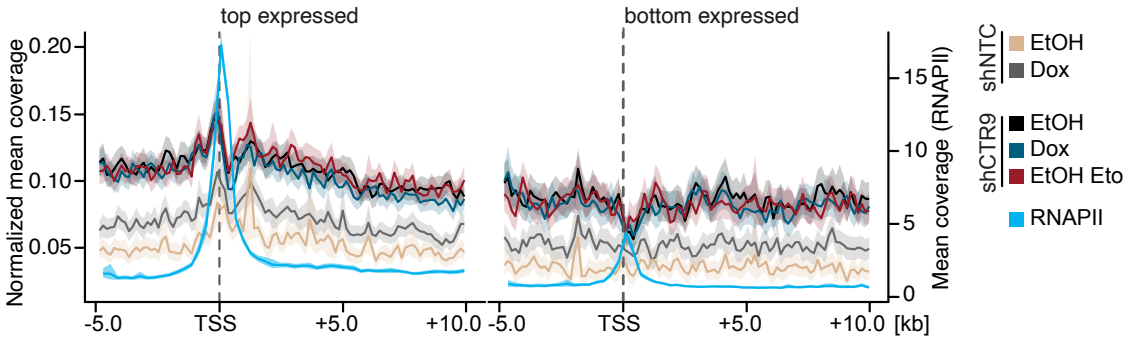

Figure 4.22: MYC promotes Double Strand Break repair in a PAF1c-dependent manner.
A) Density plot showing normalized mean coverage and estimated confidence interval of double-strand breaks (BLISS8) and total RNAPII (ChIP-Rx) around the transcription start sites (TSS). Shown are the 3,954 mostly expressed ("top", left) or the 3,012 weakly expressed ("bottom", right) genes in U2OS cells. U2OS MYC Tet-ON cells expressing stable shRNA targeting *CTR9* or non-targeting control were treated with doxycycline (1 µg/ml, 24 h) and etoposide (25 µM, 3h) where indicated. Shown is the merge of biological triplicates.
Daniel Solvie performed the bioinformatical analysis.
This figure was published in similar form in Endres et al. (2021).

Conversely to the observation in K562 MYC-AID auxin treated cells, where depletion of MYC led to a reduction of double strand breaks (see figure 4.21), induction of MYC in U2OS MYC Tet-ON cells, led to an increrase in double strand breaks in control cells. This increase was observed shortly after TSS and decreased towards the body of the gene of top expressed genes (see figure 4.22, left panel, "shNTC", "EtOH" vs. "Dox", beige line compared to grey line). Note, that the defined peak in the control condition did not get any further increased upon MYC induction. BLISS8 signal from samples of cells with CTR9 knockdown led to a visible increase in double strand breaks from the TSS onwards into the body of the gene (see figure 4.22, left panel, "shCTR9 EtOH", black line). Interestingly, addition of etoposide in *CTR9* depleted cells, did not led to a further increase (see figure 4.22, left panel, "shCTR9 EtOH Eto",

red line). Also MYC overexpression in *CTR9* depleted cells, did not lead to a change of double strand breaks (see figure 4.22, left panel, "shCTR9 EtOH," dark blue line). Bottom expressed genes followed the same pattern as highly expressed genes but did not have an enriched density after the TSS (see figure 4.22, right panel).
These data suggests that torsional stress induced by MYC's enhanced transcriptional activity is resolved by the repair of double strand breaks in promoter proximal regions in a PAF1c-dependent manner.

4.9 PAF1c knockdown reduces MYC dependent transcriptional regulation

To further study the effects of PAF1c on global MYC-dependent gene regulation, two different shRNAs targeting either *CDC73* or *CTR9* in U2OS MYC Tet-ON were used for RNA sequencing (Fellmann et al., 2013). Both constructs targeting *CDC73* and *CTR9* efficiently knocked down respective protein expression, as testified by immunoblotting (see figure 4.23 A "shCDC73", comparing "-" with "3" and "4" and figure 4.23 B "shCTR9", comparing "-" with "3" and "5"). Interestingly, MYC overexpression - which also was efficiently induced (see figure 4.23 A and B comparing "EtOH" with "Dox") - did not influence neither CTR9 nor CDC73 (see figure 4.23 A and B, "Dox").
Global gene expression profiles of the different samples were compared by RNA sequencing. RNA was isolated and libraries were prepared from different mRNA samples followed by next generation sequencing. Raw count table was further processed to calculate a $\log_2$FC.
To get a broad overview of the effect of PAF1c depletion on MYC gene regulation, a 2D bin plot was generated. Around 13,000 genes were sorted and binned according to their responsiveness to MYC activation (Walz et al., 2014). The same bins were plotted upon *CTR9* or *CDC73* depletion.
Whereas the slope of the non targeting control (see figure 4.23 C, light grey line) was around 1, the slope of the mean of all different shRNAs targeting subunits of the PAF1c was overall flatter.

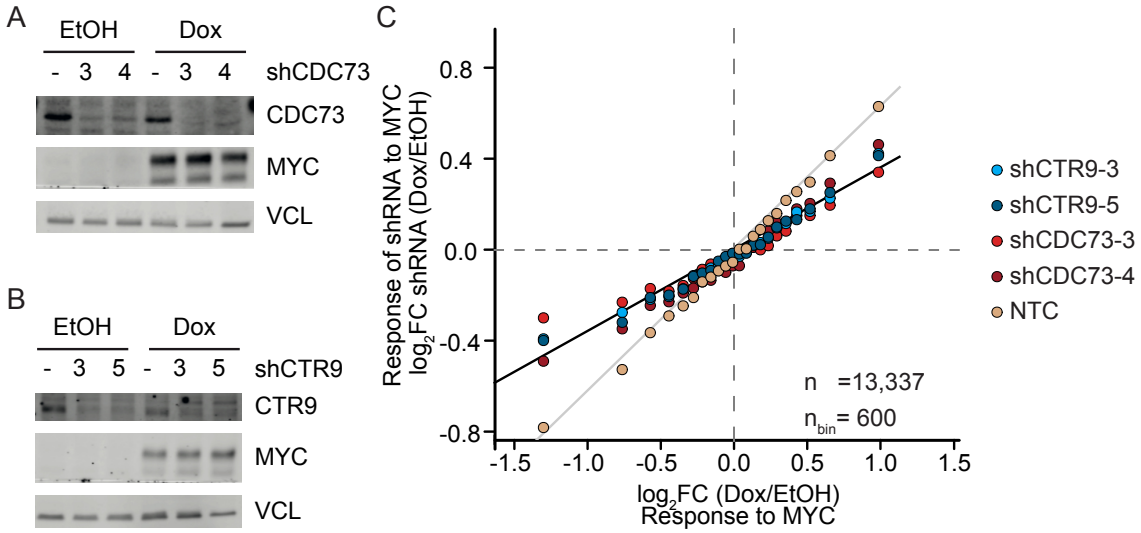

Figure 4.23: Attenuation of MYC-dependent gene expression upon PAF1c knockdown.
A) Comparison of CDC73 protein levels in control cells and upon CDC73 depletion. Cells were either infected with the pGPIZ vector containing a non targeting control ("-") or two different shRNAs targeting *CDC73*. Where indicated, cells were treated 72 h after infection with 1 µg/ml doxycycline for 24 h prior to cell lysis. Specific antibodies targeting CDC73, MYC or vinculin ("VCL") were used. VCL served as loading control.
B) Comparison of CTR9 protein levels in control cells and upon CTR9 depletion Cells were processed and analysed as described in A.
C) Bin plot summarizing RNA sequencing experiment. 13,337 genes were sorted depending on their MYC response from published in Walz et al. (2014). Genes were grouped into 23 bins 0 genes. Inducibility of MYC in U2OS MYC Tet-On cells was compared between the Non targeting control on PAF1c subunit knockdown cells. Cells were treated as described in A or B. Light grey line represents the slope of the control condition. Dark grey line represents the slope of the mean of all four shRNAs targeting the PAF1c subunits CDC73 or CTR9.
Peter Gallant performed the bioinformatical analysis.
This figure was published in similar form in Endres et al. (2021).

These result suggests that genes were less activated but also less repressed by MYC in the absence of PAF1c subunits.

To further validate that MYC's transcriptional activation is reduced upon PAF1c depletion, gene set enrichment analysis (GSEA) was performed. MYC induction showed a significantly normalized enrichment score (NES) in established "MYC-responsive" datasets from the curated signatures (C2) from the Molecular Signature Database. "MYC-responsive" data sets highlighted in table 4.1 showed a significant enriched positive NES in control samples ("shNTC") whereas PAF1c depleted samples still showed a positive NES but to a lesser extent (see 4.1, "shCDC73-3" and "shCTR9-3").

Table 4.1: MYC target gene sets activated after MYC induction in U2OS MYC-Tet-On.
Gene set enrichment analysis comparing EtOH with Dox in different conditions (NTC, shCDC73 and shCTR9). Gene expression profiles of control cells or cells with either *CDC73* or *CTR9* knockdown were compared to to published gene sets from the curated signatures (C2) from the Molecular Signature Database. U2OS MYC Tet-ON were either infected with the pGIPZ vector containing a non targeting control or shRNAs targeting either *CTR9* or *CDC73*. Cells were treated 72 h after infection with 1 µg/ml doxycycline or EtOH for 24 h prior harvest.
NES: normalized enrichment score; p: nominal p-value; q: false discovery rate.
Schumacher: SCHUHMACHER MYC TARGETS UP; Schlosser: SCHLOSSER MYC TARGETS AND SERUM RESPONSE UP.

gene sets	shNTC			shCDC73-3			shCTR9-3		
	NES	**p**	**q**	**NES**	**p**	**q**	**NES**	**p**	**q**
Schuhmacher	2.08	0.000	0.058	1.70	0.002	0.685	1.50	0.016	0.948
Schlosser	1.73	0.008	0.32	1.80	0.002	0.563	1.45	0.051	0.944

These results are in line with the results from the bin plot: Upon depletion of PAF1c subunits, MYC's transcriptional activity is subdued.

When comparing MYC induction upon knockdown of PAF1c subunits *CDC73* or *CTR9*, with control cells upon MYC induction, several gene sets, involved in DNA damage repair, showed a significant negative NES (see table 4.2). Those gene sets are part of the Molecular Signature Database in gene sets from the curated signatures (C2). Shown in table 4.2 are the gene sets with a significant negative NES upon MYC induction and PAF1c knockdown. The NES scored all within the samen negative range independent of the depletion of the PAF1c subunit and the gene set.
In sum, this data suggests that PAF1c enhances MYCs transcriptional activity and additionally acitvates genes which are involved in DNA damage repair.

Table 4.2: Gene sets repressed after PAF1c knockdown at oncogenic MYC levels. Gene set enrichment analysis comparing control cells with cells expressing an shRNA targeting *CDC73* or *CTR9* upon MYC induction. Gene expression profiles of control cells or cells with either *CDC73* or *CTR9* knockdown after MYC induction were compared to published gene sets from the curated signatures (C2) from the Molecular Signature Database. U2OS MYC Tet-ON were either infected with the pGIPZ vector containing a non targeting control ("shNTC") or shRNAs targeting either CTR9 or CDC73. Cells were treated 72 h after transfection with 1 µg/ml doxycycline for 24 h prior harvest.
NES: normalized enrichment score; p: nominal p-value; q: false discovery rate.
HR: homologous recombination; DSB: double strand break.
HR of replication independent DSB: REACTOME HOMOLOGOUS RECOMBINATION REPAIR OF REPLICATION INDEPENDEN DOUBLE STRAND BREAKS; DSB repair: REACTOME DOUBLE STRAND BREAK REPAIR; DNA repair: REACTOME DNA REPAIR; DNA repair genes: KAUFFMANN DNA REPAIR GENES.

gene sets	shCDC73-3			shCTR9-3		
	NES	**p**	**q**	**NES**	**p**	**q**
HR of replication independent DSB	-1.76	0.060	0.092	-2.00	0.000	0.036
DSB repair	-1.80	0.000	0.075	-1.88	0.000	0.066
DNA repair	-1.81	0.000	0.071	-1.76	0.000	0.095
DNA repair genes	- 1.78	0.000	0.087	-1.74	0.000	0.103

4.10 PAF1c suppresses transcription-dependent DNA damage

The attenuation of MYC-dependent gene expression upon depletion of the PAF1c subunits *CDC73* or *CTR9* shown in section 4.9, raised the question if PAF1c depletion would also have an effect on cell proliferation.

To investigate the specific contribution of PAF1c on MYC dependent cellular phenotypes, U2OS MYC Tet-On cells were infected with shRNAs targeting two different subunits of the PAF1c and their proliferation was tested with a colony formation assay.

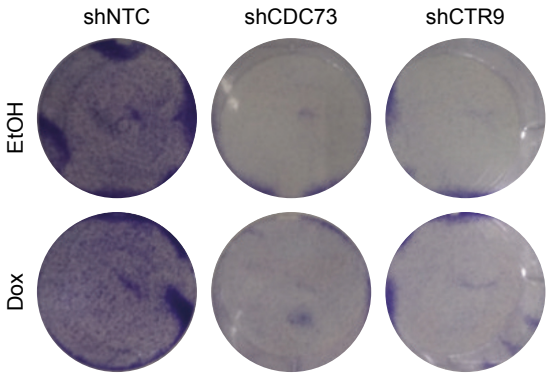

Figure 4.24: Reduced proliferation upon knockdown of PAF1c.
Crystal violet staining of control cells or PAF1c knockdown cells. U2OS MYC Tet-ON cells expressing the lentiviral pGIPZ vector including either a non targeting control (NTC) or shRNA sequences targeting *CDC73* (shCDC73) or *CTR9* (shCTR9). Where indicated, 1 µg/ml doxycycline was added for 24 h before staining. Cells were stained 96 h post infection. Representative experiment of biological triplicates is shown.
This figure was published in similar form in Endres et al. (2021).

Proliferation was retarded in cells upon depletion of either *CTR9* or *CDC73* independently of MYC induction (see figure 4.24).

To analyse the effects of PAF1c depletion upon MYC activation, cell cycle distribution was analyzed using PI-FACS. U2OS MYC-ER or MYC Tet-ON cells were infected with a non targeting control or shRNAs targeting either *CDC73* or *CTR9*. 48 h post infection cells were selected for 24 h. 24 h prior fixation with ice cold EtOH, cells were either treated with 4-OHT (U2OS MYC-ER) or doxyxycline (U2OS MYC Tet-ON). Cell distribution was analyzed based on the DNA content determined via PI intercalation.
Activation of MYC upon treatment with 4-OHT in U2OS-MYC-ER cells or induction of MYC expression upon doxycyline in U2OS MYC Tet-ON cells led to a slight increase in the proportion of cells in S-phase (see figure 4.25 A "shNTC", "4-OHT" and B, "shNTC", "Dox"). Knockdown of *CDC73* or *CTR9* led to an increase of cells arrested in S-phase upon MYC activation compared to the PAF1c depletion alone (see figure 4.25 A).

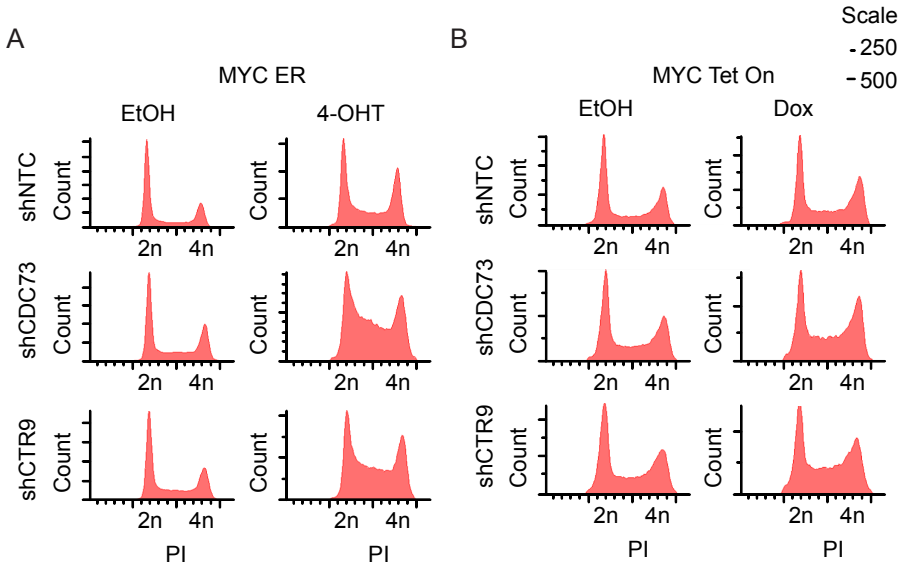

Figure 4.25: PAF1c knockdown leads to a delay in DNA replication at oncogenic MYC levels.
A) PI-FACS of control cells or cells expressing a contitutive knockdown of either *CDC73* or *CTR9* upon MYC activation. U2OS MYC-ER cells were either infected with the pGIPZ vector containing a non targeting control ("shNTC") or shRNAs targeting either *CDC73* or *CTR9*. Where indicated, cells were treated 72 h after infection with 200 nm 4-OHT for 24 h.
B) PI-FACS of control cells or cells expressing a contitutive knockdown of either *CDC73* or *CTR9* upon MYC induction. U2OS MYC Tet-ON cells were either infected with the pGIPZ vector containing a non targeting control ("shNTC") or shRNAs targeting either *CDC73* or **CTR9**. Where indicated, cells were treated 72 h after infection with 1 µg/ml doxycyclin for 24 h.
This figure was published in similar form in Endres et al. (2021).

To further investigate pathways resulting in enhanced S-phase arrest (see figure 4.25) and accumulation of double strand breaks downstream of the TSS (see figure 4.22), activation of target genes of ATM and ATR signaling pathway was determined. Activity of the ATM reflects double strand breaks while ATR is activated during replication stress.

To understand this observation immunoblot was performed with specific antibodies indicating activities of ATR or ATM kinases in U2OS MYC Tet-ON control cells or cells expressing a constitutive knockdown of the PAF1c subunits *CDC73* or *CTR9*. Activity of the ATM or ATR kinase reflects double strand breaks or replicational stress.

Protein levels of CTR9 and CDC73 were reduced upon infection with shRNAs targeting the respective proteins (see figure 4.26 A and B, "shCDC73", "shCTR9") compared to the non targeting control (figure 4.26 A and B, "shNTC"). MYC protein

levels in U2OS MYC Tet-On cells were not affected upon treatment with shRNAs targeting the two different PAF1c subunits compared to the control (see figure 4.26 A and B,"shCDC73", "shCTR9" compared to "shNTC").

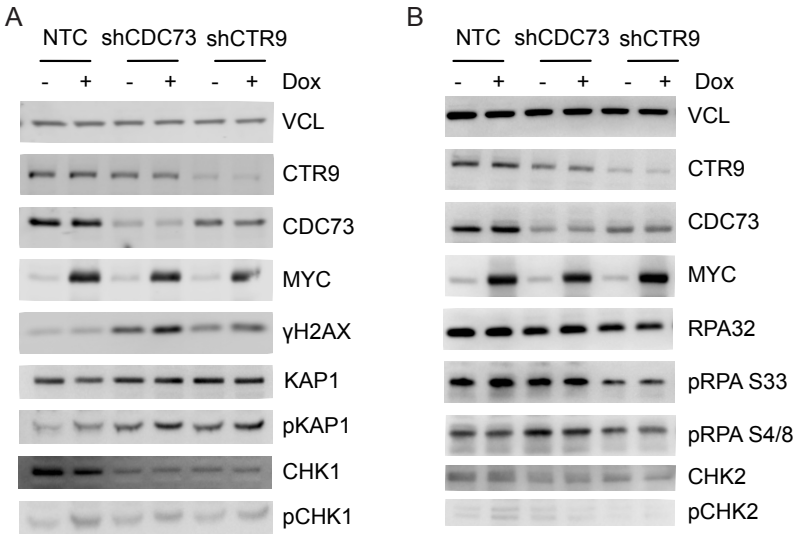

Figure 4.26: PAF1c knockdown at oncogenic MYC levels leads to an activation of the ATM kinase.
A) Comparison of protein levels in control cells and *CDC73* or *CTR9* knockdown cells. Protein lysates of U2OS MYC-ER cells. Protein lysates of U2OS MYC Tet-ON cells. Cells were either infected with the pGIPZ vector containing a non targeting control ("NTC") or shRNAs targeting either *CDC73* or *CTR9*. Were indicated, cells were treated 72 h after infection with 1 µg/ml doxycycline for 24 h prior to cell lysis. Specific antibodies targeting the indicated proteins CTR9, CDC73, MYC, γH2AX, KAP1, pKAP1 (S824), CHK1, pCHK1 (S345) or vinculin ("VCL") were used. VCL served as loading control.
B) Comparison of protein levels in control cells and CDC73 or CTR9 knockdown cells. Treatment of the cells followed by cell lysis were performed as described in A. Specific antibodies targeting CTR9, CDC73, MYC, RPA32, pRPA (S33) or pRPA (S4/8), CHK2 or pCHK2 (Thr68) or vinculin ("VCL") were used. VCL served as loading control.
This figure was published in similar form in Endres et al. (2021).

MYC induction in control cells did not induce phosphorylation of H2AX, KAP1 conveyed by the ATM kinase nor CHK1 (ATR target protein) as protein levels of γH2AX, pKAP1 (S824) and pCHK1 (S345) remained unaffected (see figure 4.26 A, "shNTC"). The same observation was made with the ATM kinase target protein CHK2 (see figure 4.26 B, "shNTC") and RPA S33 or RPA S4/8, a target protein of DNA-PK (see figure 4.26 B, "shNTC"). Depletion of either *CDC73* or *CTR9*, led to phosphorylation of H2AX or KAP1 and this was even further increased upon induction of MYC (see figure 4.26 A, "shCDC73" and "shCTR9") compared to the control condition. Knockdown of the PAF1c subunit reduced total CHK1 levels.

Considering this reduction of total CHK1 levels, PAF1c depletion also led to an increase in pCHK1 which was even more prominent upon MYC induction (see figure 4.26 A, "shCDC73" and "shCTR9"). Target proteins of the ATR kinase and DNA-PK were unaffected shown here as the phosphorylation status of RPA32 (see figure 4.26 B, "shCDC73" and "shCTR9").

To study in which phase of the cell cycle the DNA damage is most prominent in PAF1c knockdown cells upon MYC induction, immuno staining of the DNA damage marker γH2AX was performed in U2OS MYC Tet-On cells upon knockdown of *CTR9*.

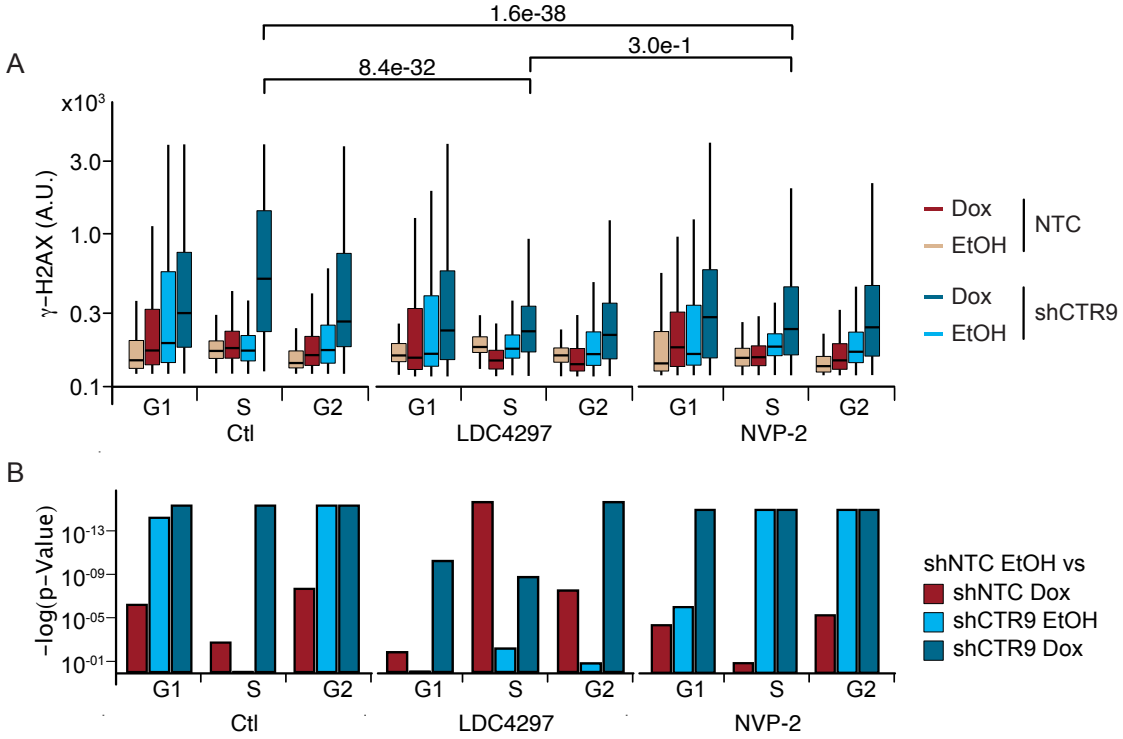

Figure 4.27: MYC-stimulated increase in DNA Damage upon PAF1c knockdown.
A) Quantitative immunofluorescence of γ-H2AX in control cells or CTR9 knockdown cells treated with the CDK7 inhibitor LDC4297 (0.5 µM) or the CDK9 inhibitor NVP-2 (1 µM) for 3 h. U2OS MYC Tet-ON cells expressing shCTR9 or shNTC as a control were employed. Where indicated, cells were treated 72 h after infection with 1 µg/ml doxycycline for 24 h. 10 µM EdU was incorporated 30 min prior fixation followed by staining. Cell cycle was stratified using Hoechst staining. Shown is a boxplot of the intensity of γ-H2AX for at least 800 cells. Statistical significance was calculated using Wilcoxon rank sum test. (n=3)
B) Significance of immunofluorescence shown in A. Pairwise comparisons were calculated with the Wilcoxon signed rank test. "NTC EtOH" serves as reference group.
This figure was published in similar form in Endres et al. (2021).

EdU is a thymidine analogue which incorporates into DNA during active DNA synthesis. Cells were co-stained with γ-H2AX and Hoechst and measured on the Operetta High Throughput operating system. EdU Click-iT® technology and Hoechst staining were used to determine the cell cycle phase of each cell. Mean intensity signal of γ-H2AX for each cell population in each cell cycle phase was determined and visualized in a boxplot shown in figure 4.27 A. Significance of the different conditions within each cell cycle phase was calculated using Wilcoxon rank sum test and visualized in a histogram plotting the negative log-change of the p-values resulting from the Wilcoxon rank sum test (see figure 4.27 B).

In G1, S and G2/M phase MYC induction led to a slight but significant increase in γ-H2AX signal (see figure 4.27 A and B, "Ctl", "Dox", "NTC", red boxplot). Knockdown of *CTR9* led to an increase of γ-H2AX in G1 or G2/M phase (see figure 4.27 A and B,"Ctl", "shCTR9", "EtOH", light blue boxplot). Cells in S-phase were unaffected. *CTR9* depletion and additional MYC induction led to a significant increase in the DNA damage marker γ-H2AX throughout the cell cycle but the most significant increase was observed in S-phase (see figure 4.27 "Ctl", "shCTR9", "Dox", dark blue boxplot).

To study, if the DNA damage in S-phase is transcription-dependent, inhibitors against CDK7 or or CDK9 (the catalytic subunit of P-TEFb) were used. Cells were treated as described above but additionally treated with DMSO, LDC4297, a CDK7 inhibitor or NVP-2, a CDK9 inhibitor for 3 h. LDC4297 inhibitor treatment significantly reduces γ-H2AX in cells with high MYC levels as well as in cells depleted for *CTR9* with oncogenic MYC levels (see figure 4.27 "LDC4297", "shCTR9", "Dox", dark blue boxplots, p=8.4e-32). A comparable effect was seen inhibiting further downstream of the transcription cycle with NVP-2 (see figure 4.27 A and B, "NVP-2", "shCTR9", "Dox", dark blue boxplots, p=1.6e-38).

The high throughput microscopy analysis of the γH2AX staining indicates that most of the DNA damage occurs during S-phase. To further investigate this γ-H2AX staining was analysed using a confocal microscope.

Cells were co-stained with EdU and γ-H2AX. To calculate the colocalisation between γ-H2AX and EdU signal, a Pearson Correlation Coefficient (PCC) was assessed. Control cells showed low levels of γ-H2AX spots with a mild overlap of the DNA synthesis marker EdU spots (see figure 4.28, "shNTC", "EtOH", PCC=0.683). As

seen before (figure 4.27 ,"Ctl", "NTC", "Dox")), DNA damage signal was slightly increased upon MYC induction (see figure 4.28, "shNTC", "Dox", PCC=0.730). *CTR9* depletion resulted in an enhanced γ-H2AX signal which did not further overlap with DNA synthesis compared to MYC induction alone (see figure 4.28 "shCTR9", "EtOH", PCC=0.748). *CTR9* depletion under MYC oncogenic levels resulted in an increased in size of γ-H2AX spot and in addition in an elevated overlap of EdU and γ-H2AX spots (see figure 4.28, "shCTR9", "Dox", PCC=0.930).

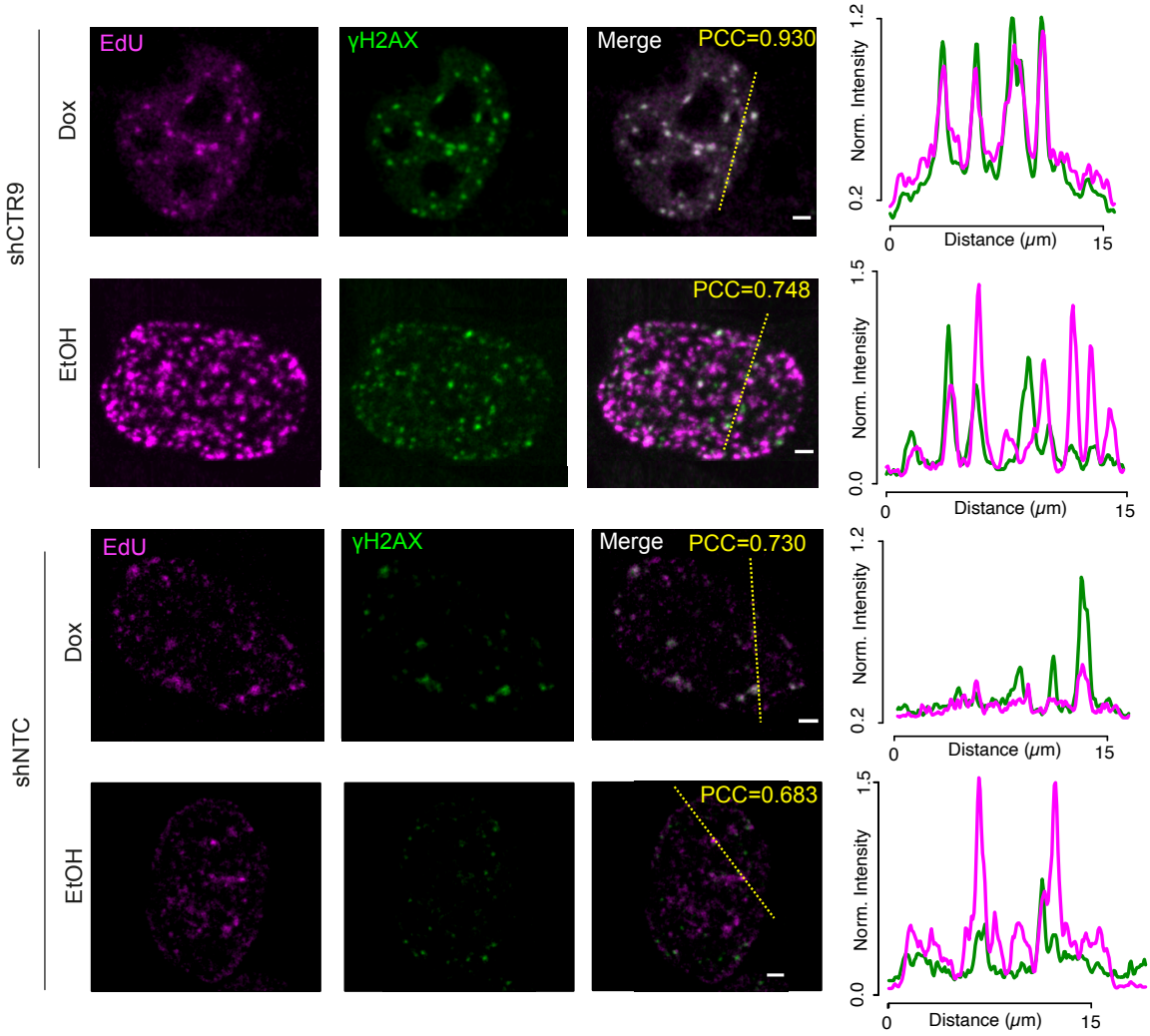

Figure 4.28: MYC-stimulated increase in DNA Damage upon PAF1c knockdown during DNA synthesis.
Confocal images of control or *CTR9* knockdown cells upon induction of MYC showing EdU incorporation immediately adjacent to γ-H2AX foci. U2OS MYC Tet-ON cells were either infected with the pGIPZ vector containing a non targeting control ("shNTC") or shRNAs targeting *CTR9*. Where indicated, cells were treated 72 h after infection with 1 µg/ml doxycycline for 24 h. 10 µM EdU was incorporated for 30 min prior fixation followed by staining. Pearson Coefficient Correlation (PCC) was calculate fo colocalization between EdU and γ-H2AX. Distance and normalized intensity of both stainings are shown in the graphs on the right and were used to calculate PCC.
Apoorva Baluapuri performed staining and analysis.
This figure was published in similar form in Endres et al. (2021).

The distribution of overlap of DNA damage marker spots with DNA synthesis marker spots using the PCC of 17-21 cells was visualized in a violin plot (see figure 4.29). At physiologic MYC conditions a broad distribution was obtained (see figure 4.29, "EtOH"). Upon oncogenic MYC levels the PCC distribution between EdU and

γ-H2AX became closer to 0.75 in all cells, resulting in a more restricted distribution (see figure 4.29, "Dox"). As already highlighted in the representative image in figure 4.28, the PCC in *CTR9* depleted cells upon MYC induction resulted close to 1 in a restricted distribution (see figure 4.29, "shCTR9", "Dox").

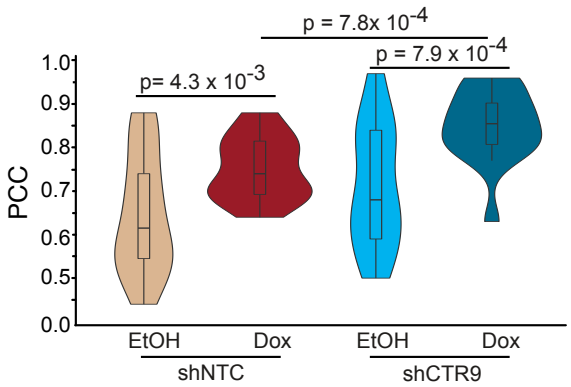

Figure 4.29: Quantification of MYC-stimulated increase in DNA Damage upon PAF1c knockdown during DNA synthesis.
Violin plot of Pearson correlation coefficient (PCC) for co-localization of DNA synthesis and γ-H2AX. Pearson correlation was performed for each of the experimental conditions (n = 17-21 cells) shown in figure 4.28. Cells were treated as described in 4.28.
Apoorva Baluapuri performed the analysis.
This figure was published in similar form in Endres et al. (2021).

This data suggests that increased portion of γ-H2AX positive cells in S-phase (figure 4.25) results from an enhanced ATM kinase activity (figure 4.26) and that the DNA damage of *CTR9* depleted cells under MYC induction is co-transcriptional (figure 4.27) and occurs during DNA synthesis (figure 4.28 and 4.29).

5 Discussion

The oncogene MYC is interacting with multiple proteins involved in all steps of the transcriptional cycle (Baluapuri et al., 2019; Büchel et al., 2017; Heidelberger et al., 2018; Kalkat et al., 2018). Jaenicke et al. (2016) proposed a model in which ubiquitin-dependent turnover of MYC is needed for transcriptional elongation at which the interaction between MYC and PAF1c play an important role. Therefore the objective of this thesis was to elucidate the underlying mechanism and function of the PAF1c-MYC interaction in the context of RNAPII transcription.

5.1 MYC directly interacts with SPT5 and PAF1c

Several interactome analyses of MYC and MYCN showed interaction of MYC proteins with PAF1c subunits CTR9 and CDC73 as well as DSIF subunit SPT5 (Baluapuri et al., 2019; Büchel et al., 2017; Heidelberger et al., 2018; Kalkat et al., 2018). Kalkat et al. (2018) used BioID to analyse interaction partners of MYC. BioID method biotinylates proteins which are in close poximity of your protein of interest. Baluapuri et al. (2019) and Büchel et al. (2017) used mass spectrometric analysis of immunoprecipitation of HA-tagged MYC or MYCN. Jaenicke et al. (2016) showed co-immunoprecipitation experiments where CTR9 or CDC73 are interacting with MYC in the presence of the proteasome inhibitor MG132. Furthermore, Jaenicke et al. (2016) suggests that PAF1c binds MYCBox I.

Importantly, all described assays could be due to indirect interactions between PAF1c and MYC as the described data resulted from immunoprecipitation or close proximity assays from cell lysates. For this reason, the direct interaction of MYC with PAF1c or with DSIF was tested here. Pulldown assays (see figure 4.3) corroborated the direct interaction between PAF1c and MYC. All subunits of PAF1c were pulled down

with GST-MYC, suggesting, that PAF1c is interacting with MYC. Regarding the interaction between DSIF and MYC, no clear conclusion could be drawn. While the subunit SPT5 directly interacted, the smaller subunit SPT4 was not even detected in the input (see figure 4.2). This might be due to suboptimal salt concentrations in washing and pulldown buffer for SPT4. Therefore, we conclude from the data, that SPT5 is interacting with MYC but a direct interaction of the complete DSIF complex with MYC could not get validated.

Enhanced interaction between phosphorylated MYCBox I peptide and the subunit CDC73 was observed (Jaenicke et al., 2016). To test, whether MYCBoxes are needed for direct interaction between PAF1c and MYC, *In vitro* pulldown experiments of MYC deletion mutants lacking either MYCBox I or MYCBox II from figure 4.4 show that neither MYCBox I nor II are necessary for the interaction. Probably, post-translational modifications of MYC such as phosphorylation and ubiquitylation control its function: this suggests, that phosphorylation of MYCBox I enhances the interaction between PAF1c and MYC but is not necessary for the direct interaction.

Despite of the classical paradigm which claims that proteins are only functional when folded properly in a defined structure (Anfinsen, 1973), more recent data show, that transcription factors bearing low complexity structures (frequently named intrinsically disordered domains, IDRs), mostly found in eukaryotes, have a functionality or even multifunctionality (Tarczewska and Greb-Markiewicz, 2019). It is believed that in brHLHLZ transcription factors (as MYC) those IDRs seve as hubs for other factors - even for those which contain IDR but do not contain a brHLHLZ motif themselves - to expand their network (Iakoucheva et al., 2004; Sharma et al., 2015). PAF1c contains as well IDRs (Vos et al., 2018a). IDRs are also proposed to serve as a 'hub' for multiple cancer events (Lasorella et al., 2014) suggesting that MYC-PAF1c interaction is one of those events which might be benefical for tumor cells.

Those observations lead to the conclusion that MYC and PAF1c interact through their IDR and that phosphorylations might enhance this interaction similarily to what was observed for the enhanced interaction between the tail of CDC73 with the phoshorylated CTD of the RNAPII (Amrich et al., 2012).

Due to the large accessibility of different residues within IDR of proteins, they can be easily posttranslationally modified (Iakoucheva et al., 2004). Therefore, enhanced interaction between MYC and PAF1c might be counteracted by another modification

of MYC: the ubiquitylation. There are several observations leading to this idea: First, Jaenicke et al. (2016) observed enhanced interaction between PAF1c and MYC upon treatement with the proteasome inhibitor MG132. Second, HUWE1 turned out to be the top hit in a PLA based siRNA screen targeting E3 ligases (see figure 4.20 and Endres et al. (2021)). Cells treated with siRNA targeting *HUWE1* showed enhanced interaction between PAF1 and MYC. And third, Heidelberger et al. (2018) suggests, that HUWE1 ubiquitylates MYC at K148 which is in turn removed from chromatin by VCP. Overall, this suggests that phosphorylated chromatin-bound MYC is interacting with PAF1c to bring the complex in close proximity to the RNAPII. As soon as HUWE1 ubiquitylates MYC and the CTD of the RNAPII is phosphorylated, the affinity between the interaction partners is changing and PAF1c is transferred onto the RNAPII while MYC is dissociating from the chromatin via VCP (see figure 5.1).

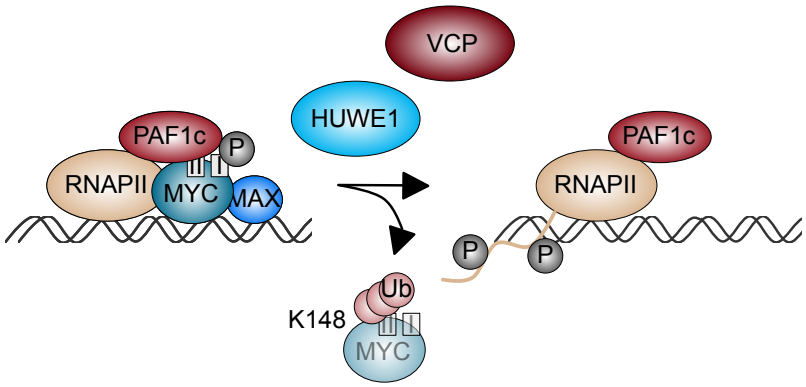

Figure 5.1: Suggested transfer model of PAF1c from MYC onto RNAPII via PTMs. Phosphorylation of MYC at MYCBox I enhances interaction with PAF1c. PAF1c is transferred from MYC onto RNAPII after ubiquitylation of MYC and phosphorylation at Ser2 of the CTD of the RNAPII.

5.2 SPT5 and MYC: an interaction to keep the chromatin accessible

After confirming the direct interaction between MYC and SPT5, we next investigated its biological relevance. DSIF has two roles during transcription: on the one hand, it induces promoter proximal pausing in collaboration with NELF (Vos et al., 2018b),

on the other hand, it promotes elongation, as part of the activated elongation complex consisting of RNAPII, DSIF, SPT6 and PAF1c (Vos et al., 2018a). DSIF is transferred onto the RNAPII during the initiation step of transcription in a CDK7-dependent manner (Fisher, 2019). Interestingly, Baluapuri et al. (2019) showed that MYC hands over the DSIF subunit SPT5 in dependency of CDK7 onto the RNAPII. This observation is in line with other publications that MYC promotes different steps of the transcription cycle (Büchel et al., 2017; de Pretis et al., 2017; Rahl and Young, 2014; Walz et al., 2014), and that the transfer of SPT5 from MYC onto RNAPII is relevant for elongation but not initiation (Baluapuri et al., 2019; de Pretis et al., 2017). Accordingly, we showed that RNAPII is initiated and starts to elongate upon SPT5 depletion, but a portion of RNAPII does not reach the end of the gene (see figure 4.11). This assumption is additionally confirmed by the calculated processivity score (see figure 4.11 D). Furthermore, Baluapuri et al. (2019) observed that not only processivity is positively affected by MYC but also directionality meaning that MYC prevents the RNAPII in traveling in antisense direction.

Intriguingly, figure 4.13 showed that upon oncogenic MYC levels, SPT5 is squelched from the RNAPII; this, in combination with the reduced processivity upon lack of SPT5 suggests that at oncogenic MYC levels RNAPII is less productive. Interestingly, a high portion of unproductive RNAPII remains bound to chromatin.

But what would be the benefit for an oncogenic cell, to have less productive RNAPII bound to chromatin? This finding opens to an intriguing scenario, in which the SPT5-MYC interaction is required to keep chromatin accessible. This would support the function of the interaction of MYC with another major partner: WDR5. Strickingly, the WDR5-MYC interaction promotes not only MYC recruitment to its target promoters, but also chromatin accessibility (Thomas et al., 2015). In this view, the SPT5-MYC interaction would then be required to keep promoters active and SPT5, when squelched from RNAPII would prevent heterochromatization by keeping unproductive RNAPII close to promoter regions.

5.3 PAF1c and MYC: another interaction partner at the elongation step?

In vitro pulldown experiments showed direct interaction between MYC and PAF1c. Consequently, the underlying mechanism of this interaction was investigated in more detail. All active promoters are occupied by MYC. By forming a heterodimer with MAX, MYC can bind EBoxes thanks to its brHLHLZ motif. But only one third of MYC binding sites contains canonical EBox motif sequences. Additionally, MYC/MAX heterodimers have a significant preference towards an EBox motif but they also display a high affinity towards any DNA (Guo et al., 2014). Lorenzin et al. (2016) concluded that there are two high affinity classes of MYC binding sites: one contains a consensus EBox and the other one non-specific DNA motif to which MYC is recruited thanks to other factors such as WDR5.

MYC ChIP-Rx data (see figures 4.9 and 4.6) showed a reduction of MYC upon PAF1c depletion. This concludes that PAF1c is an important factor for MYC's occupancy on chromatin. Since it was shown in *Drosophila melanogaster*, that LEO1 subunit helps to recruit MYC to chromatin (Gerlach et al., 2017), the mechanism might be conserved.

Chen et al. (2017b) suggested that PAF1c regulates promoter proximal pause release via enhancer activity. This activation upon depletion of the PAF1 subunit led to enhanced pause release of RNAPII in nearby PAF1c activated genes. Additionally, knockout of PAF1c regulated enhancers, abolished this effect.

We therefore investigated if the MYC-PAF1c interaction is relevant for enhancer binding of MYC proteins. Analysis of MYC binding to chromatin at promoter or enhancer regions upon PAF1c depletion showed, that reduced MYC occupancy was negatively affected at promoters but not enhancers (see figure 4.7 and 4.10). These observations suggest that PAF1c-MYC interaction is mostly important at active genes. Next, we investigated the potential, converse role of MYC in PAF1c chromatin recruitment.

Considering the different models which are based on observations of different MYC levels (see introduction subsection 1.2.3), a comprehensive analysis of PAF1c occupancy upon MYC level manipulation was performed using two different cell

lines, U2OS cell line (p53 wildtype) and K562 cell line (p53 null mutant) and three different MYC manipulation methods. U2OS cells either expressed ectopic MYC levels resulting in up to five times higher MYC protein level (see figure 4.8) or a MYC-ER system to activate MYC via translocation from the cytoplasm into the nucleus. Both systems resulted in higher MYC levels. The K562 cell line includes a MYC-AID system (Muhar et al., 2018), by which the MYC protein is degraded within a short time period (see 4.18). In U2OS expressing ectopic MYC, CTR9 and CDC73 were recruited to gene bodies upon high MYC levels (see figure 4.14). The PAF1c is not directly DNA bound but indirectly bound to chromatin via RNAPII. To bring this observation in line with the previously made conclusion, it would suggest that a preformed MYC-PAF1c complex is recruited to chromatin and PAF1c subsequently is transferred onto the RNAPII, traveling alongside until the TES is reached.

Interestingly, it appears that CTR9 is already recruited at the TSS whereas CDC73 is only efficiently chromatin-bound after the TSS. Distinct binding patterns on chromatin in between the different subunits of PAF1c were already described in the literature (Yang et al., 2016). Xie et al. (2018) showed, that CTR9 and PAF1 subunits form a subcomplex in yeast which is needed for the PAF1c to assemble completely. Amrich et al. (2012) reported that the subunits CDC73 and RTF1 are needed to bind elongating RNAPII. Thus, in combination with the observation that LEO1 is as well important for MYC recruitment to promoters (Gerlach et al., 2017) and that LEO1 interacts directly with PAF1 (Chu et al., 2013) it is conceivable that MYC and CTR9-PAF1-LEO1 are forming a subcomplex, which is recruited to the chromatin. When the CTR9-PAF1-LEO1 subcomplex is transferred onto the RNAPII, a stable PAF1c is assembling on the elongating RNAPII via a CDC73-RTF1 subcomplex to promote elongation. This leads to the speculation that MYC serves as a "hub" for PAF1c to assemble properly and spatially-precisely (see figure 5.3). A less provocative and more technical interpretation for this observation would be, that the antibody binding site is differently accessible for the different subunits and might be blocked by another subunit ending up in a different occupancy pattern.

The next question we investigated concerned the speed of the transfer of PAF1c from MYC onto the RNAPII. This matter was addressed by taking advantage of a fast system of MYC activation (U2OS MYC-ER). Two different timepoints were chosen:

one very short time point for 10 minutes of activation and the other one after 30 minutes when MYC levels are saturated on known promoter regions depending on their occupancy (see figure 4.15). Strikingly, global MYC occupancy shot up within 10 minutes and was reduced again after 30 minutes of tamoxifen treatment (see figure 4.16). This is in keeping with the known literature about MYC turnover that indicates that HUWE1 drives the transfer of PAF1c onto RNAPII (see figure 4.20) by ubiquitylating MYC so that VCP can extract MYC from chromatin (Heidelberger et al., 2018). In this view, 10 minutes of MYC activation are not enough for an efficient MYC ubiquitylation-chromatin-extraction process but after 30 minutes the HUWE1-VCP machinery had adapted to the MYC overload.

The elongating form of RNAPII (pS2) showed a constant increase into the gene body already after 10 minutes MYC activation (see figure 4.17). Even though MYC regulates different steps of the transcriptional process, it is predominantly promoting transcriptional elongation. (Baluapuri et al., 2019; de Pretis et al., 2017; Herold et al., 2019; Rahl et al., 2010; Rahl and Young, 2014). Interestingly, CTR9 ChIP-Rx did not follow the same pattern as the elongating RNAPII and an efficient PAF1c enrichment was observed only after 30 minutes of MYC activation (see figure 4.17) suggesting that other "earlier" co-factors are important for MYC-induced elongating RNAPII. One of those factors - as already discussed - could be SPT5 (see section 5.2). MYC-dependent transfer of SPT5 onto the RNAPII happens in a CDK7-dependent manner (Baluapuri et al., 2019). Additionally, DSIF facilitates PAF1c recruitment onto the RNAPII (Wier et al., 2013), and NELF is blocking the binding site of PAF1c (Vos et al., 2018b). Collectively, this suggests a model in which - within 10 minutes- WDR5 enhances MYC occupancy at active promoters, another MYC molecule transfers SPT5 in a CDK7-dependent manner, and a third MYC molecule recruits PAF1c to a later timepoint to assemble properly on the elongation RNAPII-SPT5 complex allowing an efficient elongation complex to be formed (see figure 5.2).

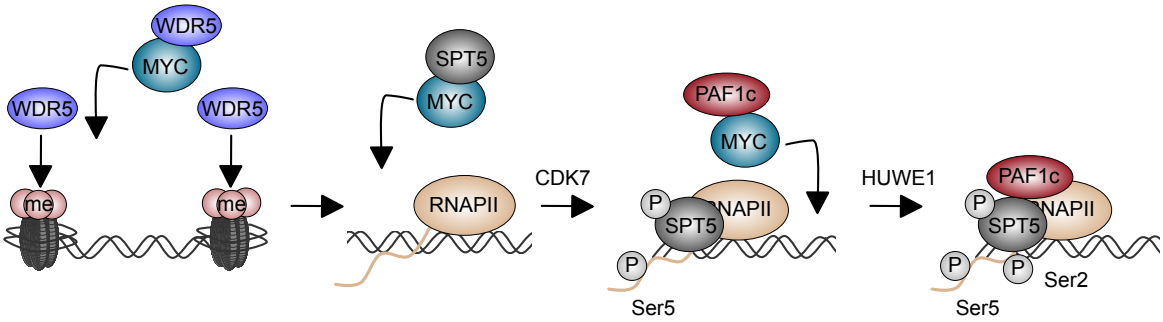

Figure 5.2: Proposed model for MYCs involvement in the transcriptional cycle. MYCs interaction with WDR5 for recruiting MYC to active promoters. Interaction with SPT5 for processivity and open chromatin. Interaction with PAF1c at the transition to elongation. P: phosphorylation; me: methylation.

Next, we investigated how PAF1c occupancy is changing in cells which contain high MYC levels and in addition harbour a p53 null mutation which is common in several cancer entities. K562 cells containing a MYC-AID construct (Muhar et al., 2018) were used to acutely deplete MYC acutely (30 minutes). Importantly, the phenotype mirrors the one observed in the U2OS MYC-ER cells after 30 minutes of MYC activation: whereas total RNAPII was mildly affected by acute MYC depletion, CDC73 occupancy was reduced in the body of the gene (see figure 4.19).

Taken together, the MYC-mediated PAF1c transfer onto the RNAPII appears to be robust and quick in cells bearing oncogenic MYC levels and promotes an assembly of a activated elongation complex. Endres et al. (2021) and figure 4.20 show that the MYC-dependent transfer of PAF1c happens ubiquitin-dependent and CDK9-independent. This is in line with Aoi et al. (2020). There they suggest a two step pausing in promoter regions: The first pausing is NELF-dependent while the second one is independent of NELF. In this context, our observations suggest that MYC first transfers SPT5 in a CDK7-dependent manner onto the RNAPII (Baluapuri et al., 2019), where it pauses with NELF (Vos et al., 2018b). Subsequently, MYC promotes the assembly of a CTR9-PAF1-LEO1 subcomplex whereas concomitantly CDC73-RTF1 subcomplex assembles with DSIF onto the RNAPII. As soon as NELF dissociates from the paused RNAPII and HUWE1 and VCP extract MYC from chromatin, the PAF1c subcomplex is transferred onto the RNAPII forming an activated elongation complex consisting of RNAPII, DSIF, SPT6 and PAF1c (see figure 5.3). Additionally, all those assemblies are likely to be controlled by

post-translational modifications which allow fast respones to changes within the cellular environment: Phosphorylation of MYCBox I enhances the interaction between PAF1c and MYC (Jaenicke et al., 2016) whereas the transfer of PAF1c onto RNAPII is ubiquitin-dependent.

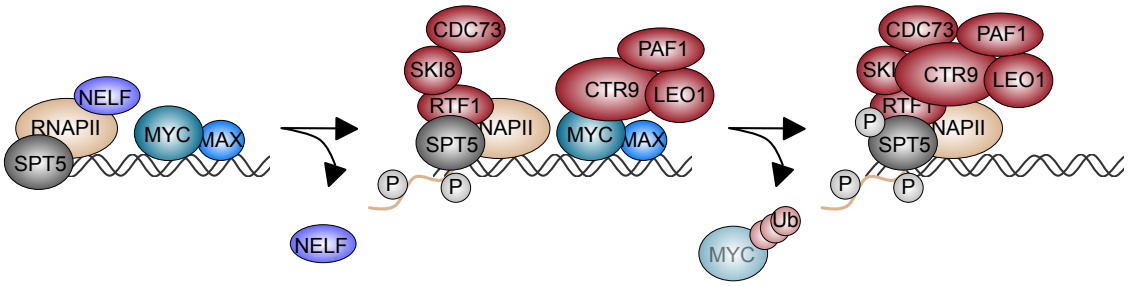

Figure 5.3: Proposed model for subcomplex assembly of MYC, PAF1c and RNAPII. PAF1c assembles as two subcomplexes: CTR9, PAF1 and LEO1 congregate on MYC and RTF1, SKI8 and CDC73 join the RNAPII. NELF binding to RNAPII shares the same binding site as the subunits CTR9 and SKI8. The dissociation of NELF frees the binding site on the RNAPII for CTR9 and PAF1 and LEO1. Ubiquitylation of MYC leads to the transfer and consecutively the formation of the complete PAF1c onto the RNAPII allowing to form an elongation complex consisting of DSIF, PAF1C, SPT6 (not shown) and RNAPII.

5.4 PAF1c and MYC - interactors for the DNA damage repair

Ubiquitin-dependent transfer of PAF1c from MYC onto the RNAPII is triggered by the E3 ligase HUWE1 and inhibition of HUWE1 reduces ubiquitylation of H2B (see figure 4.20). Ubiquitylation of H2B has different functions in elongation (Fuchs et al., 2014; Weake and Workman, 2008), replication (Trujillo and Osley, 2012) and DNA Damage Response (Giannattasio et al., 2005; Moyal et al., 2011; Nakamura et al., 2011; Northam and Trujillo, 2016). The PAF1c is as well involved in controlling histone modifications including (amongst others) the stimulation of H2B monoubiquitylation (Oss et al., 2017). The PAF1c subunit RTF1 directly interacts with RAD6/BRE1 (RNF20/40) to stimulate H2Bub independently of transcription (Van Oss et al., 2016). Additionally it is known, that RNF20/40 in combination with RAD6 lead to H2Bub to promote double strand break repair (Giannattasio et al., 2005; Oliveira et al., 2014; Zheng et al., 2018). Due to torsional stress, double strand breaks can

occur. Recruitment of topoisomerase I or II can release torsional stress. Inhibition of topoisomerase II results in torsional stress not only in gene bodies but specifically downstream of active promoters (Gothe et al., 2019; Kouzine et al., 2013; Singh et al., 2020). We investigated if the observed reduction of H2Bub upon HUWE1 inhibition - and therefore the turnover of MYC - is linked to double strand break repair. To detect double strand breaks, BLISS was performed. Figure 4.21 showed that in unperturbed cells, double strand breaks accumulated preferentially at promoters of active genes (defined as the most expressed ones). This observation is in line with Madabhushi et al. (2015) where early-response gene expression in neurons is accompanied with double strand breaks resulting from topoisomerase II activity. Topoisomerase II inhibition led to an increase in double strand breaks shortly after the TSS and this increase was more prominent upon acute depletion of MYC. Intriguingly the sole MYC depletion led to a reduction of double strand breaks - which might be due to an overall decrease in transcription rate. These findings suggest that MYC is required to reduce double strand break accumulation at active promoters. Strickingly, PAF1c depletion alone led to an increase in double strand breaks close to the TSS of active genes (see figure 4.22). Topoisomerase II inhibitor did not further increase this DNA damage but, even more importantly, MYC induction did not reduce the double strand breaks which were induced by PAF1c depletion. Overall, these observations indicate that MYC promotes double strand break repair in a PAF1c-dependent manner.

Genes which are actively transcribed are vulnerable to DNA damage. To maintain genomic stability DNA repair is of high importance for the cell and consequently a tightly regulated process (Gregersen and Svejstrup, 2018; Lans et al., 2019). On the one side, transcriptional processes are sensitive to DNA damage, on the other side, DNA damage is induced upon transcription or even needed for transcriptional activity (Baranello et al., 2016; Bunch et al., 2015; Ju et al., 2006; Kouzine et al., 2013; Puc et al., 2015). Torsional stress is accompanied with transcriptional activity and one major cause for DNA double strand breaks (Cheung and Cramer, 2012; Kouzine et al., 2013; Wang et al., 1998). To promote transcriptional elongation, torsional stress has to be relaxed (Bunch et al., 2015; Ju et al., 2006; Puc et al., 2015). Thus, this process is regulated by - for example - the stimulation of topoisomerase I activity via the phosphorylation on the CTD of the RNAPII (Baranello et al., 2016). Additionally, MYC and MYCN are interacting with topoisomerases (Baluapuri et al., 2019; Büchel

et al., 2017). Even though there are processes to relax torsional stress, double strand breaks are observed shortly after the TSS of active genes (Chiarle et al., 2011; Gothe et al., 2019; Klein et al., 2011).

Here we suggest that the MYC-PAF1c interaction plays a major role in promoting double strand break repair (see figure 5.4, right side). Upon transcription induced double strand breaks PAF1c and MYC are co-recruited to the promoter regions. PAF1c is transferred onto the RNAPII to stimulate H2B ubiquitylation via RNF20/40 as already described in Van Oss et al. (2016). H2B ubiquitylation in turn opens up the chromatin structure so that a DNA repair machinery can be recruited to resolve the double strand break (Giannattasio et al., 2005; Oliveira et al., 2014; Zheng et al., 2018).

5.5 MYC-dependent PAF1c transfer: a struggle to maintain the integrity of the genome?

In section 5.4 we suggest that MYC promotes double strand break repair at active promoters.

PAF1c is classified as a positive elongation factor, once it is transferred onto the RNAPII and it forms an activated elongation complex consisting of RNAPII, DSIF, SPT6 and PAF1c (Vos et al., 2018a). So we wondered if PAF1c affects MYC transcriptional activity.

MYC induction alone led to an activation of MYC target genes as earlier described in Walz et al. (2014) (see figure 4.23). Upon depletion of two different subunits of the PAF1c, namely CTR9 and CDC73, MYC transcriptional activation as well as repression were attenuated. This observation suggests that, upon depletion of PAF1c, MYC occupancy on chromatin is reduced (see figures 4.6 and 4.9), resulting in the effect observed in RNA sequencing: attenuation of activation and repression of MYC-dependent genes. Still, it was surprising that the depletion of the potent positive elongation factor PAF1c had a relatively mild effect on MYC regulated genes. Independently of normal or oncogenic MYC expression, PAF1c depletion resulted in reduced proliferation (see figure 4.24). In combination with the attenuated transcriptional activity of MYC, we investigated whether PAF1c depletion has an

effect on cell cycle progression in a MYC dependent context. MYC activation or PAF1c knockdown alone resulted in a modest accumulation of cells in S-phase. Interestingly, this effect was more prominent at oncogenic MYC levels upon PAF1c knockdown (see figure 4.25).

To better understand this phenotype, we analyzed DNA damage response markers in different cell cycle phases. Upon DNA damage, cells arrest either to protect DNA replication and chromatin segregation. Major regulators of the DNA double strand break repair are the kinases ATM or ATR as well as DNA-PK (Stiff et al., 2004; Ward and Chen, 2001; Yang et al., 2003). γH2AX accumulates around the DNA lesions and is thus a marker for general DNA damage (Smith et al., 2020).

Whereas the ATR kinase target RPA S33 or the DNA-PK target RPA S4/8 were not affected upon knockdown of CDC73 or CTR9, ATM kinase activity was shown via phosphorylation of its target KAP (S824) and was even more visible at oncogenic MYC levels (see figure 4.26). While MYC activation alone did not lead to γH2AX accumulation, PAF1c knockdown induced γH2AX signal and the effect was even more prominent upon additional induction of MYC. Most of the DNA damage upon PAF1c depletion, represented by the general DNA damage marker γH2AX, was detected in S-phase (see figure 4.27). These observation suggest that PAF1c plays a role in preventing replication-transcription conflicts at oncogenic MYC levels. To underpin this statement, the cells were treated with the CDK7 and CDK9 inhibitors, LDC4297 (Hutterer et al., 2015) and NVP-2 (Olson et al., 2018). Inhibition of transcription led - indeed - to a reduced γH2AX foci in PAF1c depleted cells (see figure 4.27). Confocal images showed a strong overlap of EdU positive signal and γH2AX foci in cells upon *CTR9* knockdown compared to knockdown or MYC induction alone leading to the conclusion that the observed DNA synthesis is repair-associated DNA synthesis rather than replication based DNA synthesis (see figure 4.28 and figure 4.29). These data strongly support the idea, that MYC dependent double strand break repair happens co-transcriptionally.

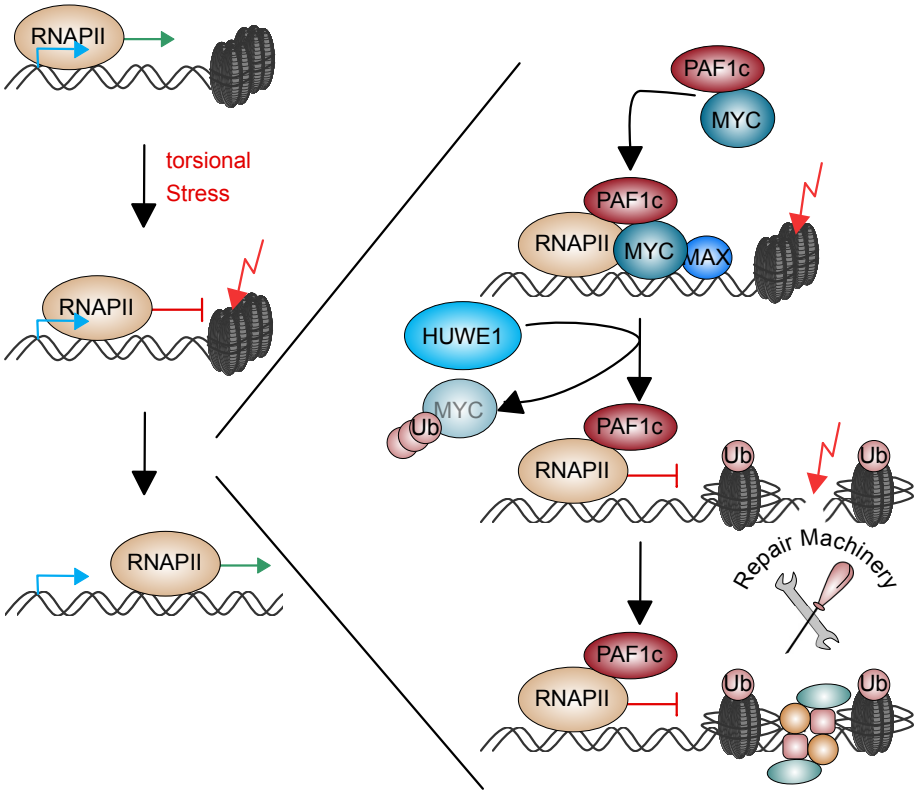

Figure 5.4: MYC-PAF1c interaction controls genomic integrity in an oncogenic environment.
The transcription process causes torsional stress and its relief is critical for productive elongation. Here we suggest that PAF1c and MYC are recruited to promoters which encounter torsional stress followed by double strand breaks. The turnover of MYC driven by HUWE1 leads to the transfer of PAF1c from MYC onto RNAPII. PAF1c promotes H2B monoubiquitylation to open up the chromatin so that the double strand break is accessible for the repair machinery. As soon as the double strand break is resolved the RNAPII is able to elongate.

All together, these data suggest a model by which PAF1c and MYC are recruited to promoters which encounter DNA damage because of transcription-induced torsional stress (see figure 5.4). After turnover of MYC, PAF1c is transferred onto the stalled RNAPII. PAF1c in turn, interacts with RNF20/40 to recruit RAD6 (Van Oss et al., 2016) to promote H2B monoubiquitylation. This leads to chromatin opening to make the double strand break accessible to the repair machinery. As soon as the DNA damage is resolved, transcription can restart. Collectively, this models suggests that MYC controls genomic integrity via PAF1c.

5.6 PAF1c and MYC - a gene regulation-independent function of MYC

The different models of MYC function (see Introduction, subsection MYC and the models) are based on common observations: First, MYC binds to virtually all open promoters. MYC-bound genes are as well occupied by the RNAPII. MYC countains a transactivation domain and a DNA binding domain which - in combination with the earlier statement - suggests that MYC is a transcription factor and therefore able to alter gene expression. Specific binding of MYC is required for its transcriptional activation but the binding affinity to its target sequences is not sufficient to explain the MYC function (Gerlach et al., 2017; Lorenzin et al., 2016). Second, the changes on gene expression of individual genes are weak and often depending on MYC levels and/or tumor entities. Changes in mRNA levels are rather indirect and oncogenic MYC levels do not affect steady-state mRNA levels (Tesi et al., 2019).
To understand MYC function, we need to understand why MYC is bound at all active promoters and how this occupancy is linked to tumorigenesis.
A third, yet another interesting observation is, that MYC interacts with many factors involved in different processes in the nucleus (Baluapuri et al., 2019; Büchel et al., 2017; Heidelberger et al., 2018; Kalkat et al., 2018). This observation leads to the idea that the interaction of MYC with other factors is of relevance for MYC function. Additional factors besides of the co-factor MAX are needed for the specificity of MYC binding to active promoters. Only one third of MYC binding sites are canonical and contain the sequence specific motif. Therefore Lorenzin et al. (2016) suggests that other factors are required for MYC-specific binding to chromatin - specifically for sites which are mainly occupied by MYC at oncogenic levels. Nevertheless, the observation that MYC binds at specific sites and the number of sites on which MYC is bound is increasing at oncogenic levels alone does not explain MYC function as steady-state mRNA levels remain unaffected.
Here we show that the effect of PAF1c knockdown on transcription was rather mild and led to the conclusion that PAF1c-MYC interaction is not important for enhanced transcription at oncogenic MYC levels. We concluded, that the main - yet unknown - function of this interaction is the repair of DSB caused by oncogenic transcription

induced stress.

In this case MYC serves as a "guardian" of the RNAPII to maintain genomic integrity in an oncogenic environment. MYC "guards" the RNAPII through its transcriptional cycle by absorbing the stress which occurs in an oncogenic environment. There are other transcription factors which lead to an in-balance of transcription and -in turn- result in enhanced torsional stress. SPT5 function is depending on MYC level whereas lightly elevated MYC level recruit SPT5 onto the RNAPII, high oncogenic MYC level squelch SPT5 from the RNAPII ending up in unproductive RNAPII to keep the chromatin accessible but also resulting in additional torsional stress (Baluapuri et al., 2019). In neuroblastoma, MYCN recruits BRCA1 to promoters to prevent accumulation of unproductive RNAPII (Herold et al., 2019). Here we show that MYC recruits PAF1c to promoters to prevent accummulation of double strand breaks to guarantee productive elongation in an oncogenic environment where different stressors might affect transcription negatively. Leading to the conclusion that MYC function is gene-regulation independent.

Thus, the MYC-PAF1c-axis as described in this study helps to maintain genomic integrity at oncogenic MYC levels and makes it therefore a suitable target for future therapeutic approaches: By disrupting the interaction between MYC and PAF1c, the MYC-driven oncogenic cell accumulates double strand breaks which would in the end result in apoptosis and therefore sensitise the cells towards DNA damaging agents.

Bibliography

Adhikary, S. and Eilers, M. (2005). Transcriptional regulation and transformation by myc proteins. *Nat Rev Mol Cell Biol*, 6(8):635–45.

Allshire, R. C. and Ekwall, K. (2015). Epigenetic regulation of chromatin states in schizosaccharomyces pombe. *Cold Spring Harb Perspect Biol*, 7(7):a018770.

Amemiya, H. M., Kundaje, A., and Boyle, A. P. (2019). The encode blacklist: Identification of problematic regions of the genome. *Scientific Reports*, 9(1):9354.

Amrich, C. G., Davis, C. P., Rogal, W. P., Shirra, M. K., Heroux, A., Gardner, R. G., Arndt, K. M., and VanDemark, A. P. (2012). Cdc73 subunit of paf1 complex contains c-terminal ras-like domain that promotes association of paf1 complex with chromatin *. *Journal of Biological Chemistry*, 287(14):10863–10875.

Anfinsen, C. B. (1973). Principles that govern the folding of protein chains. *Science*, 181(4096):223–230.

Aoi, Y., Smith, E. R., Shah, A. P., Rendleman, E. J., Marshall, S. A., Woodfin, A. R., Chen, F. X., Shiekhattar, R., and Shilatifard, A. (2020). Nelf regulates a promoter-proximal step distinct from rna pol ii pause-release. *Molecular Cell*, 78(2):261–274.e5.

Baejen, C., Andreani, J., Torkler, P., Battaglia, S., Schwalb, B., Lidschreiber, M., Maier, K. C., Boltendahl, A., Rus, P., Esslinger, S., Söding, J., and Cramer, P. (2017). Genome-wide analysis of rna polymerase ii termination at protein-coding genes. *Mol Cell*, 66(1):38–49.e6.

Bahrampour, S. and Thor, S. (2016). Ctr9, a key component of the paf1 complex, affects proliferation and terminal differentiation in the developing drosophila nervous system. *G3 (Bethesda)*, 6(10):3229–3239.

Baluapuri, A., Hofstetter, J., Dudvarski Stankovic, N., Endres, T., Bhandare, P., Vos, S. M., Adhikari, B., Schwarz, J. D., Narain, A., Vogt, M., Wang, S.-Y., Düster, R., Jung, L. A., Vanselow, J. T., Wiegering, A., Geyer, M., Maric, H. M., Gallant, P., Walz, S., Schlosser, A., Cramer, P., Eilers, M., and Wolf, E. (2019). Myc recruits spt5 to rna polymerase ii to promote processive transcription elongation. *Molecular Cell*, 74(4):674–687.e11.

Baluapuri, A., Wolf, E., and Eilers, M. (2020). Target gene-independent functions of myc oncoproteins. *Nat Rev Mol Cell Biol*, 21(5):255–267.

Baranello, L., Wojtowicz, D., Cui, K., Devaiah, B. N., Chung, H. J., Chan-Salis, K. Y., Guha, R., Wilson, K., Zhang, X., Zhang, H., Piotrowski, J., Thomas, C. J., Singer, D. S., Pugh, B. F., Pommier, Y., Przytycka, T. M., Kouzine, F., Lewis,

B. A., Zhao, K., and Levens, D. (2016). Rna polymerase ii regulates topoisomerase 1 activity to favor efficient transcription. *Cell*, 165(2):357–71.

Barnum, K. J. and O'Connell, M. J. (2014). Cell cycle regulation by checkpoints. *Methods Mol Biol*, 1170:29–40.

Bentley, D. L. (2014). Coupling mrna processing with transcription in time and space. *Nature Reviews Genetics*, 15(3):163–175.

Bernecky, C., Plitzko, J. M., and Cramer, P. (2017). Structure of a transcribing rna polymerase ii–dsif complex reveals a multidentate dna–rna clamp. *Nat. Struct. Mol. Biol.*, 24.

Beroukhim, R., Mermel, C. H., Porter, D., Wei, G., Raychaudhuri, S., Donovan, J., Barretina, J., Boehm, J. S., Dobson, J., Urashima, M., Mc Henry, K. T., Pinchback, R. M., Ligon, A. H., Cho, Y. J., Haery, L., Greulich, H., Reich, M., Winckler, W., Lawrence, M. S., Weir, B. A., Tanaka, K. E., Chiang, D. Y., Bass, A. J., Loo, A., Hoffman, C., Prensner, J., Liefeld, T., Gao, Q., Yecies, D., Signoretti, S., Maher, E., Kaye, F. J., Sasaki, H., Tepper, J. E., Fletcher, J. A., Tabernero, J., Baselga, J., Tsao, M. S., Demichelis, F., Rubin, M. A., Janne, P. A., Daly, M. J., Nucera, C., Levine, R. L., Ebert, B. L., Gabriel, S., Rustgi, A. K., Antonescu, C. R., Ladanyi, M., Letai, A., Garraway, L. A., Loda, M., Beer, D. G., True, L. D., Okamoto, A., Pomeroy, S. L., Singer, S., Golub, T. R., Lander, E. S., Getz, G., Sellers, W. R., and Meyerson, M. (2010). The landscape of somatic copy-number alteration across human cancers. *Nature*, 463(7283):899–905.

Berwanger, B., Hartmann, O., Bergmann, E., Bernard, S., Nielsen, D., Krause, M., Kartal, A., Flynn, D., Wiedemeyer, R., Schwab, M., Schäfer, H., Christiansen, H., and Eilers, M. (2002). Loss of a fyn-regulated differentiation and growth arrest pathway in advanced stage neuroblastoma. *Cancer Cell*, 2(5):377–86.

Besche, H. C., Haas, W., Gygi, S. P., and Goldberg, A. L. (2009). Isolation of mammalian 26s proteasomes and p97/vcp complexes using the ubiquitin-like domain from hhr23b reveals novel proteasome-associated proteins. *Biochemistry*, 48.

Blackwood, E. M., Kretzner, L., and Eisenman, R. N. (1992). Myc and max function as a nucleoprotein complex. *Current Opinion in Genetics Development*, 2(2):227–235.

Blanco-Bose, W. E., Murphy, M. J., Ehninger, A., Offner, S., Dubey, C., Huang, W., Moore, D. D., and Trumpp, A. (2008). C-myc and its target foxm1 are critical downstream effectors of constitutive androstane receptor (car) mediated direct liver hyperplasia. *Hepatology*, 48(4):1302–11.

Boehning, M., Dugast-Darzacq, C., Rankovic, M., Hansen, A. S., Yu, T., Marie-Nelly, H., McSwiggen, D. T., Kokic, G., Dailey, G. M., Cramer, P., Darzacq, X., and Zweckstetter, M. (2018). Rna polymerase ii clustering through carboxy-terminal domain phase separation. *Nature Structural Molecular Biology*, 25(9):833–840.

Brodeur, G. M., Seeger, R. C., Schwab, M., Varmus, H. E., and Bishop, J. M. (1984). Amplification of n-myc in untreated human neuroblastomas correlates with advanced disease stage. *Science*, 224(4653):1121–4.

Büchel, G., Carstensen, A., Mak, K. Y., Roeschert, I., Leen, E., Sumara, O., Hofstetter, J., Herold, S., Kalb, J., Baluapuri, A., Poon, E., Kwok, C., Chesler, L., Maric, H. M., Rickman, D. S., Wolf, E., Bayliss, R., Walz, S., and Eilers, M. (2017). Association with aurora-a controls n-myc-dependent promoter escape and pause release of rna polymerase ii during the cell cycle. *Cell Rep*, 21(12):3483–3497.

Bunch, H., Lawney, B. P., Lin, Y.-F., Asaithamby, A., Murshid, A., Wang, Y. E., Chen, B. P. C., and Calderwood, S. K. (2015). Transcriptional elongation requires dna break-induced signalling. *Nature Communications*, 6(1):10191.

Bushnell, D. A., Westover, K. D., Davis, R. E., and Kornberg, R. D. (2004). Structural basis of transcription: an rna polymerase ii–tfiib cocrystal at 4.5 angstroms. *Science*, 303.

Cao, Q. F., Yamamoto, J., Isobe, T., Tateno, S., Murase, Y., Chen, Y., Handa, H., and Yamaguchi, Y. (2015). Characterization of the human transcription elongation factor rtf1: Evidence for nonoverlapping functions of rtf1 and the paf1 complex. *Mol Cell Biol*, 35(20):3459–70.

Casey, S. C., Tong, L., Li, Y., Do, R., Walz, S., Fitzgerald, K. N., Gouw, A. M., Baylot, V., Gütgemann, I., Eilers, M., and Felsher, D. W. (2016). Myc regulates the antitumor immune response through cd47 and pd-l1. *Science*, 352(6282):227–31.

Chatterjee, N. and Walker, G. C. (2017). Mechanisms of dna damage, repair, and mutagenesis. *Environ Mol Mutagen*, 58(5):235–263.

Chen, D., Kon, N., Li, M., Zhang, W., Qin, J., and Gu, W. (2005). Arf-bp1/mule is a critical mediator of the arf tumor suppressor. *Cell*, 121(7):1071–1083.

Chen, F. X., Smith, E. R., and Shilatifard, A. (2018a). Born to run: control of transcription elongation by rna polymerase ii. *Nat. Rev. Mol. Cell Biol.*, 19.

Chen, F. X., Woodfin, A. R., Gardini, A., Rickels, R. A., Marshall, S. A., Smith, E. R., Shiekhattar, R., and Shilatifard, A. (2015). Paf1, a molecular regulator of promoter-proximal pausing by rna polymerase ii. *Cell*, 162(5):1003–15.

Chen, F. X., Xie, P., Collings, C. K., Cao, K., Aoi, Y., Marshall, S. A., Rendleman, E. J., Ugarenko, M., Ozark, P. A., Zhang, A., Shiekhattar, R., Smith, E. R., Zhang, M. Q., and Shilatifard, A. (2017a). Paf1 regulation of promoter-proximal pause release via enhancer activation. *Science (New York, N.Y.)*, 357(6357):1294–1298.

Chen, F. X., Xie, P., Collings, C. K., Cao, K., Aoi, Y., Marshall, S. A., Rendleman, E. J., Ugarenko, M., Ozark, P. A., Zhang, A., Shiekhattar, R., Smith, E. R., Zhang, M. Q., and Shilatifard, A. (2017b). Paf1 regulation of promoter-proximal pause release via enhancer activation. *Science (New York, N.Y.)*, 357(6357):1294–1298.

Chen, H., Liu, H., and Qing, G. (2018b). Targeting oncogenic myc as a strategy for cancer treatment. *Signal Transduction and Targeted Therapy*, 3(1):5.

Chen, H. T. and Hahn, S. (2004). Mapping the location of tfiib within the rna polymerase ii transcription preinitiation complex: a model for the structure of the pic. *Cell*, 119.

Cheung, A. C. and Cramer, P. (2011). Structural basis of rna polymerase ii backtracking, arrest and reactivation. *Nature*, 471.

Cheung, A. C. M. and Cramer, P. (2012). A movie of rna polymerase ii transcription. *Cell*, 149(7):1431–1437.

Chiarle, R., Zhang, Y., Frock, R. L., Lewis, S. M., Molinie, B., Ho, Y. J., Myers, D. R., Choi, V. W., Compagno, M., Malkin, D. J., Neuberg, D., Monti, S., Giallourakis, C. C., Gostissa, M., and Alt, F. W. (2011). Genome-wide translocation sequencing reveals mechanisms of chromosome breaks and rearrangements in b cells. *Cell*, 147(1):107–19.

Cho, W.-K., Spille, J.-H., Hecht, M., Lee, C., Li, C., Grube, V., and Cisse, I. I. (2018). Mediator and rna polymerase ii clusters associate in transcription-dependent condensates. *Science*, 361(6400):412–415.

Chong, S., Dugast-Darzacq, C., Liu, Z., Dong, P., Dailey, G. M., Cattoglio, C., Heckert, A., Banala, S., Lavis, L., Darzacq, X., and Tjian, R. (2018). Imaging dynamic and selective low-complexity domain interactions that control gene transcription. *Science*, 361(6400):eaar2555.

Chu, X., Qin, X., Xu, H., Li, L., Wang, Z., Li, F., Xie, X., Zhou, H., Shen, Y., and Long, J. (2013). Structural insights into paf1 complex assembly and histone binding. *Nucleic Acids Res*, 41(22):10619–29.

Chu, Y., Simic, R., Warner, M. H., Arndt, K. M., and Prelich, G. (2007). Regulation of histone modification and cryptic transcription by the bur1 and paf1 complexes. *The EMBO Journal*, 26(22):4646–4656.

Cisse, I. I., Izeddin, I., Causse, S. Z., Boudarene, L., Senecal, A., Muresan, L., Dugast-Darzacq, C., Hajj, B., Dahan, M., and Darzacq, X. (2013). Real-time dynamics of rna polymerase ii clustering in live human cells. *Science*, 341(6146):664–667.

Clouaire, T., Rocher, V., Lashgari, A., Arnould, C., Aguirrebengoa, M., Biernacka, A., Skrzypczak, M., Aymard, F., Fongang, B., Dojer, N., Iacovoni, J. S., Rowicka, M., Ginalski, K., Côté, J., and Legube, G. (2018). Comprehensive mapping of histone modifications at dna double-strand breaks deciphers repair pathway chromatin signatures. *Molecular Cell*, 72(2):250–262.e6.

Conaway, J. W., Shilatifard, A., Dvir, A., and Conaway, R. C. (2000). Control of elongation by rna polymerase ii. *Trends Biochem. Sci.*, 25.

Cortazar, M. A., Sheridan, R. M., Erickson, B., Fong, N., Glover-Cutter, K., Brannan, K., and Bentley, D. L. (2019). Control of rna pol ii speed by pnuts-pp1 and spt5 dephosphorylation facilitates termination by a x201c;sitting duck torpedox201d; mechanism. *Molecular Cell*, 76(6):896–908.e4.

Costa, R. M., Chigançcas, V., Galhardo Rda, S., Carvalho, H., and Menck, C. F. (2003). The eukaryotic nucleotide excision repair pathway. *Biochimie*, 85(11):1083–99.

Cramer, P. (2019). Organization and regulation of gene transcription. *Nature*.

Dalla-Favera, R., Bregni, M., Erikson, J., Patterson, D., Gallo, R. C., and Croce, C. M. (1982). Human c-myc onc gene is located on the region of chromosome 8 that is translocated in burkitt lymphoma cells. *Proc Natl Acad Sci U S A*, 79(24):7824–7.

Dang, C. V. (2006). The c-myc target gene network. *Semin. Cancer Biol.*, 16.

Dauch, D., Rudalska, R., Cossa, G., Nault, J. C., Kang, T. W., Wuestefeld, T., Hohmeyer, A., Imbeaud, S., Yevsa, T., Hoenicke, L., Pantsar, T., Bozko, P., Malek, N. P., Longerich, T., Laufer, S., Poso, A., Zucman-Rossi, J., Eilers, M., and Zender, L. (2016). A myc-aurora kinase a protein complex represents an actionable drug target in p53-altered liver cancer. *Nat Med*, 22(7):744–53.

de Pretis, S., Kress, T. R., Morelli, M. J., Sabò, A., Locarno, C., Verrecchia, A., Doni, M., Campaner, S., Amati, B., and Pelizzola, M. (2017). Integrative analysis of rna polymerase ii and transcriptional dynamics upon myc activation. *Genome Research*, 27(10):1658–1664.

Decker, T. M. (2020). Mechanisms of transcription elongation factor dsif (spt4-spt5). *J Mol Biol*, page 166657.

Dermody, J. L. and Buratowski, S. (2010). Leo1 subunit of the yeast paf1 complex binds rna and contributes to complex recruitment. *J Biol Chem*, 285(44):33671–9.

Diamant, G., Bahat, A., and Dikstein, R. (2016). The elongation factor spt5 facilitates transcription initiation for rapid induction of inflammatory-response genes. *Nature Communications*, 7(1):11547.

Diefenbacher, M. E., Chakraborty, A., Blake, S. M., Mitter, R., Popov, N., Eilers, M., and Behrens, A. (2015). Usp28 counteracts fbw7 in intestinal homeostasis and cancer. *Cancer Res*, 75(7):1181–6.

Dubois, N. C., Adolphe, C., Ehninger, A., Wang, R. A., Robertson, E. J., and Trumpp, A. (2008). Placental rescue reveals a sole requirement for c-myc in embryonic erythroblast survival and hematopoietic stem cell function. *Development*, 135(14):2455–65.

Duesberg, P. H. and Vogt, P. K. (1979). Avian acute leukemia viruses mc29 and mh2 share specific rna sequences: evidence for a second class of transforming genes. *Proc Natl Acad Sci U S A*, 76(4):1633–7.

Easwaran, H., Johnstone, S. E., Van Neste, L., Ohm, J., Mosbruger, T., Wang, Q., Aryee, M. J., Joyce, P., Ahuja, N., Weisenberger, D., Collisson, E., Zhu, J., Yegnasubramanian, S., Matsui, W., and Baylin, S. B. (2012). A dna hypermethylation module for the stem/progenitor cell signature of cancer. *Genome Research*, 22(5):837–849.

Egly, J. M. and Coin, F. (2011). A history of tfiih: two decades of molecular biology on a pivotal transcription/repair factor. *DNA Repair (Amst.)*, 10.

Ehara, H., Yokoyama, T., Shigematsu, H., Yokoyama, S., Shirouzu, M., and Sekine, S.-i. (2017). Structure of the complete elongation complex of rna polymerase ii with basal factors. *Science*, 357(6354):921–924.

Eick, D. and Geyer, M. (2013). The rna polymerase ii carboxy-terminal domain (ctd) code. *Chem. Rev.*, 113.

Eilers, M., Picard, D., Yamamoto, K. R., and Bishop, J. M. (1989). Chimaeras of myc oncoprotein and steroid receptors cause hormone-dependent transformation of cells. *Nature*, 340.

Endres, T., Solvie, D., Heidelberger, J. B., Andrioletti, V., Baluapuri, A., Ade, C. P., Muhar, M., Eilers, U., Vos, S. M., Cramer, P., Zuber, J., Beli, P., Popov, N., Wolf, E., Gallant, P., and Eilers, M. (2021). Ubiquitylation of myc couples transcription elongation with double-strand break repair at active promoters. *Molecular Cell*.

Farrell, A. S. and Sears, R. C. (2014). Myc degradation. *Cold Spring Harb. Perspect. Med.*

Fellmann, C., Hoffmann, T., Sridhar, V., Hopfgartner, B., Muhar, M., Roth, M., Lai, D. Y., Barbosa, I. A., Kwon, J. S., Guan, Y., Sinha, N., and Zuber, J. (2013). An optimized microrna backbone for effective single-copy rnai. *Cell Rep*, 5(6):1704–13.

Fisher, R. P. (2019). Cdk7: a kinase at the core of transcription and in the crosshairs of cancer drug discovery. *Transcription*, 10(2):47–56.

Fitz, J., Neumann, T., and Pavri, R. (2018). Regulation of rna polymerase ii processivity by spt5 is restricted to a narrow window during elongation. *The EMBO Journal*, 37(8):e97965.

Fong, N., Brannan, K., Erickson, B., Kim, H., Cortazar, M. A., Sheridan, R. M., Nguyen, T., Karp, S., and Bentley, D. L. (2015). Effects of transcription elongation rate and xrn2 exonuclease activity on rna polymerase ii termination suggest widespread kinetic competition. *Mol Cell*, 60(2):256–67.

Fonseca, G. J., Cohen, M. J., and Mymryk, J. S. (2014). Adenovirus e1a recruits the human paf1 complex to enhance transcriptional elongation. *Journal of virology*, 88(10):5630–5637.

Fonseca, G. J., Cohen, M. J., Nichols, A. C., Barrett, J. W., and Mymryk, J. S. (2013). Viral retasking of hbre1/rnf20 to recruit hpaf1 for transcriptional activation. *PLoS Pathog*, 9(6):e1003411.

Fuchs, G., Hollander, D., Voichek, Y., Ast, G., and Oren, M. (2014). Cotranscriptional histone h2b monoubiquitylation is tightly coupled with rna polymerase ii elongation rate. *Genome Res*, 24(10):1572–83.

Gabay, M., Li, Y., and Felsher, D. W. (2014). Myc activation is a hallmark of cancer initiation and maintenance. *Cold Spring Harb Perspect Med*, 4(6).

Gebhardt, A., Frye, M., Herold, S., Benitah, S. A., Braun, K., Samans, B., Watt, F. M., Elsässer, H.-P., and Eilers, M. (2006). Myc regulates keratinocyte adhesion and differentiation via complex formation with miz1. *The Journal of cell biology*, 172(1):139–149.

Gerlach, J. M., Furrer, M., Gallant, M., Birkel, D., Baluapuri, A., Wolf, E., and Gallant, P. (2017). Paf1 complex component leo1 helps recruit

drosophila myc to promoters. *Proceedings of the National Academy of Sciences*, 114(44):E9224–E9232.

Giannattasio, M., Lazzaro, F., Plevani, P., and Muzi-Falconi, M. (2005). The dna damage checkpoint response requires histone h2b ubiquitination by rad6-bre1 and h3 methylation by dot1. *J Biol Chem*, 280(11):9879–86.

Giglia-Mari, G., Zotter, A., and Vermeulen, W. (2011). Dna damage response. *Cold Spring Harb Perspect Biol*, 3(1):a000745.

Gomez-Roman, N., Grandori, C., Eisenman, R. N., and White, R. J. (2003). Direct activation of rna polymerase iii transcription by c-myc. *Nature*, 421(6920):290–4.

Gorrini, C., Squatrito, M., Luise, C., Syed, N., Perna, D., Wark, L., Martinato, F., Sardella, D., Verrecchia, A., Bennett, S., Confalonieri, S., Cesaroni, M., Marchesi, F., Gasco, M., Scanziani, E., Capra, M., Mai, S., Nuciforo, P., Crook, T., Lough, J., and Amati, B. (2007). Tip60 is a haplo-insufficient tumour suppressor required for an oncogene-induced dna damage response. *Nature*, 448(7157):1063–1067.

Gothe, H. J., Bouwman, B. A. M., Gusmao, E. G., Piccinno, R., Petrosino, G., Sayols, S., Drechsel, O., Minneker, V., Josipovic, N., Mizi, A., Nielsen, C. F., Wagner, E.-M., Takeda, S., Sasanuma, H., Hudson, D. F., Kindler, T., Baranello, L., Papantonis, A., Crosetto, N., and Roukos, V. (2019). Spatial chromosome folding and active transcription drive dna fragility and formation of oncogenic mll translocations. *Molecular Cell*, 75(2):267–283.e12.

Grandori, C., Gomez-Roman, N., Felton-Edkins, Z. A., Ngouenet, C., Galloway, D. A., Eisenman, R. N., and White, R. J. (2005). c-myc binds to human ribosomal dna and stimulates transcription of rrna genes by rna polymerase i. *Nature Cell Biology*, 7(3):311–318.

Gregersen, L. H. and Svejstrup, J. Q. (2018). The cellular response to transcription-blocking dna damage. *Trends in Biochemical Sciences*, 43(5):327–341.

Gressel, S., Schwalb, B., Decker, T. M., Qin, W., Leonhardt, H., Eick, D., and Cramer, P. (2017). Cdk9-dependent rna polymerase ii pausing controls transcription initiation. *eLife*, 6:e29736.

Grohmann, D., Nagy, J., Chakraborty, A., Klose, D., Fielden, D., Ebright, R. H., Michaelis, J., and Werner, F. (2011). The initiation factor tfe and the elongation factor spt4/5 compete for the rnap clamp during transcription initiation and elongation. *Molecular Cell*, 43(2):263–274.

Guo, J., Li, T., Schipper, J., Nilson, K. A., Fordjour, F. K., Cooper, J. J., Gordân, R., and Price, D. H. (2014). Sequence specificity incompletely defines the genome-wide occupancy of myc. *Genome Biology*, 15(10):482.

Hanks, S., Perdeaux, E. R., Seal, S., Ruark, E., Mahamdallie, S. S., Murray, A., Ramsay, E., Del Vecchio Duarte, S., Zachariou, A., de Souza, B., Warren-Perry, M., Elliott, A., Davidson, A., Price, H., Stiller, C., Pritchard-Jones, K., and Rahman, N. (2014). Germline mutations in the paf1 complex gene ctr9 predispose to wilms tumour. *Nat Commun*, 5:4398.

He, T. C., Sparks, A. B., Rago, C., Hermeking, H., Zawel, L., da Costa, L. T., Morin, P. J., Vogelstein, B., and Kinzler, K. W. (1998). Identification of c-myc as a target of the apc pathway. *Science*, 281(5382):1509–12.

Heidelberger, J. B., Voigt, A., Borisova, M. E., Petrosino, G., Ruf, S., Wagner, S. A., and Beli, P. (2018). Proteomic profiling of vcp substrates links vcp to k6-linked ubiquitylation and c-myc function. *EMBO reports*, 19(4):e44754.

Herkert, B., Dwertmann, A., Herold, S., Abed, M., Naud, J.-F., Finkernagel, F., Harms, G. S., Orian, A., Wanzel, M., and Eilers, M. (2010). The arf tumor suppressor protein inhibits miz1 to suppress cell adhesion and induce apoptosis. *Journal of Cell Biology*, 188(6):905–918.

Herold, S., Kalb, J., Buchel, G., Ade, C. P., Baluapuri, A., Xu, J., Koster, J., Solvie, D., Carstensen, A., Klotz, C., Rodewald, S., Schulein-Volk, C., Dobbelstein, M., Wolf, E., Molenaar, J., Versteeg, R., Walz, S., and Eilers, M. (2019). Recruitment of brca1 limits mycn-driven accumulation of stalled rna polymerase. *Nature*, 567(7749):545–549.

Herold, S., Wanzel, M., Beuger, V., Frohme, C., Beul, D., Hillukkala, T., Syvaoja, J., Saluz, H. P., Haenel, F., and Eilers, M. (2002). Negative regulation of the mammalian uv response by myc through association with miz-1. *Mol Cell*, 10(3):509–21.

Hnisz, D., Shrinivas, K., Young, R. A., Chakraborty, A. K., and Sharp, P. A. (2017). A phase separation model for transcriptional control. *Cell*, 169.

Ho, J. W. K., Jung, Y. L., Liu, T., Alver, B. H., Lee, S., Ikegami, K., Sohn, K.-A., Minoda, A., Tolstorukov, M. Y., Appert, A., Parker, S. C. J., Gu, T., Kundaje, A., Riddle, N. C., Bishop, E., Egelhofer, T. A., Hu, S. S., Alekseyenko, A. A., Rechtsteiner, A., Asker, D., Belsky, J. A., Bowman, S. K., Chen, Q. B., Chen, R. A. J., Day, D. S., Dong, Y., Dose, A. C., Duan, X., Epstein, C. B., Ercan, S., Feingold, E. A., Ferrari, F., Garrigues, J. M., Gehlenborg, N., Good, P. J., Haseley, P., He, D., Herrmann, M., Hoffman, M. M., Jeffers, T. E., Kharchenko, P. V., Kolasinska-Zwierz, P., Kotwaliwale, C. V., Kumar, N., Langley, S. A., Larschan, E. N., Latorre, I., Libbrecht, M. W., Lin, X., Park, R., Pazin, M. J., Pham, H. N., Plachetka, A., Qin, B., Schwartz, Y. B., Shoresh, N., Stempor, P., Vielle, A., Wang, C., Whittle, C. M., Xue, H., Kingston, R. E., Kim, J. H., Bernstein, B. E., Dernburg, A. F., Pirrotta, V., Kuroda, M. I., Noble, W. S., Tullius, T. D., Kellis, M., MacAlpine, D. M., Strome, S., Elgin, S. C. R., Liu, X. S., Lieb, J. D., Ahringer, J., Karpen, G. H., and Park, P. J. (2014). Comparative analysis of metazoan chromatin organization. *Nature*, 512(7515):449–452.

Hu, S. S., Lai, M. M., and Vogt, P. K. (1979). Genome of avian myelocytomatosis virus mc29: analysis by heteroduplex mapping. *Proc Natl Acad Sci U S A*, 76(3):1265–8.

Hutterer, C., Eickhoff, J., Milbradt, J., Korn, K., Zeitträger, I., Bahsi, H., Wagner, S., Zischinsky, G., Wolf, A., Degenhart, C., Unger, A., Baumann, M., Klebl, B., and Marschall, M. (2015). A novel cdk7 inhibitor of the pyrazolotriazine class exerts

broad-spectrum antiviral activity at nanomolar concentrations. *Antimicrob Agents Chemother*, 59(4):2062–71.

Iakoucheva, L. M., Radivojac, P., Brown, C. J., O'Connor, T. R., Sikes, J. G., Obradovic, Z., and Dunker, A. K. (2004). The importance of intrinsic disorder for protein phosphorylation. *Nucleic Acids Res*, 32(3):1037–49.

Inoue, S., Hao, Z., Elia, A. J., Cescon, D., Zhou, L., Silvester, J., Snow, B., Harris, I. S., Sasaki, M., Li, W. Y., Itsumi, M., Yamamoto, K., Ueda, T., Dominguez-Brauer, C., Gorrini, C., Chio, I., Haight, J., You-Ten, A., McCracken, S., Wakeham, A., Ghazarian, D., Penn, L. J., Melino, G., and Mak, T. W. (2013). Mule/huwe1/arf-bp1 suppresses ras-driven tumorigenesis by preventing c-myc/miz1-mediated down-regulation of p21 and p15. *Genes Dev*, 27(10):1101–14.

Iyama, T. and Wilson, D. M., r. (2013). Dna repair mechanisms in dividing and non-dividing cells. *DNA Repair (Amst)*, 12(8):620–36.

Jacquet, K. (2016). The tip60 complex regulates bivalent chromatin recognition by 53bp1 through direct h4k20me binding and h2ak15 acetylation. *Mol. Cell*, 62.

Jaenicke, L. A., von Eyss, B., Carstensen, A., Wolf, E., Xu, W., Greifenberg, A. K., Geyer, M., Eilers, M., and Popov, N. (2016). Ubiquitin-dependent turnover of myc antagonizes myc/paf1c complex accumulation to drive transcriptional elongation. *Mol Cell*, 61(1):54–67.

Jiricny, J. (2006). The multifaceted mismatch-repair system. *Nat Rev Mol Cell Biol*, 7(5):335–46.

Ju, B.-G., Lunyak, V. V., Perissi, V., Garcia-Bassets, I., Rose, D. W., Glass, C. K., and Rosenfeld, M. G. (2006). A topoisomerase iiß-mediated dsdna break required for regulated transcription. *Science*, 312(5781):1798–1802.

Kalkat, M., Resetca, D., Lourenco, C., Chan, P. K., Wei, Y., Shiah, Y. J., Vitkin, N., Tong, Y., Sunnerhagen, M., Done, S. J., Boutros, P. C., Raught, B., and Penn, L. Z. (2018). Myc protein interactome profiling reveals functionally distinct regions that cooperate to drive tumorigenesis. *Mol Cell*, 72(5):836–848.e7.

Karmakar, S., Seshacharyulu, P., Lakshmanan, I., Vaz, A. P., Chugh, S., Sheinin, Y. M., Mahapatra, S., Batra, S. K., and Ponnusamy, M. P. (2017). hpaf1/pd2 interacts with oct3/4 to promote self-renewal of ovarian cancer stem cells. *Oncotarget*, 8(9):14806–14820.

Kastenhuber, E. R. and Lowe, S. W. (2017). Putting p53 in context. *Cell*, 170(6):1062–1078.

Kieffer-Kwon, K. R., Nimura, K., Rao, S. S. P., Xu, J., Jung, S., Pekowska, A., Dose, M., Stevens, E., Mathe, E., Dong, P., Huang, S. C., Ricci, M. A., Baranello, L., Zheng, Y., Tomassoni Ardori, F., Resch, W., Stavreva, D., Nelson, S., McAndrew, M., Casellas, A., Finn, E., Gregory, C., St Hilaire, B. G., Johnson, S. M., Dubois, W., Cosma, M. P., Batchelor, E., Levens, D., Phair, R. D., Misteli, T., Tessarollo, L., Hager, G., Lakadamyali, M., Liu, Z., Floer, M., Shroff, H., Aiden, E. L., and

Casellas, R. (2017). Myc regulates chromatin decompaction and nuclear architecture during b cell activation. *Mol Cell*, 67(4):566–578.e10.

Kikuchi, I., Takahashi-Kanemitsu, A., Sakiyama, N., Tang, C., Tang, P.-J., Noda, S., Nakao, K., Kassai, H., Sato, T., Aiba, A., and Hatakeyama, M. (2016). Dephosphorylated parafibromin is a transcriptional coactivator of the wnt/hedgehog/notch pathways. *Nature Communications*, 7(1):12887.

Kim, J., Guermah, M., and Roeder, R. G. (2010). The human paf1 complex acts in chromatin transcription elongation both independently and cooperatively with sii/tfiis. *Cell*, 140(4):491–503.

Kim, S. Y., Herbst, A., Tworkowski, K. A., Salghetti, S. E., and Tansey, W. P. (2003). Skp2 regulates myc protein stability and activity. *Mol Cell*, 11(5):1177–88.

Kim, T. K., Ebright, R. H., and Reinberg, D. (2000). Mechanism of atp-dependent promoter melting by transcription factor iih. *Science*, 288.

Klein, I. A., Resch, W., Jankovic, M., Oliveira, T., Yamane, A., Nakahashi, H., Di Virgilio, M., Bothmer, A., Nussenzweig, A., Robbiani, D. F., Casellas, R., and Nussenzweig, M. C. (2011). Translocation-capture sequencing reveals the extent and nature of chromosomal rearrangements in b lymphocytes. *Cell*, 147(1):95–106.

Kohl, N. E., Gee, C. E., and Alt, F. W. (1984). Activated expression of the n-myc gene in human neuroblastomas and related tumors. *Science*, 226(4680):1335–7.

Kornberg, R. D. (1999). Eukaryotic transcriptional control. *Trends Cell Biol.*, 9.

Kornberg, R. D. (2005). Mediator and the mechanism of transcriptional activation. *Trends Biochem. Sci.*, 30.

Kortlever, R. M., Sodir, N. M., Wilson, C. H., Burkhart, D. L., Pellegrinet, L., Brown Swigart, L., Littlewood, T. D., and Evan, G. I. (2017). Myc cooperates with ras by programming inflammation and immune suppression. *Cell*, 171(6):1301–1315.e14.

Kouzine, F., Gupta, A., Baranello, L., Wojtowicz, D., Ben-Aissa, K., Liu, J., Przytycka, T. M., and Levens, D. (2013). Transcription-dependent dynamic supercoiling is a short-range genomic force. *Nature Structural Molecular Biology*, 20(3):396–403.

Kress, T. R., Sabo, A., and Amati, B. (2015). Myc: connecting selective transcriptional control to global rna production. *Nat. Rev. Cancer*, 15.

Krogan, N. J., Dover, J., Wood, A., Schneider, J., Heidt, J., Boateng, M. A., Dean, K., Ryan, O. W., Golshani, A., Johnston, M., Greenblatt, J. F., and Shilatifard, A. (2003). The paf1 complex is required for histone h3 methylation by compass and dot1p: linking transcriptional elongation to histone methylation. *Mol Cell*, 11(3):721–9.

Kuehner, J. N., Pearson, E. L., and Moore, C. (2011). Unravelling the means to an end: Rna polymerase ii transcription termination. *Nature Reviews Molecular Cell Biology*, 12(5):283–294.

Kwak, H. and Lis, J. T. (2013). Control of transcriptional elongation. *Annu. Rev. Genet.*, 47.

Landick, R. (2006). The regulatory roles and mechanism of transcriptional pausing. *Biochem. Soc. Trans.*, 34.

Langmead, B. and Salzberg, S. L. (2012). Fast gapped-read alignment with bowtie 2. *Nature Methods*, 9(4):357–359.

Lans, H., Hoeijmakers, J. H. J., Vermeulen, W., and Marteijn, J. A. (2019). The dna damage response to transcription stress. *Nature Reviews Molecular Cell Biology*, 20(12):766–784.

Lasorella, A., Benezra, R., and Iavarone, A. (2014). The id proteins: master regulators of cancer stem cells and tumour aggressiveness. *Nat Rev Cancer*, 14(2):77–91.

Lee, Y., Park, D., and Iyer, V. R. (2017). The atp-dependent chromatin remodeler chd1 is recruited by transcription elongation factors and maintains h3k4me3/h3k36me3 domains at actively transcribed and spliced genes. *Nucleic Acids Res*, 45(12):7180–7190.

Lewis, L. M., Edwards, M. C., Meyers, Z. R., Talbot, C. Conover, J., Hao, H., Blum, D., and Reproducibility Project: Cancer, B. (2018). Replication study: Transcriptional amplification in tumor cells with elevated c-myc. *eLife*, 7:e30274.

Lin, C. Y., Lovén, J., Rahl, P. B., Paranal, R. M., Burge, C. B., Bradner, J. E., Lee, T. I., and Young, R. A. (2012). Transcriptional amplification in tumor cells with elevated c-myc. *Cell*, 151(1):56–67.

Lorenzin, F., Benary, U., Baluapuri, A., Walz, S., Jung, L. A., von Eyss, B., Kisker, C., Wolf, J., Eilers, M., and Wolf, E. (2016). Different promoter affinities account for specificity in myc-dependent gene regulation. *eLife*, 5:e15161.

Lu, X., Zhu, X., Li, Y., Liu, M., Yu, B., Wang, Y., Rao, M., Yang, H., Zhou, K., Wang, Y., Chen, Y., Chen, M., Zhuang, S., Chen, L. F., Liu, R., and Chen, R. (2016). Multiple p-tefbs cooperatively regulate the release of promoter-proximally paused rna polymerase ii. *Nucleic Acids Res*, 44(14):6853–67.

Madabhushi, R., Gao, F., Pfenning, A. R., Pan, L., Yamakawa, S., Seo, J., Rueda, R., Phan, T. X., Yamakawa, H., Pao, P. C., Stott, R. T., Gjoneska, E., Nott, A., Cho, S., Kellis, M., and Tsai, L. H. (2015). Activity-induced dna breaks govern the expression of neuronal early-response genes. *Cell*, 161(7):1592–605.

Marshall, N. F. and Price, D. H. (1995). Purification of p-tefb, a transcription factor required for the transition into productive elongation. *J. Biol. Chem.*, 270.

Mayer, A., Lidschreiber, M., Siebert, M., Leike, K., Söding, J., and Cramer, P. (2010). Uniform transitions of the general rna polymerase ii transcription complex. *Nat Struct Mol Biol*, 17(10):1272–8.

Mbogning, J., Nagy, S., Pagé, V., Schwer, B., Shuman, S., Fisher, R. P., and Tanny, J. C. (2013). The paf complex and prf1/rtf1 delineate distinct cdk9-dependent

pathways regulating transcription elongation in fission yeast. *PLoS Genet*, 9(12):e1004029.

McMahon, S. B., Buskirk, H. A., Dugan, K. A., Copeland, T. D., and Cole, M. D. (1998). The novel atm-related protein trrap is an essential cofactor for the c-myc and e2f oncoproteins. *Cell*, 94.

Meyer, N. and Penn, L. Z. (2008). Reflecting on 25 years with myc. *Nat. Rev. Cancer*, 8.

Minsky, N., Shema, E., Field, Y., Schuster, M., Segal, E., and Oren, M. (2008). Monoubiquitinated h2b is associated with the transcribed region of highly expressed genes in human cells. *Nature Cell Biology*, 10(4):483–488.

Mosimann, C., Hausmann, G., and Basler, K. (2006). Parafibromin/hyrax activates wnt/wg target gene transcription by direct association with beta-catenin/armadillo. *Cell*, 125(2):327–41.

Moyal, L., Lerenthal, Y., Gana-Weisz, M., Mass, G., So, S., Wang, S. Y., Eppink, B., Chung, Y. M., Shalev, G., Shema, E., Shkedy, D., Smorodinsky, N. I., van Vliet, N., Kuster, B., Mann, M., Ciechanover, A., Dahm-Daphi, J., Kanaar, R., Hu, M. C., Chen, D. J., Oren, M., and Shiloh, Y. (2011). Requirement of atm-dependent monoubiquitylation of histone h2b for timely repair of dna double-strand breaks. *Mol Cell*, 41(5):529–42.

Mueller, C. L., Porter, S. E., Hoffman, M. G., and Jaehning, J. A. (2004). The paf1 complex has functions independent of actively transcribing rna polymerase ii. *Mol Cell*, 14(4):447–56.

Muhar, M., Ebert, A., Neumann, T., Umkehrer, C., Jude, J., Wieshofer, C., Rescheneder, P., Lipp, J. J., Herzog, V. A., Reichholf, B., Cisneros, D. A., Hoffmann, T., Schlapansky, M. F., Bhat, P., von Haeseler, A., Köcher, T., Obenauf, A. C., Popow, J., Ameres, S. L., and Zuber, J. (2018). Slam-seq defines direct gene-regulatory functions of the brd4-myc axis. *Science*, 360(6390):800–805.

Mullins, E. A., Rodriguez, A. A., Bradley, N. P., and Eichman, B. F. (2019). Emerging roles of dna glycosylases and the base excision repair pathway. *Trends in Biochemical Sciences*, 44(9):765–781.

Murphy, D. M., Buckley, P. G., Bryan, K., Watters, K. M., Koster, J., van Sluis, P., Molenaar, J., Versteeg, R., and Stallings, R. L. (2011). Dissection of the oncogenic mycn transcriptional network reveals a large set of clinically relevant cell cycle genes as drivers of neuroblastoma tumorigenesis. *Mol Carcinog*, 50(6):403–11.

Nagaike, T., Logan, C., Hotta, I., Rozenblatt-Rosen, O., Meyerson, M., and Manley, J. L. (2011). Transcriptional activators enhance polyadenylation of mrna precursors. *Mol Cell*, 41(4):409–18.

Nakamura, K., Kato, A., Kobayashi, J., Yanagihara, H., Sakamoto, S., Oliveira, D. V., Shimada, M., Tauchi, H., Suzuki, H., Tashiro, S., Zou, L., and Komatsu, K. (2011). Regulation of homologous recombination by rnf20-dependent h2b ubiquitination. *Mol Cell*, 41(5):515–28.

Nau, M. M., Brooks, B. J., Battey, J., Sausville, E., Gazdar, A. F., Kirsch, I. R., McBride, O. W., Bertness, V., Hollis, G. F., and Minna, J. D. (1985). L-myc, a new myc-related gene amplified and expressed in human small cell lung cancer. *Nature*, 318(6041):69–73.

Ng, H. H., Dole, S., and Struhl, K. (2003a). The rtf1 component of the paf1 transcriptional elongation complex is required for ubiquitination of histone h2b. *J Biol Chem*, 278(36):33625–8.

Ng, H. H., Robert, F., Young, R. A., and Struhl, K. (2003b). Targeted recruitment of set1 histone methylase by elongating pol ii provides a localized mark and memory of recent transcriptional activity. *Mol Cell*, 11(3):709–19.

Nie, Z., Hu, G., Wei, G., Cui, K., Yamane, A., Resch, W., Wang, R., Green, D. R., Tessarollo, L., Casellas, R., Zhao, K., and Levens, D. (2012). c-myc is a universal amplifier of expressed genes in lymphocytes and embryonic stem cells. *Cell*, 151(1):68–79.

Nordick, K., Hoffman, M. G., Betz, J. L., and Jaehning, J. A. (2008). Direct interactions between the paf1 complex and a cleavage and polyadenylation factor are revealed by dissociation of paf1 from rna polymerase ii. *Eukaryot Cell*, 7(7):1158–67.

Northam, M. R. and Trujillo, K. M. (2016). Histone h2b mono-ubiquitylation maintains genomic integrity at stalled replication forks. *Nucleic Acids Research*, 44(19):9245–9255.

Nozawa, K., Schneider, T. R., and Cramer, P. (2017). Core mediator structure at 3.4 Å extends model of transcription initiation complex. *Nature*, 545.

Oliveira, D. V., Kato, A., Nakamura, K., Ikura, T., Okada, M., Kobayashi, J., Yanagihara, H., Saito, Y., Tauchi, H., and Komatsu, K. (2014). Histone chaperone fact regulates homologous recombination by chromatin remodeling through interaction with rnf20. *J Cell Sci*, 127(Pt 4):763–72.

Olson, C. M., Jiang, B., Erb, M. A., Liang, Y., Doctor, Z. M., Zhang, Z., Zhang, T., Kwiatkowski, N., Boukhali, M., Green, J. L., Haas, W., Nomanbhoy, T., Fischer, E. S., Young, R. A., Bradner, J. E., Winter, G. E., and Gray, N. S. (2018). Pharmacological perturbation of cdk9 using selective cdk9 inhibition or degradation. *Nat Chem Biol*, 14(2):163–170.

Orlando, D. A., Chen, M. W., Brown, V. E., Solanki, S., Choi, Y. J., Olson, E. R., Fritz, C. C., Bradner, J. E., and Guenther, M. G. (2014). Quantitative chip-seq normalization reveals global modulation of the epigenome. *Cell Reports*, 9(3):1163–1170.

Oss, S. B., Cucinotta, C. E., and Arndt, K. M. (2017). Emerging insights into the roles of the paf1 complex in gene regulation. *Trends Biochem. Sci.*, 42.

Otto, T., Horn, S., Brockmann, M., Eilers, U., Schüttrumpf, L., Popov, N., Kenney, A. M., Schulte, J. H., Beijersbergen, R., Christiansen, H., Berwanger, B., and Eilers, M. (2009). Stabilization of n-myc is a critical function of aurora a in human neuroblastoma. *Cancer Cell*, 15(1):67–78.

Palangat, M., Renner, D. B., Price, D. H., and Landick, R. (2005). A negative elongation factor for human rna polymerase ii inhibits the anti-arrest transcript-cleavage factor tfiis. *Proc. Natl Acad. Sci. USA*, 102.

Palomero, T., Lim, W. K., Odom, D. T., Sulis, M. L., Real, P. J., Margolin, A., Barnes, K. C., O'Neil, J., Neuberg, D., Weng, A. P., Aster, J. C., Sigaux, F., Soulier, J., Look, A. T., Young, R. A., Califano, A., and Ferrando, A. A. (2006). Notch1 directly regulates c-myc and activates a feed-forward-loop transcriptional network promoting leukemic cell growth. *Proc Natl Acad Sci U S A*, 103(48):18261–6.

Peter, S., Bultinck, J., Myant, K., Jaenicke, L. A., Walz, S., Müller, J., Gmachl, M., Treu, M., Boehmelt, G., Ade, C. P., Schmitz, W., Wiegering, A., Otto, C., Popov, N., Sansom, O., Kraut, N., and Eilers, M. (2014). Tumor cell-specific inhibition of myc function using small molecule inhibitors of the huwe1 ubiquitin ligase. *EMBO Molecular Medicine*, 6(12):1525–1541.

Piro, A. S., Mayekar, M. K., Warner, M. H., Davis, C. P., and Arndt, K. M. (2012). Small region of rtf1 protein can substitute for complete paf1 complex in facilitating global histone h2b ubiquitylation in yeast. *Proceedings of the National Academy of Sciences*, 109(27):10837–10842.

Plaschka, C., Larivière, L., Wenzeck, L., Seizl, M., Hemann, M., Tegunov, D., Petrotchenko, E. V., Borchers, C. H., Baumeister, W., Herzog, F., Villa, E., and Cramer, P. (2015). Architecture of the rna polymerase ii–mediator core initiation complex. *Nature*, 518(7539):376–380.

Popov, N., Herold, S., Llamazares, M., Schülein, C., and Eilers, M. (2007). Fbw7 and usp28 regulate myc protein stability in response to dna damage. *Cell Cycle*, 6(19):2327–31.

Porrua, O. and Libri, D. (2015). Transcription termination and the control of the transcriptome: why, where and how to stop. *Nature Reviews Molecular Cell Biology*, 16(3):190–202.

Prendergast, G. C. and Ziff, E. B. (1991). Methylation-sensitive sequence-specific dna binding by the c-myc basic region. *Science*, 251(4990):186–9.

Prieto-Garcia, C., Hartmann, O., Reissland, M., Braun, F., Fischer, T., Walz, S., Schülein-Völk, C., Eilers, U., Ade, C. P., Calzado, M. A., Orian, A., Maric, H. M., Münch, C., Rosenfeldt, M., Eilers, M., and Diefenbacher, M. E. (2020). Maintaining protein stability of np63 via usp28 is required by squamous cancer cells. *EMBO Molecular Medicine*, 12(4):e11101.

Puc, J., Kozbial, P., Li, W., Tan, Y., Liu, Z., Suter, T., Ohgi, K. A., Zhang, J., Aggarwal, A. K., and Rosenfeld, M. G. (2015). Ligand-dependent enhancer activation regulated by topoisomerase-i activity. *Cell*, 160(3):367–380.

Qiu, H., Hu, C., Gaur, N. A., and Hinnebusch, A. G. (2012). Pol ii ctd kinases bur1 and kin28 promote spt5 ctr-independent recruitment of paf1 complex. *Embo j*, 31(16):3494–505.

Qiu, H., Hu, C., Wong, C. M., and Hinnebusch, A. G. (2006). The spt4p subunit of yeast dsif stimulates association of the paf1 complex with elongating rna polymerase ii. *Mol Cell Biol*, 26(8):3135–48.

Quinlan, A. R. and Hall, I. M. (2010). Bedtools: a flexible suite of utilities for comparing genomic features. *Bioinformatics*, 26(6):841–842.

Rahl, P. B., Lin, C. Y., Seila, A. C., Flynn, R. A., McCuine, S., Burge, C. B., Sharp, P. A., and Young, R. A. (2010). c-myc regulates transcriptional pause release. *Cell*, 141(3):432–45.

Rahl, P. B. and Young, R. A. (2014). Myc and transcription elongation. *Cold Spring Harbor perspectives in medicine*, 4(1):a020990–a020990.

Ramírez, F., Ryan, D. P., Grüning, B., Bhardwaj, V., Kilpert, F., Richter, A. S., Heyne, S., Dündar, F., and Manke, T. (2016). deeptools2: a next generation web server for deep-sequencing data analysis. *Nucleic Acids Research*, 44(W1):W160–W165.

Richards, M. W., Burgess, S. G., Poon, E., Carstensen, A., Eilers, M., Chesler, L., and Bayliss, R. (2016). Structural basis of n-myc binding by aurora-a and its destabilization by kinase inhibitors. *Proceedings of the National Academy of Sciences*, 113(48):13726–13731.

Rogakou, E. P., Pilch, D. R., Orr, A. H., Ivanova, V. S., and Bonner, W. M. (1998). Dna double-stranded breaks induce histone h2ax phosphorylation on serine 139. *J Biol Chem*, 273(10):5858–68.

Rozenblatt-Rosen, O., Nagaike, T., Francis, J. M., Kaneko, S., Glatt, K. A., Hughes, C. M., LaFramboise, T., Manley, J. L., and Meyerson, M. (2009). The tumor suppressor cdc73 functionally associates with cpsf and cstf 3 mrna processing factors. *Proceedings of the National Academy of Sciences*, 106(3):755–760.

Sabari, B. R., Dall'Agnese, A., Boija, A., Klein, I. A., Coffey, E. L., Shrinivas, K., Abraham, B. J., Hannett, N. M., Zamudio, A. V., Manteiga, J. C., Li, C. H., Guo, Y. E., Day, D. S., Schuijers, J., Vasile, E., Malik, S., Hnisz, D., Lee, T. I., Cisse, I. I., Roeder, R. G., Sharp, P. A., Chakraborty, A. K., and Young, R. A. (2018). Coactivator condensation at super-enhancers links phase separation and gene control. *Science*, 361(6400):eaar3958.

Sabò, A., Kress, T. R., Pelizzola, M., de Pretis, S., Gorski, M. M., Tesi, A., Morelli, M. J., Bora, P., Doni, M., Verrecchia, A., Tonelli, C., Fagà, G., Bianchi, V., Ronchi, A., Low, D., Müller, H., Guccione, E., Campaner, S., and Amati, B. (2014). Selective transcriptional regulation by myc in cellular growth control and lymphomagenesis. *Nature*, 511(7510):488–492.

Sadeghi, L., Prasad, P., Ekwall, K., Cohen, A., and Svensson, J. P. (2015). The paf1 complex factors leo1 and paf1 promote local histone turnover to modulate chromatin states in fission yeast. *EMBO reports*, 16(12):1673–1687.

Saha, N., Ropa, J., Chen, L., Hu, H., Mysliwski, M., Friedman, A., Maillard, I., and Muntean, A. G. (2019). The paf1c subunit cdc73 is required for mouse

hematopoietic stem cell maintenance but displays leukemia-specific gene regulation. *Stem Cell Reports*, 12(5):1069–1083.

Schones, D. E., Cui, K., Cuddapah, S., Roh, T. Y., Barski, A., Wang, Z., Wei, G., and Zhao, K. (2008). Dynamic regulation of nucleosome positioning in the human genome. *Cell*, 132(5):887–98.

Seoane, J., Le, H. V., and Massagué, J. (2002). Myc suppression of the p21(cip1) cdk inhibitor influences the outcome of the p53 response to dna damage. *Nature*, 419(6908):729–34.

Sharma, P., Chinaranagari, S., and Chaudhary, J. (2015). Inhibitor of differentiation 4 (id4) acts as an inhibitor of id-1, -2 and -3 and promotes basic helix loop helix (bhlh) e47 dna binding and transcriptional activity. *Biochimie*, 112:139–50.

Sharma, V. M., Calvo, J. A., Draheim, K. M., Cunningham, L. A., Hermance, N., Beverly, L., Krishnamoorthy, V., Bhasin, M., Capobianco, A. J., and Kelliher, M. A. (2006). Notch1 contributes to mouse t-cell leukemia by directly inducing the expression of c-myc. *Mol Cell Biol*, 26(21):8022–31.

Sheiness, D. and Bishop, J. M. (1979). Dna and rna from uninfected vertebrate cells contain nucleotide sequences related to the putative transforming gene of avian myelocytomatosis virus. *J Virol*, 31(2):514–21.

Shen, L., Shao, N., Liu, X., and Nestler, E. (2014). ngs.plot: Quick mining and visualization of next-generation sequencing data by integrating genomic databases. *BMC Genomics*, 15(1):284.

Shou, Y., Martelli, M. L., Gabrea, A., Qi, Y., Brents, L. A., Roschke, A., Dewald, G., Kirsch, I. R., Bergsagel, P. L., and Kuehl, W. M. (2000). Diverse karyotypic abnormalities of the c-myc locus associated with c-myc dysregulation and tumor progression in multiple myeloma. *Proc Natl Acad Sci U S A*, 97(1):228–33.

Simabuco, F. M., Morale, M. G., Pavan, I. C. B., Morelli, A. P., Silva, F. R., and Tamura, R. E. (2018). p53 and metabolism: from mechanism to therapeutics. *Oncotarget*, 9(34):23780–23823.

Singh, S., Szlachta, K., Manukyan, A., Raimer, H. M., Dinda, M., Bekiranov, S., and Wang, Y. H. (2020). Pausing sites of rna polymerase ii on actively transcribed genes are enriched in dna double-stranded breaks. *J Biol Chem*, 295(12):3990–4000.

Smith, H. L., Southgate, H., Tweddle, D. A., and Curtin, N. J. (2020). Dna damage checkpoint kinases in cancer. *Expert Rev Mol Med*, 22:e2.

Smith, T., Heger, A., and Sudbery, I. (2017). Umi-tools: modeling sequencing errors in unique molecular identifiers to improve quantification accuracy. *Genome Research*, 27(3):491–499.

Smolle, M. and Workman, J. L. (2013). Transcription-associated histone modifications and cryptic transcription. *Biochimica et Biophysica Acta (BBA) - Gene Regulatory Mechanisms*, 1829(1):84–97.

Soucek, L., Nasi, S., and Evan, G. I. (2004). Omomyc expression in skin prevents myc-induced papillomatosis. *Cell Death Differ.*, 11.

Staller, P., Peukert, K., Kiermaier, A., Seoane, J., Lukas, J., Karsunky, H., Möröy, T., Bartek, J., Massagué, J., Hänel, F., and Eilers, M. (2001). Repression of p15ink4b expression by myc through association with miz-1. *Nat Cell Biol*, 3(4):392–9.

Stiff, T., O'Driscoll, M., Rief, N., Iwabuchi, K., Löbrich, M., and Jeggo, P. A. (2004). Atm and dna-pk function redundantly to phosphorylate h2ax after exposure to ionizing radiation. *Cancer Res*, 64(7):2390–6.

Stine, Z. E., Walton, Z. E., Altman, B. J., Hsieh, A. L., and Dang, C. V. (2015). Myc, metabolism and cancer. *Cancer Discov.*, 5.

Takahashi, A., Tsutsumi, R., Kikuchi, I., Obuse, C., Saito, Y., Seidi, A., Karisch, R., Fernandez, M., Cho, T., Ohnishi, N., Rozenblatt-Rosen, O., Meyerson, M., Neel, B. G., and Hatakeyama, M. (2011). Shp2 tyrosine phosphatase converts parafibromin/cdc73 from a tumor suppressor to an oncogenic driver. *Mol Cell*, 43(1):45–56.

Talbert, P. B., Meers, M. P., and Henikoff, S. (2019). Old cogs, new tricks: the evolution of gene expression in a chromatin context. *Nat. Rev. Genet.*, 20.

Tarczewska, A. and Greb-Markiewicz, B. (2019). The significance of the intrinsically disordered regions for the functions of the bhlh transcription factors. *International journal of molecular sciences*, 20(21):5306.

Tasselli, L., Xi, Y., Zheng, W., Tennen, R. I., Odrowaz, Z., Simeoni, F., Li, W., and Chua, K. F. (2016). Sirt6 deacetylates h3k18ac at pericentric chromatin to prevent mitotic errors and cellular senescence. *Nature Structural Molecular Biology*, 23(5):434–440.

Taub, R., Kirsch, I., Morton, C., Lenoir, G., Swan, D., Tronick, S., Aaronson, S., and Leder, P. (1982). Translocation of the c-myc gene into the immunoglobulin heavy chain locus in human burkitt lymphoma and murine plasmacytoma cells. *Proc Natl Acad Sci U S A*, 79(24):7837–41.

Tesi, A., de Pretis, S., Furlan, M., Filipuzzi, M., Morelli, M. J., Andronache, A., Doni, M., Verrecchia, A., Pelizzola, M., Amati, B., and Sabò, A. (2019). An early myc-dependent transcriptional program orchestrates cell growth during b-cell activation. *EMBO Rep*, 20(9):e47987.

Thomas, L. R., Foshage, A. M., Weissmiller, A. M., Popay, T. M., Grieb, B. C., Qualls, S. J., Ng, V., Carboneau, B., Lorey, S., Eischen, C. M., and Tansey, W. P. (2016). Interaction of myc with host cell factor-1 is mediated by the evolutionarily conserved myc box iv motif. *Oncogene*, 35(27):3613–8.

Thomas, L. R., Wang, Q., Grieb, B. C., Phan, J., Foshage, A. M., Sun, Q., Olejniczak, E. T., Clark, T., Dey, S., Lorey, S., Alicie, B., Howard, G. C., Cawthon, B., Ess, K. C., Eischen, C. M., Zhao, Z., Fesik, S. W., and Tansey, W. P. (2015). Interaction with wdr5 promotes target gene recognition and tumorigenesis by myc. *Mol Cell*, 58(3):440–52.

Topper, M. J., Vaz, M., Chiappinelli, K. B., DeStefano Shields, C. E., Niknafs, N., Yen, R. C., Wenzel, A., Hicks, J., Ballew, M., Stone, M., Tran, P. T., Zahnow, C. A., Hellmann, M. D., Anagnostou, V., Strissel, P. L., Strick, R., Velculescu, V. E., and Baylin, S. B. (2017). Epigenetic therapy ties myc depletion to reversing immune evasion and treating lung cancer. *Cell*, 171(6):1284–1300.e21.

Trujillo, K. M. and Osley, M. A. (2012). A role for h2b ubiquitylation in dna replication. *Mol Cell*, 48(5):734–46.

Tsai, K.-L., Yu, X., Gopalan, S., Chao, T.-C., Zhang, Y., Florens, L., Washburn, M. P., Murakami, K., Conaway, R. C., Conaway, J. W., and Asturias, F. J. (2017). Mediator structure and rearrangements required for holoenzyme formation. *Nature*, 544(7649):196–201.

Tu, W. B., Shiah, Y. J., Lourenco, C., Mullen, P. J., Dingar, D., Redel, C., Tamachi, A., Ba-Alawi, W., Aman, A., Al-Awar, R., Cescon, D. W., Haibe-Kains, B., Arrowsmith, C. H., Raught, B., Boutros, P. C., and Penn, L. Z. (2018). Myc interacts with the g9a histone methyltransferase to drive transcriptional repression and tumorigenesis. *Cancer Cell*, 34(4):579–595.e8.

Van Oss, S. B., Shirra, M. K., Bataille, A. R., Wier, A. D., Yen, K., Vinayachandran, V., Byeon, I. L., Cucinotta, C. E., Héroux, A., Jeon, J., Kim, J., VanDemark, A. P., Pugh, B. F., and Arndt, K. M. (2016). The histone modification domain of paf1 complex subunit rtf1 directly stimulates h2b ubiquitylation through an interaction with rad6. *Mol Cell*, 64(4):815–825.

Venkatesh, S. and Workman, J. L. (2013). Set2 mediated h3 lysine 36 methylation: regulation of transcription elongation and implications in organismal development. *Wiley Interdiscip Rev Dev Biol*, 2(5):685–700.

Vera, J., Raatz, Y., Wolkenhauer, O., Kottek, T., Bhattacharya, A., Simon, J. C., and Kunz, M. (2015). Chk1 and wee1 control genotoxic-stress induced g2-m arrest in melanoma cells. *Cell Signal*, 27(5):951–60.

von der Lehr, N., Johansson, S., Wu, S., Bahram, F., Castell, A., Cetinkaya, C., Hydbring, P., Weidung, I., Nakayama, K., Nakayama, K. I., Söderberg, O., Kerppola, T. K., and Larsson, L. G. (2003). The f-box protein skp2 participates in c-myc proteosomal degradation and acts as a cofactor for c-myc-regulated transcription. *Mol Cell*, 11(5):1189–200.

Vos, S. M., Farnung, L., Boehning, M., Wigge, C., Linden, A., Urlaub, H., and Cramer, P. (2018a). Structure of activated transcription complex pol ii-dsif-paf-spt6. *Nature*, 560(7720):607–612.

Vos, S. M., Farnung, L., Urlaub, H., and Cramer, P. (2018b). Structure of paused transcription complex pol ii–dsif–nelf. *Nature*, 560.

Wade, P. A., Werel, W., Fentzke, R. C., Thompson, N. E., Leykam, J. F., Burgess, R. R., Jaehning, J. A., and Burton, Z. F. (1996). A novel collection of accessory factors associated with yeast rna polymerase ii. *Protein Expr Purif*, 8(1):85–90.

Walz, S., Lorenzin, F., Morton, J., Wiese, K. E., von Eyss, B., Herold, S., Rycak, L., Dumay-Odelot, H., Karim, S., Bartkuhn, M., Roels, F., Wüstefeld, T., Fischer, M., Teichmann, M., Zender, L., Wei, C.-L., Sansom, O., Wolf, E., and Eilers, M. (2014). Activation and repression by oncogenic myc shape tumour-specific gene expression profiles. *Nature*, 511(7510):483–487.

Wang, M. D., Schnitzer, M. J., Yin, H., Landick, R., Gelles, J., and Block, S. M. (1998). Force and velocity measured for single molecules of rna polymerase. *Science*, 282(5390):902–907.

Wang, P. F., Tan, M. H., Zhang, C., Morreau, H., and Teh, B. T. (2005). Hrpt2, a tumor suppressor gene for hyperparathyroidism-jaw tumor syndrome. *Horm Metab Res*, 37(6):380–3.

Wanzel, M., Kleine-Kohlbrecher, D., Herold, S., Hock, A., Berns, K., Park, J., Hemmings, B., and Eilers, M. (2005). Akt and 14-3-3η regulate miz1 to control cell-cycle arrest after dna damage. *Nature Cell Biology*, 7(1):30–41.

Ward, I. M. and Chen, J. (2001). Histone h2ax is phosphorylated in an atr-dependent manner in response to replicational stress *. *Journal of Biological Chemistry*, 276(51):47759–47762.

Warner, M. H., Roinick, K. L., and Arndt, K. M. (2007). Rtf1 is a multifunctional component of the paf1 complex that regulates gene expression by directing cotranscriptional histone modification. *Mol Cell Biol*, 27(17):6103–15.

Weake, V. M. and Workman, J. L. (2008). Histone ubiquitination: triggering gene activity. *Mol Cell*, 29(6):653–63.

Welcker, M., Orian, A., Jin, J., Grim, J. E., Harper, J. W., Eisenman, R. N., and Clurman, B. E. (2004). The fbw7 tumor suppressor regulates glycogen synthase kinase 3 phosphorylation-dependent c-myc protein degradation. *Proc Natl Acad Sci U S A*, 101(24):9085–90.

Wen, H., Li, Y., Xi, Y., Jiang, S., Stratton, S., Peng, D., Tanaka, K., Ren, Y., Xia, Z., Wu, J., Li, B., Barton, M. C., Li, W., Li, H., and Shi, X. (2014). Zmynd11 links histone h3.3k36me3 to transcription elongation and tumour suppression. *Nature*, 508(7495):263–268.

Weng, A. P., Millholland, J. M., Yashiro-Ohtani, Y., Arcangeli, M. L., Lau, A., Wai, C., Del Bianco, C., Rodriguez, C. G., Sai, H., Tobias, J., Li, Y., Wolfe, M. S., Shachaf, C., Felsher, D., Blacklow, S. C., Pear, W. S., and Aster, J. C. (2006). c-myc is an important direct target of notch1 in t-cell acute lymphoblastic leukemia/lymphoma. *Genes Dev*, 20(15):2096–109.

Wier, A. D., Mayekar, M. K., Héroux, A., Arndt, K. M., and VanDemark, A. P. (2013). Structural basis for spt5-mediated recruitment of the paf1 complex to chromatin. *Proceedings of the National Academy of Sciences*, 110(43):17290–17295.

Wiese, K. E., Haikala, H. M., von Eyss, B., Wolf, E., Esnault, C., Rosenwald, A., Treisman, R., Klefström, J., and Eilers, M. (2015). Repression of srf target genes is critical for myc-dependent apoptosis of epithelial cells. *Embo j*, 34(11):1554–71.

Wolf, E., Gebhardt, A., Kawauchi, D., Walz, S., von Eyss, B., Wagner, N., Renninger, C., Krohne, G., Asan, E., Roussel, M. F., and Eilers, M. (2013). Miz1 is required to maintain autophagic flux. *Nature Communications*, 4(1):2535.

Wolf, E., Lin, C. Y., Eilers, M., and Levens, D. L. (2015). Taming of the beast: shaping myc-dependent amplification. *Trends Cell Biol*, 25(4):241–8.

Wood, A., Schneider, J., Dover, J., Johnston, M., and Shilatifard, A. (2003). The paf1 complex is essential for histone monoubiquitination by the rad6-bre1 complex, which signals for histone methylation by compass and dot1p. *J Biol Chem*, 278(37):34739–42.

Wu, L., Li, L., Zhou, B., Qin, Z., and Dou, Y. (2014). H2b ubiquitylation promotes rna pol ii processivity via paf1 and ptefb. *Mol Cell*, 54(6):920–931.

Xiao, W. and Samson, L. (1993). In vivo evidence for endogenous dna alkylation damage as a source of spontaneous mutation in eukaryotic cells. *Proceedings of the National Academy of Sciences of the United States of America*, 90(6):2117–2121.

Xie, Y., Zheng, M., Chu, X., Chen, Y., Xu, H., Wang, J., Zhou, H., and Long, J. (2018). Paf1 and ctr9 subcomplex formation is essential for paf1 complex assembly and functional regulation. *Nature communications*, 9(1):3795–3795.

Yada, M., Hatakeyama, S., Kamura, T., Nishiyama, M., Tsunematsu, R., Imaki, H., Ishida, N., Okumura, F., Nakayama, K., and Nakayama, K. I. (2004). Phosphorylation-dependent degradation of c-myc is mediated by the f-box protein fbw7. *The EMBO journal*, 23(10):2116–2125.

Yamaguchi, Y., Shibata, H., and Handa, H. (2013). Transcription elongation factors dsif and nelf: promoter-proximal pausing and beyond. *Biochim. Biophys. Acta*, 1829.

Yang, J., Yu, Y., Hamrick, H. E., and Duerksen-Hughes, P. J. (2003). Atm, atr and dna-pk: initiators of the cellular genotoxic stress responses. *Carcinogenesis*, 24(10):1571–80.

Yang, Y., Li, W., Hoque, M., Hou, L., Shen, S., Tian, B., and Dynlacht, B. D. (2016). Paf complex plays novel subunit-specific roles in alternative cleavage and polyadenylation. *PLOS Genetics*, 12(1):e1005794.

Yeh, E., Cunningham, M., Arnold, H., Chasse, D., Monteith, T., Ivaldi, G., Hahn, W. C., Stukenberg, P. T., Shenolikar, S., Uchida, T., Counter, C. M., Nevins, J. R., Means, A. R., and Sears, R. (2004). A signalling pathway controlling c-myc degradation that impacts oncogenic transformation of human cells. *Nature Cell Biology*, 6(4):308–318.

Yin, X. Y., Grove, L., Datta, N. S., Katula, K., Long, M. W., and Prochownik, E. V. (2001). Inverse regulation of cyclin b1 by c-myc and p53 and induction of tetraploidy by cyclin b1 overexpression. *Cancer Res*, 61(17):6487–93.

Yu, M., Yang, W., Ni, T., Tang, Z., Nakadai, T., Zhu, J., and Roeder, R. G. (2015). Rna polymerase ii-associated factor 1 regulates the release and phosphorylation of paused rna polymerase ii. *Science*, 350(6266):1383–6.

Yustein, J. T., Liu, Y. C., Gao, P., Jie, C., Le, A., Vuica-Ross, M., Chng, W. J., Eberhart, C. G., Bergsagel, P. L., and Dang, C. V. (2010). Induction of ectopic myc target gene jag2 augments hypoxic growth and tumorigenesis in a human b-cell model. *Proc Natl Acad Sci U S A*, 107(8):3534–9.

Zhang, H., Rigo, F., and Martinson, H. G. (2015). Poly(a) signal-dependent transcription termination occurs through a conformational change mechanism that does not require cleavage at the poly(a) site. *Mol Cell*, 59(3):437–48.

Zhang, N., Ichikawa, W., Faiola, F., Lo, S. Y., Liu, X., and Martinez, E. (2014). Myc interacts with the human staga coactivator complex via multivalent contacts with the gcn5 and trrap subunits. *Biochim Biophys Acta*, 1839(5):395–405.

Zhao, X., Heng, J. I., Guardavaccaro, D., Jiang, R., Pagano, M., Guillemot, F., Iavarone, A., and Lasorella, A. (2008). The hect-domain ubiquitin ligase huwe1 controls neural differentiation and proliferation by destabilizing the n-myc oncoprotein. *Nat Cell Biol*, 10(6):643–53.

Zheng, S., Li, D., Lu, Z., Liu, G., Wang, M., Xing, P., Wang, M., Dong, Y., Wang, X., Li, J., Zhang, S., Peng, H., Ira, G., Li, G., and Chen, X. (2018). Bre1-dependent h2b ubiquitination promotes homologous recombination by stimulating histone eviction at dna breaks. *Nucleic acids research*, 46(21):11326–11339.

Zhi, X., Giroux-Leprieur, E., Wislez, M., Hu, M., Zhang, Y., Shi, H., Du, K., and Wang, L. (2015). Human rna polymerase ii associated factor 1 complex promotes tumorigenesis by activating c-myc transcription in non-small cell lung cancer. *Biochem Biophys Res Commun*, 465(4):685–90.

Zhou, Q., Li, T., and Price, D. H. (2012). Rna polymerase ii elongation control. *Annu. Rev. Biochem.*, 81.

Zhu, B., Mandal, S. S., Pham, A. D., Zheng, Y., Erdjument-Bromage, H., Batra, S. K., Tempst, P., and Reinberg, D. (2005). The human paf complex coordinates transcription with events downstream of rna synthesis. *Genes Dev*, 19(14):1668–73.

List of Publications

Endres, T., Solvie, D., Heidelberger, J. B., Andrioletti, V., Baluapuri, A., Ade, C. P., Muhar, M., Eilers, U., Vos, S. M., Cramer, P., Zuber, J., Beli, P., Popov, N., Wolf, E., Gallant, P., and Eilers, M. (2021). Ubiquitylation of myc couples transcription elongation with double-strand break repair at active promoters. *Molecular Cell*.

Baluapuri, A., Hofstetter, J., Dudvarski Stankovic, N., **Endres, T.**, Bhandare, P., Vos, S. M., Adhikari, B., Schwarz, J. D., Narain, A., Vogt, M., Wang, S.-Y., Düster, R., Jung, L. A., Vanselow, J. T., Wiegering, A., Geyer, M., Maric, H. M., Gallant, P., Walz, S., Schlosser, A., Cramer, P., Eilers, M., and Wolf, E. (2019). Myc recruits spt5 to rna polymerase ii to promote processive transcription elongation. *Molecular Cell*, 74(4):674–687.e11.

Papadopoulos, D., Kalb, J., Solvie, D., Baluapuri, A., Herold, S., **Endres, T.**, Giansanti, C., Schülein-Völk, C., Ade, C. P., Schneider, C., Fischer, U., Dobbelstein, M., Wolf, E., and Eilers, M. (2021). The mycn oncoprotein resolves conflicts of stalling rna polymerase with the replication fork. **Under revision, Mol Cell*.

Acknowledgments

First of all, I would like to thank Prof. Dr. Martin Eilers for supervising this thesis and for giving me the opportunity to work on this project. I am very grateful for his support, helpful advices and fruitfull discussions which lead in the end to a successfull project.

I would also like to thank Prof. Dr. Elmar Wolf for his advices and support as second supervisor and part of my thesis committee.

I thank Prof. Dr. Caroline Kisker and Prof. Dr. Patrick Cramer for being a member of my thesis committee.

I thank the GRK2243 members. I enjoyed the discussions and the nice atmosphere during the journal club, retreats or social get together.

I want to express my gratitude towards the Graduate School of Life Science for their support and for providing soft skill trainings.

I also would like to acknowledge scientists outside the department. For getting to know new technologies and scientific concepts, I am grateful to members of the Patrick Cramer lab and the Kisker lab, especially Seychelle Vos and Jochen Kuper.

Additionally, I would like to thank the whole department. This department provides an exceptionally friendly and helpful environment in which I loved to work. I liked my role as associated member of AG Wolf. I also loved the spontaneous discussions on the corridor, the daily excursions to mensa and the various social get together for different reasons. I got to know very special, motivated people which helped me a lot beyond the scientific part. I want to thank Carsten and Peter for their constant support in regard to bioinformatic problems. Special thanks goes to my office, the "Weinkenner", the "Antiquity" group and the "wisky amigos". Specifically I want to thank Gabriele and Giacomo for their advices as "experienced postdocs". Many thanks to them and Steffi for offering corrections on this thesis. I thank Irem, "my plus one" in always being so honest with me and for offering help also after she left the lab. A special thank you goes to Daniel for the "dream team" work during the "PAF1c-HUWE1" project. At that time I enjoyed being friends and our meetings for "pumpen". I also want to thank Apoorva for being a good friend who went with me for "Spaziergang" so many times, to discuss life, science and the future in always a very helpful but at the same time nerdy and philosophic level. I always liked working with you, also when it

appears to others that we are "fighting".
I also want to thank Seteam, Amelie and Selena. I appreciate, that we always support each other and I am so grateful for that.
Last but not least, I want to thank my family for their help and their continuous encouragement, support and love - specially when so much was going on. And during all those difficult times we became even stronger as a family. I simply cannot thank you enough!

Affidavit

I hereby confirm that my thesis entitled "PAF1 complex and MYC couple transcription elongation with double-strand break repair" is the result of my own work. I did not receive any help or support from commercial consultants. All sources and / or materials applied are listed and specified in the thesis.

Furthermore, I confirm that this thesis has not yet been submitted as part of another examination process neither in identical nor in similar form.

Wuerzburg, August 17, 2021

Place, Date Signature

Eidesstattliche Erklärung

Hiermit erkläre ich an Eidesstatt, die Dissertation "Koordination von Transkriptionselongation und Doppelstrangbruchreparatur durch den PAF1 Komplex und MYC" , eigenständig, d.h. insbesondere selbständig und ohne Hilfe eines kommerziellen Promotionsberaters, angefertigt und keine anderen als die von mir angegebenen Quellen und Hilfsmittel verwendet zu haben.

Ich erkäre außerdem, dass die Dissertation weder in gleicher noch in Ahnlicher Form bereits in einem anderen Prüfungsverfahren vorgelegen hat.

Wuerzburg, August 17, 2021

Ort, Datum Unterschrift